An experimental and numerical investigation of predictive control with different building-integrated thermal storage systems

Anastasios C. Papachristou

A Thesis

In the Department

of

Building, Civil and Environmental Engineering

Presented in Partial Fulfillment of the Requirements

for the Degree of Master of Applied Science (Building Engineering) at

Concordia University

Montreal, Quebec, Canada

October 2016

© Anastasios Papachristou, 2016

CONCORDIA UNIVERSITY

CONCORDIA UNIVERSITY
School of Graduate Studies

This is to certify that the thesis prepared

By: Anastasios Papachristou

Entitled: An Experimental and Numerical Investigation of Predictive Control With Different Building-Integrated Thermal Storage Systems

and submitted in partial fulfillment of the requirements for the degree of
Master of Applied Science (Building Engineering)

complies with the regulations of the University and meets the accepted standards with respect to originality and quality.

Signed by the final examining committee:

_____ Chair
Dr. R. Zmeureanu

_____ Supervisor
Dr. A. Athienitis

_____ Examiner
Dr. M. Paraschivoiu External (to program)

_____ Examiner
Dr. L. Wang

_____ Examiner
Dr. R. Zmeureanu

_____ Examiner
Dr. A. Daoud

Approved by _____
Dr. F. Haghighat, GPD
Department of Building, Civil and Environmental Engineering

_____
Dr. Amir Asif, Dean
Faculty of Engineering and Computer Science

Date _____

Abstract

An experimental and numerical investigation of predictive control with different building-integrated thermal storage systems

Anastasios Papachristou

This thesis presents a numerical and experimental investigation of predictive control with different building-integrated thermal storage systems. The purpose is to utilize efficiently the available thermal mass of a space in order to reduce the peak demand and energy consumption while maintaining occupant comfort.

Two case studies are performed together with model development. The first one is a zone of a perimeter office with floor heating, convective cooling and a carpeted concrete floor. Various floor configurations are simulated to study the effect of thermal mass and its cover in predictive control. The window-to-wall (WWR) ratio is 75%, resulting in high solar gains. These solar gains are useful in winter but in summer they need to be reduced by controlling the shades to reduce total cooling load. The simulations results show that an exposed concrete floor (no carpet) can lead to significantly lower peak (about 35% in cooling and 41% in heating) in the auxiliary cooling/ heating as compared to a carpeted floor.

The second case study presents a simulation and experimental implementation of simple predictive control strategies in a test cell using a phase change material (PCM) as a means of thermal storage exposed to simulated outdoor conditions in a large environmental chamber. The PCM, embedded in a wall of the test cell, is actively charged through forced air circulation. The objective of the study is to investigate how model predictive control (MPC) can be used to leverage the thermal capacity of a PCM wall. This study also shows how a low-order thermal network model can be

used as an effective tool in the design of the MPC strategy. The proposed MPC algorithm uses a set of linear ramp functions to change the room temperature setpoint to reduce and shift peak power demand. These ramp setpoint profiles allow the effective charging and discharging of the wall-integrated PCM. The algorithm applied in the experimental facility uses the outdoor temperature as input to select the best charging and discharging rates over a prediction horizon. A low-order model of the room and the PCM wall is used in the predictive control algorithm. It was found that this model can predict accurately the peak power demand and the temperature profile in the room. As the process moves forward in time, the weather profile is updated periodically and the algorithm calculates the new outputs over the new control horizon. The whole procedure is automated and the outputs of the algorithm are transferred to the local variables of the controller of the test room through BACnet.

Dedication

To my father, Christos

Acknowledgements

I would like to express my deep gratitude to my supervisor, Dr. Andreas K. Athienitis, for his guidance, support and motivation. Thank you for giving me the opportunity to work on real case studies, study systems of real buildings and gaining so much practical knowledge. Thank you for allowing me to participate in numerous meetings and interesting projects at Concordia University. I will be always thankful for trusting me the letting me be part of your team. It has been an honor working with you!

I want to thank everyone in Regulvar Head Office in Laval for their help during my time there. Especially I would like to thank Marc Dugré, Gabriel Mainville and Marc-André Lagacé for providing me with all the necessary tools and advice for my work at Regulvar.

I would like to acknowledge the technical and financial support from the NSERC/Hydro-Quebec Industrial Research Chair and the Faculty of Engineering and Computer Science of Concordia University. Thank you to Ahmed Daoud, Karine Lavigne and Jocelyn Milette from Hydro-Quebec for their continuous help and sharing their time and expertise. Also, I want to thank José Candanedo from NRC CanmetENERGY for sharing his knowledge in Matlab and Simulink and inspiring me during my studies.

I want to thank all of my colleagues within the Centre for Zero Energy Building Studies. It was very interesting and though-provoking working in a multidisciplinary team. Thank you all for your friendship, enthusiasm, helpful ideas and cooperation. I would like to specially thank Harry Vallianos, Vasken Dermardiros, Zissis Ioannidis and Costa Kapsis for their valuable help during the simulations and experimental part of my work. Without you I would still be writing code in

Matlab! Thank you Vasken Dermardiros for letting me continue part of your project, guiding me and sharing your passion for controls.

From the administrative team, I would like to thank Gerald Parnis, Jacques Payer, Lyne Dee, Jenny Drapeau, Olga Soares, Debbie Walker and Linda Swinden. From the technical team, I would like to thank Luc Desmers and Jaime Yeargans for their help in the lab. Dr. Jiwu Rao deserves special thanks for sharing his technical and software expertise through the course of this experimental work and especially for his valuable help in BACnet communication.

Finally, I want to thank all of my friends and my family for believing in me and supporting me during these years. Last, I want to thank Stefania Strantza who has always been there for me, motivating me and making me stronger.

Table of Contents

List of Figures

List of Tables

Nomenclature

Variables

C_i	Thermal capacitance of node i	J/ ºC
Δh	Enthalpy of fusion	$J \cdot kg^{-1}$
$C(T)_i^j$	Capacitance as a function of its temperature	J/ ºC
C_{air}	Thermal capacitance of the room air	J/ ºC
C_{eff}	Effective thermal capacitance of the room	J/ ºC
$C_{p\ ,\ average}$	Average specific heat of PCM in the sensible range	$J \cdot kg^{-1} \cdot K^{-1}$
F_{ij}	View factor, surface i to j	
k_i	Integral gain	W/(ºC·s)
k_p	Proportional gain	W/ºC
$\dot{m}_{air}$	Air mass flow rate	kgs^{-1}
q_{aux}	Auxiliary heat (cooling or heating)	W
Q_{heater}	Auxiliary heat from an electric heater	W
$\dot{Q}$i	Heat flow into the node	W
R_{COND}	Thermal resistance for conductive heat transfer	$(ºCm^2)/W$
R_{CONV}	Thermal resistance for convective heat transfer	$(ºCm^2)/W$
R_{eff}	Effective thermal resistance of the room	$(ºCm^2)/W$
R_{floor}	Thermal resistance of the floor	$(ºCm^2)/W$
R_{ij}	Thermal resistance between nodes i and j	$(ºCm^2)/W$
R_{RAD}	Thermal resistance for radiative heat transfer	$(ºCm^2)/W$
skew	Skewness factor	
S_{rad}	Solar radiation transmitted through the window	W
T_c	Approximate temperature of peak phase change	°C
T_m	Mean Radiant Temperature	°C
T_{sp}	Room air setpoint	°C
$T_{surface}$	Average temperature of the front and back PCM surfaces	°C
U_{ij}	Thermal conductance between nodes i and j	$W/(ºCm^2)$
Δt	Simulation time step	s

Greek letters

ε	Emissivity	
ρ	Density	Kg/m^3
σ	Stefan-Boltzmann constant $5.67\times10-8$	$W/(m^2K^4)$
ω	Temperature range of phase change	°C

Abbreviation

4SID	Subspace State Space System Identification
ANSI	American National Standards Institute
ARMAX	Autoregressive Moving Average with exogenous input
ASHRAE	American Society of Heating, Refrigerating, and Air-Conditioning Engineers
BACnet	Building automation and control networks
BCVTB	Building Control Virtual Test Bed
CTES	Cool thermal energy storage
CV-RMSE	Coefficient of variation of the root mean squared error
DSPM	Deterministic Semi – Physical Modeling
FDM	Finite Difference Method
HVAC	Heating, Ventilation and Air Conditioning
IRA	Integrated Room Automation
LHES	Latent Heat Energy Storage
MPC	Model-based Predictive Control
MRI	MPC Relevant Identification
NMBE	Normalized Mean Bias Error
NSERC	Natural Sciences and Engineering Research Council of Canada
PCM - TES	Phase-Change Material Thermal Energy Storage
PEM	Prediction Error Methods
PI	Proportional-Integral
PID	Proportional-Integral-Derivative
PMV	Predicted Mean Vote
PPD	Predicted Percentage of Dissatisfied
PSPM	Probabilistic Semi – Physical Modeling
RBC	Rule-based Control
SSEC	Solar Simulator Environmental Chamber
TES	Thermal Energy Storage
UDI	Useful Daylight Illuminance
WWR	Window-to-Wall Ratio

1 Introduction

1.1 Background and Motivation

It is widely accepted that to reduce greenhouse gas emissions we need to replace fossil energy sources by renewable energy wherever possible (Wolisz et al. 2015). Buildings are major energy consumers globally. Reports show that buildings account for about 30 % of final energy consumption in Europe (Eurostat 2016; Wolisz et al. 2015) and more than 70% of electricity consumption in US (DOE US 2016). In Quebec commercial, institutional and residential buildings consume 51% of electricity (Dermardiros 2015; Natural Resources Canada 2013). Among other techniques that have been proposed to reduce energy consumption in buildings, control of building thermal mass does not require installation of additional equipment (Li and Malkawi 2016). Storing thermal energy into the thermal mass and releasing it later may offset the peak demand and improve the thermal comfort (Athienitis et al. 1997; Dincer 2002; Fernandes et al. 2012). Phase-change material-thermal energy storage systems (PCM-TES) may help in that direction, increasing the thermal capacity without much volume or additional weight.

The type of control is also important. Feedback controllers, such as proportional-integral (PI) controllers, are commonly used in buildings. These approaches fail to efficiently control slow responding dynamic processes (Afram and Janabi-Sharifi 2014). A promising solution for that is model-based predictive control (MPC) that takes into account the inertia of the system. MPC uses future information about occupancy, weather and internal loads, in order to take the best action to minimize a cost function which can be energy consumption reduction and thermal comfort enhancement. The performance improvement in buildings when forecast information is used can

be done by load shifting (or active storage) and optimization (Ma et al. 2012). An MPC strategy combines these two mechanisms.

This thesis covers simulation and experimental results of predictive control strategies in two different thermal mass configurations. The first case study that is investigated describes a room with a concrete floor covered with carpet. The effect of thermal and its thermal coupling with the room on peak load reductions and temperature fluctuations are investigated in here. The second case study includes a chamber with PCM integrated into its back wall with an air channel between the PCM panels for active thermal storage. A low order model of the system is created and calibrated experimentally. Then this model is used in a predictive control strategy which is implemented in a test room in an environmental chamber.

1.2 Objectives

The objectives of this thesis are as follows:

1. To develop predictive control strategies for different thermal mass configurations for perimeter zones and study the effect of model resolution on peak and total load. Also this study will aim to develop calibrated models that can be easily used in predictive control.
2. To investigate different types of thermal mass, in particular concrete and phase change materials, and study through predictive control strategies the effect on peak and total load and temperature fluctuations in a room using different setpoint profiles.

1.3 Outline of the thesis

Chapter 1 presents an introduction including the background and motivation and also the objectives of this thesis and the thesis outline.

Chapter 2 presents a literature review focusing on predictive control and some topics related to that. These topics include the thermal energy storage and the role of thermal mass, the thermal comfort, types of controls in buildings and model-based predictive control (MPC).

Chapter 3 presents the first case study; a perimeter office zone with a radiant floor heating system and a chilled beam. The impact of thermal mass on peak load reduction and temperature variations in the room in studied through predictive control strategies.

Chapter 4 presents the second case study which is a test room with PCM integrated into its back wall. A model of the test room is created and used in a predictive control scheme implemented in the lab.

Chapter 5 presents the conclusions of this thesis, main contributions and recommendations for future work.

2 Literature review

2.1 Thermal energy storage

Thermal energy storage (TES) systems contribute to more efficient, harmless to the environment energy use in building heating and cooling, space power and utility applications (Dincer 2002). Dincer (2002) classifies three type of TES: sensible, latent and thermochemical. He states that among other parameters, the selection of TES system mainly depends on the storage period required (e.g. diurnal or seasonal), economic viability and operating conditions. TES lead to significant energy savings when using waste energy and surplus heat, reducing electrical demand charges, and avoiding heating, cooling or air-conditioning equipment purchases. Dincer and Rosen (2001) also explain some other benefits of TES, including increased generation capacity and shifting energy purchases to low cost periods. The thermal mass of the building or phase change materials (PCM) integrated into the structure of the building or the HVAC system act as thermal energy storage systems.

Another study from Parameshwaran et al. (2012) mentions the need of developing efficient and sustainable energy technologies using TES systems to decrease the difference between the energy supply and energy demand. They estimate that energy savings of around 10–15% of space conditioning can be accomplished, if passive design is combined with latent heat energy storage (LHES) systems in buildings. In case of buildings using cool thermal energy storage (CTES), the energy savings could be around 45–55%. They state that using highly energy efficient TES system methods while maintaining occupancy comfort, overall energy-cost savings in buildings on long term basis, can be possible.

2.1.1 Thermal mass

Thermal mass can store thermal energy and release it later, reducing the heating or cooling load of the building system (Balaras 1996; Chen 2013). Pre-conditioning of a space can shift the peak load and reduce the peak (Braun 2003; Peng Xu 2009). Xu (2009) also mentioned that "*Pre-cooling can be very effective if the building mass is relatively heavy*". The amount of thermal mass and the thermal coupling with the thermal zone are crucial to avoid large temperature fluctuations and maintain acceptable thermal comfort in the zone (ASHRAE 2007; Chen 2013).

The type and thickness of the material covering the floor are the most important parameters in the design of radiant floor heating systems (Sattari and Farhanieh 2006). (Seo et al. 2011) also showed that the thermal transfer performance dependents on the flooring thickness and installation method. Song et al. studied the buttock responses to finishing materials over the ONDOL floor heating system in Korea. Their study revealed that the covering material with the lower contact coefficient led to more stable temperature fluctuations on the floor surface and the buttock skin. The contact coefficient was defined as $(\lambda \cdot c \cdot \rho)^{0.5}$, where λ is the thermal conductivity (W/m K), c the specific heat (J/kg K) and ρ the specific mass (kg/m^3).

Wolisz et al. (2015) showed that furniture and floor covering have distinct impact on simulated room temperatures under dynamic set temperature conditions. However, for short period temperature reductions, such as a night setback, they state that the differences are not significant. In case when the room thermal mass is used as a means of load shifting, the temperature differences between empty and furnished rooms are noticeable. Their results present 1.2 K temperature difference between an empty massive room and the same room modelled with laminate flooring and furniture inside, after 4 hours of increased set temperature.

Materials that are commonly used as floor covering include carpet, area rugs, and resilient flooring such as linoleum or vinyl flooring and materials called flooring include wood flooring, tiles and parquet (WIKIPEDIA 2016). Typically, a carpet has very low thermal conductivity (0.06 W/m°C) as compared to concrete (about 1.7 W/m^{o}C; depending on density) (ASHRAE 2009). Therefore, the carpet introduces a thermal resistance that reduces the effectiveness of concrete as thermal mass. Also, a carpet blocks the direct solar gains from charging the concrete layer under it.

2.1.2 PCM

Latent TES systems are generally used with PCM (Caliskan, Dincer, and Hepbasli 2012). Latent heat storage is met when a storage material undergoes a phase change, absorbing or releasing heat (Fernandes et al. 2012). Phase change materials (PCM) can increase the thermal capacitance of a building with minimal burden on its structure (Sharma et al. 2009). They can be used to retrofit a thermally light-weight building with more thermal mass, which acts as a thermal buffer dampening temperature fluctuations within a space (Tyagi and Buddhi 2007; Zalba et al. 2003). PCM included in the walls reduce overheating and enhance thermal comfort (Kuznik and Virgone 2009). Athienitis et al. (1997) studied the thermal performance of gypsum board impregnated with a phase change material. The experimental results showed a substantial reduction of room mean radiant temperature (about 4^{o}C) as a result of the absorption of solar gains in the PCM board and the phase change of the material. They concluded that PCM applied over a large surface area in a passive solar building can store the solar gains and improve the thermal comfort.

PCM allow the use of smaller size mechanical equipment (boilers, chillers, electric heaters etc.) and to save energy and operational costs (Dermardiros 2015; Dincer, Dost, and Li 1997; Dincer and Rosen 2001a). Among numerous applications of PCM in buildings are their use in heating and cooling (Telkes 1975), free-cooling (Fukai et al. 2000; Py, Olives, and Mauran 2001) and window-

integrated. Ismail and Henriquez (2001) studied a double glazed window with PCM filled between its glazings. They showed that the PCM filling filters out the thermal radiation and reduces the heat gain or loss because most of the energy transferred is absorbed during the phase change of the PCM. Merker et al. (2002) also studied a PCM-shading system that prevents overheating around the window area.

Dermardiros (2015) studied a thermal energy system (TES) using PCM integrated into a wall (Figure 2-1). An air channel between the PCM panels and a plenum fan on the ceiling enable the active charge and discharge of the material through air circulation.

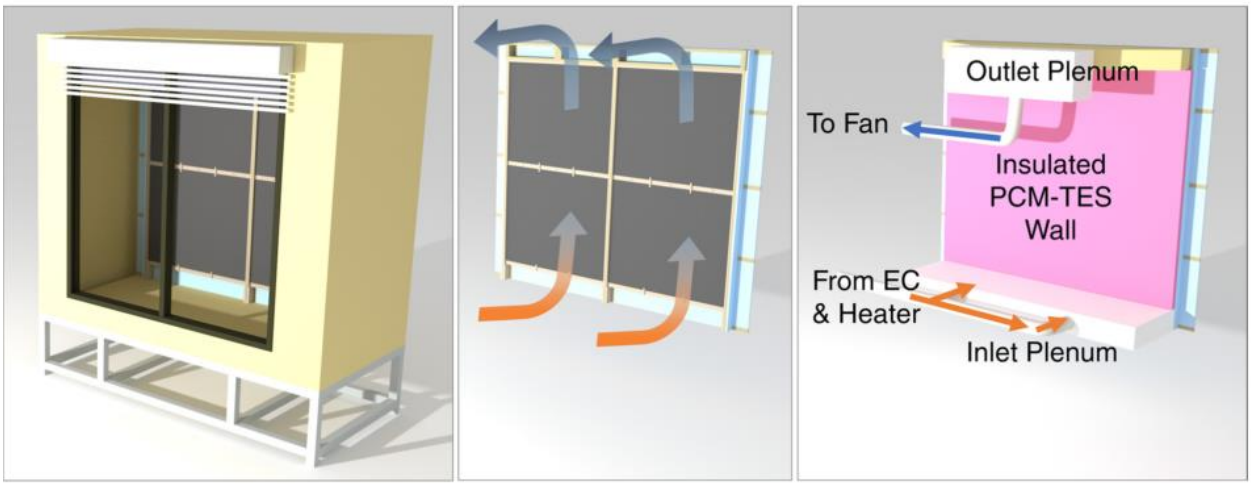

Figure 2-1: Renderings of the PCM test room showing the active PCM-TES system setup (Left) PCM test room; (Center) active PCM wall: warm air enters from the bottom inlet plenum where it exchanges heat to a pre-cooled system and exits cooled through the outlet plenum; (Right) The front of the PCM surface is insulated to isolate the system from the room; the inlet and outlet plenums are ducted (Dermardiros 2015)

He created a 30th order non-linear model for the PCM-TES with varying thermal capacitance to account for the phase change {C(T)} and used the experimental data to validate the model (Dermardiros et al. 2016). Reducing the model resolution he showed that a simplified 2nd order model can adequately predict the dynamic response of the system for thermal charging/discharging (1.7% error between the model and the experiment in the energy balance during charging and 4.1% during discharging after 6 hours). The simplified model can be used into model-based control systems to reduce and shift peak load. However, he states that there are no control algorithms implemented in this work. The two models are presented in Figure 2-2 and Figure 2-3.

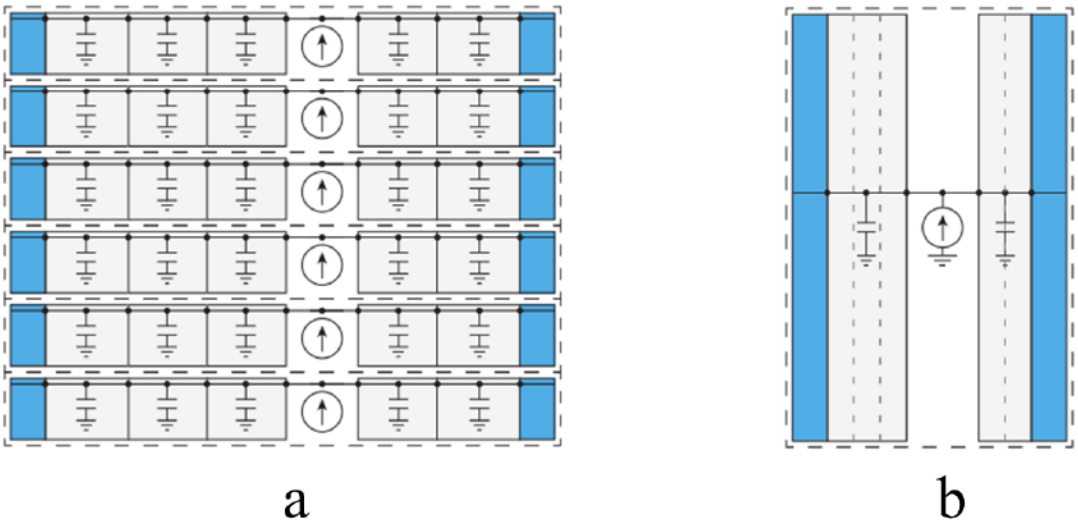

Figure 2-2:(a) 6 section, 5 capacitance per section, 30th order model (b) 1 section, 2 capacitance per section, 2nd order model (Dermardiros 2015)

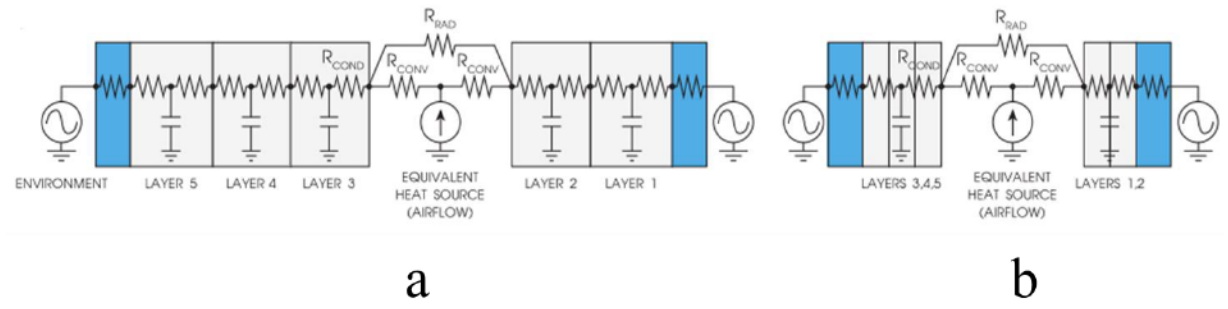

Figure 2-3: Thermal network of the (a) detailed 5-capacitance vertical section, and (b) simplified 2-capacitance section (Dermardiros 2015)

He simulated a simple office with a multi-channel PCM-TES system is incorporated to study its effect on the heating load during the morning peak. The simulation results of the simplified 2nd order non-linear PCM-TES shown to reduce the peak by at least 50% for the simulated conditions.

Dermardiros studied variations of this system, where the PCM can be integrated into the HVAC system or zone-coupled (Figure 2-4). He studied the impact of PCM-TES on heating peak during the morning start-up for varying amounts of PCM and for different HVAC activation times (Dermardiros and Athienitis 2016). Starting the HVAC system at earlier times, the peak demand was significantly reduced. The use of an active PCM-TES led to further peak reduction.

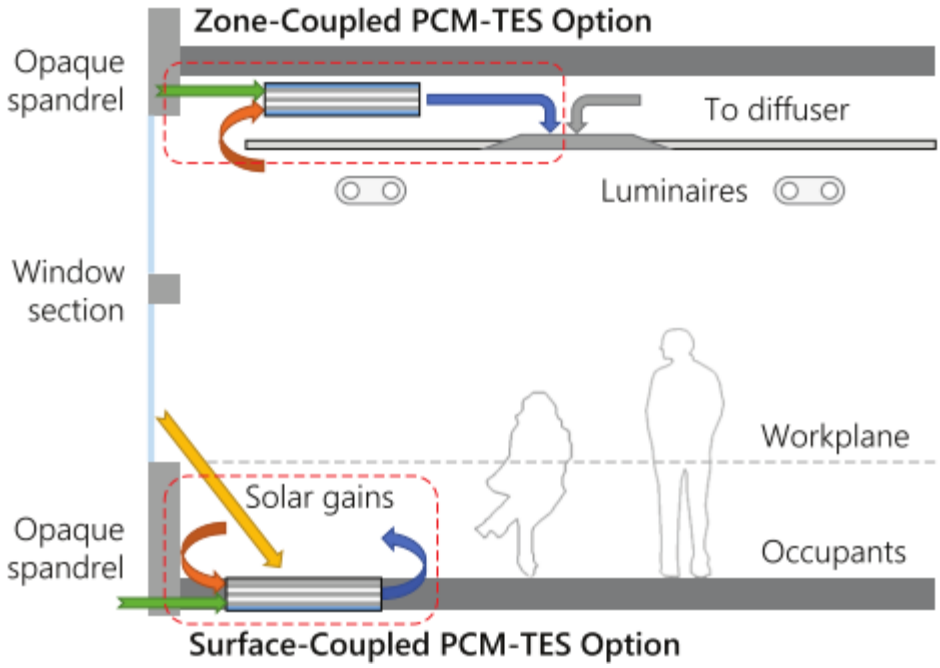

Figure 2-4: PCM-TES configurations: zone-coupled and surface-coupled (Dermardiros and Athienitis 2016)

Dermardiros also showed that increasing the number of air channels between the PCM panels (Figure 2-5), the charging and discharging durations decrease and lead to faster and more easily controllable thermal energy storage (Dermardiros and Athienitis 2015). A pre-cooled TES system can be used to reduce peak cooling demand and a pre-heated one to reduce peak heating demand.

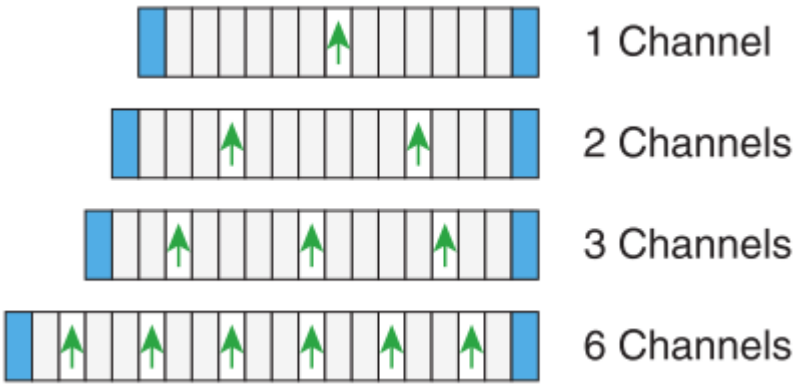

Figure 2-5: Isolated single/multiple channel systems: The blue rectangles represent insulation, the grey, a PCM panel, and the green arrow, an air channel (Dermardiros and Athienitis 2015)

The results of charging and discharging time for heating and cooling sets are presented in Figure 2-6 for 3 different systems of 1.2, 2.4 or 3.6 m. These systems were obtained by putting identical 1.2 m systems in series.

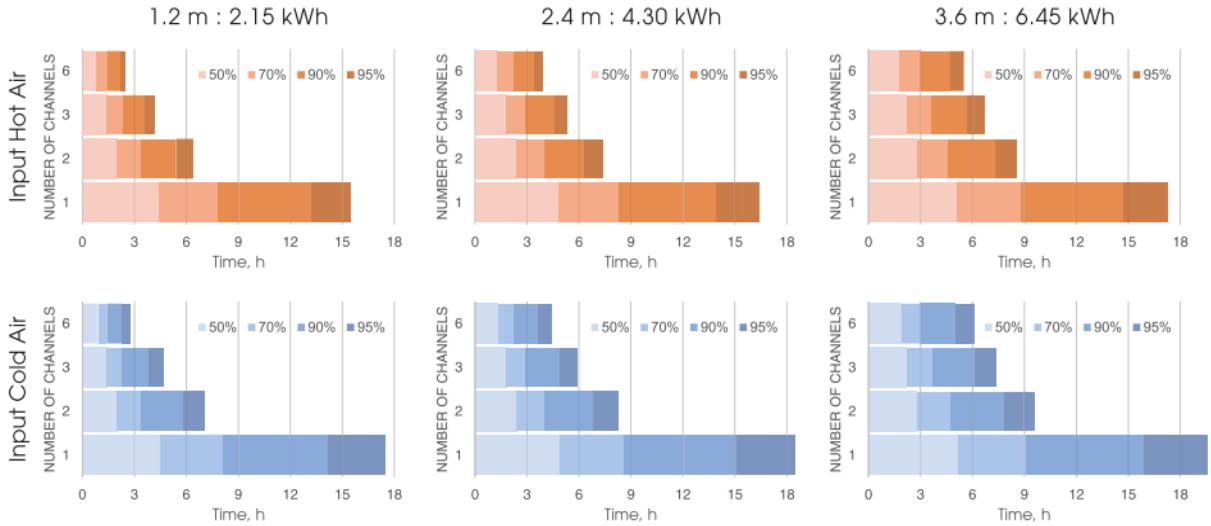

Figure 2-6: Time required to charge the TES system to a certain percentage of its steady state energy value: (top) hot air introduced in an initially cold TES system; (bottom) cold air introduced in an initially hot TES system (Dermardiros and Athienitis 2015)

2.2 Thermal comfort

According to ASHRAE Standard-55, thermal comfort is defined as "*that condition of mind which expresses satisfaction with the thermal environment and is assessed by subjective evaluation*" (ASHRAE 2010). Six main factors that affect thermal comfort are the metabolic rate (met), clothing insulation (clo), air temperature, mean radiant temperature, air speed and relative humidity. Thermal discomfort may be caused by asymmetry: radiant temperature asymmetry, temperature stratification between feet and head and fluctuating air velocities (Appleby et al. 2008; Frontczak and Wargocki 2011). For instance sitting next to a cold window may cause discomfort due to radiative heat losses.

2.2.1 Main models

There two approaches to thermal comfort evaluation: climate chamber tests and field studies. The first one, based on heat exchange processes of the body, determines steady-state thermal comfort models and the second one adaptive thermal comfort models and standards, studying thermal comfort in the real world (Taleghani et al. 2013). The first heat-balance approach developed by Fanger uses the predicted mean vote (PMV) index which incorporates the seven-point ASHRAE thermal sensation scale (-3 cold, -2 cool, -1 slightly cool, 0 neutral, +1 slightly warm, +2 warm and +3 hot) (Athienitis and O'Brien 2015; ISO7730 2005; Yang, Yan, and Lam 2014). At the energy balance calculation, when the heat leaving the human body is greater than the heat entering the human body, the thermal perception is "cold." When the opposite happens the thermal perception is "warm" or "hot" (AUTODESK 2016).

The adaptive model is based on field surveys of thermal comfort, taking into consideration the real environment where users live (La Gennusa et al. 2010; Nicol and Humphreys 2002). This approach models thermal comfort taking into account factors such as the thermal history, culture,

psychological factors and interaction with the environment (Athienitis and O'Brien 2015; La Gennusa et al. 2010; I and Dear 1998). It relies on occupants' response according to their thermal experience. For example, they will tolerate higher indoor temperatures when ambient temperature is higher (Appleby et al. 2008).

Yang, Yan and Lam (2014) concluded that PMV models work well in air-conditioned buildings but not in naturally ventilated places, where occupants are able to interact with their surroundings to adapt and be more comfortable. They also state that adaptive comfort models could lead to significant energy savings, because they have a wider range of comfort temperature.

2.2.2 Thermal comfort and productivity

Thermal comfort affects the performance and enables better work productivity (Appleby et al. 2008; Frontczak and Wargocki 2011; Kosonen and Tan 2004a, 2004b; Roelofsen 2015; Simmonds 1993; Yang et al. 2014). Kosonen and Tan (2004b) studied the effect of perceived indoor air quality on productivity loss. They stated that productivity could improve by increasing outdoor airflow rate, reducing emissions and improving ventilation efficiency. However, they claim that the usage of minimum airflow rate design principle leads to 5–13% productivity loss. They suggest that displacement ventilation, compared to traditional mixing system may improve indoor air quality in a way that increases productivity.

Simmonds (1993) studied thermal comfort of indoor environment according to Fanger's PMV index. The results show that low air changes per hour in the ventilation system can obtain higher comfort levels in the workspace. He also showed that a control strategy for comfort control is simpler and can be easily optimized and save energy. He states that the necessary energy to

maintain the desired conditions is less when the operation is based on comfort conditions and not temperatures.

Roelofsen (2015) proposes a computer model for the assessment of employee performance loss as a function of thermal discomfort or degree of heat stress. His model uses validated mathematical models (human thermophysiological model and Wet Bulb Globe Temperature Index model) and various mathematical performance (loss) models, based on comfort and heat stress indices. The objective is to present design tool for a variety of disciplines that are involved in the design of the indoor environment of buildings.

The cost of productivity translated into employee's salaries may surpass the costs of operation and maintenance of the building. A study of Woods (1989) has shown that the salaries of workers in the US office buildings have exceeded the cost of utilities, maintenance, annualized construction and rental by a factor of 100. A similar study in Norway (J.E. Skåret 1992) estimated that increased productivity caused by an enhanced indoor climate is at least 10–100 times greater than the operational and maintenance costs.

2.3 Thermal and daylight control in buildings

The thermal comfort is influenced by the control strategy of temperature, humidity and air distribution in the room. Nevertheless, the type of control has an impact not only on occupant comfort, but on energy consumption as well (Appleby et al. 2008). The combination of the control system and the thermal dynamics of the building is necessary for the regulation of building thermal variables (Buonomano et al. 2014; Prívara et al. 2013). Therefore, building automation and control systems provide great opportunities for improving building energy efficiency and thermal comfort (Buonomano et al. 2014; Li and Wen 2014). Among other control variables, two that are widely

used to enhance occupancy comfort are the indoor temperature profile and the position of the shades.

2.3.1 Room setpoint profile control

A common practice, during the heating season in Canada, is to lower the temperature setpoint during the night to save energy (Manning et al. 2007; Moon and Han 2011). This setpoint change can either be performed manually or using a programmable thermostat. Although programmable thermostats are installed in houses to save energy, their misuse can result in an increased energy consumption over manually operated cases. Moreover, occupants complain about the complexity of the modern thermostats and the discomfort due to their wrong use (Peffer et al. 2011).

A shortcoming of a night setback strategy is that the return to the daytime setpoint, often implemented as a step change, results in a sudden increase in power demand (Candanedo et al. 2015). Date et al. (2015) studied the use of ramp functions instead of the conventional night time setback and succeeded 25% reduction in peak power demand. Candanedo et al. (2015) used a simple curve for near-optimal transition between constant temperature setpoints and reduced the peak demand (about 8%) compared to the case of linear ramps. Braun developed methods to determine demand-limiting setpoint trajectories in buildings using short-term measurements (Lee and Braun 2008). Their results show peak load reductions of 22–32W/m^2 (2–3W/ft^2) of peak cooling load (Leea and Braun 2008).

Large commercial buildings usually have thermal mass in the form of exposed concrete or tiled concrete floors. Anticipatory controls are beneficial since they address the delay between the supplied heating/cooling and its effect on the room temperature. Typically, feedback controllers, such as proportional-integral (PI) controllers, are used in these buildings. These approaches fail to

efficiently control slow responding dynamic processes (Afram and Janabi-Sharifi 2014). The time lag of the temperature response and the associated occupant discomfort are affected by many parameters, including the amount of effective thermal mass and its thermal coupling with the occupied space (ASHRAE 2007; Chen 2013).

2.3.2 Control of daylight with motorized shades

There are many studies about the automatic control of motorized shades showing that their efficient operation may contribute to peak load reduction (Shen and Tzempelikos 2012; Zhang and Lam 2011) and uniform daylight distribution in the room (Athienitis and Tzempelikos 2002; Reinhart, Mardaljevic, and Rogers 2013; Wienold 2007).

Shen and Tzempelikos (2012) studied the balance between daylighting and energy consumption through control of incident direct solar radiation for each facade in private office spaces. Their results show that windows occupying 30–50% of the façade lead to lower total energy consumption for most cases with automated shading. They used useful daylight illuminances between 500 and 1000 lux (UDI500-1000), because at this range there is enough natural light to offset electric lighting and also reduce the risk of glare. They found that this index can be maximized for specific WWR and it depends on the glazing and shading properties for each orientation.

Zhang and Lam (2011) studied the effect of two shading control algorithms, an ideal and an implementable, on office building thermal and lighting loads over a year's period through energy simulation in four different climatic contexts in USA. The implementable algorithm was used to simulate the real world cases, where a lot of information is not always available. They used EnergyPlus to calculate annual thermal and lighting loads and Building Control Virtual Test Bed

(BCVTB) to implement the control algorithm. The results show a maximum reduction of 6.7% in building total loads by the internal shading device. They also concluded that both algorithms result in net reduction in building total loads (heating, cooling and lighting), without daylighting control. The performance difference between the two algorithms is significant in this case. When daylighting control is activated, both algorithms result in increase of total load.

Wienold (2007) presented a method of evaluation of different control strategties (manual and automated) for shading devices. He used RADIANCE and DAYSIM to investigate energy, daylight and visual comfort. His results show that the commonly used manual control strategies hardly activate the shading in summer. From the automated strategies, the cut-off approach offers a good compromise between energy and comfort, especially in summer. This approach calculates the maximum open position of the shades to block entirely the direct solar radiation.

Athienitis and Tzempelikos (2002) presented a methodology of control of daylight room illuminance distribution and light dimming for a room, with motorized shades. The test room has a double-glazed window with motorized highly reflective blinds installed between the two glazings (Figure 2-7). They found energy savings from the daylighting and dimming control for the particular system that exceed 75% for overcast days and 90% for clear days. An important parameter for on-line control is the blind tilt angle that minimizes glare and at the same time allows the maximum possible amount of daylight into the room.

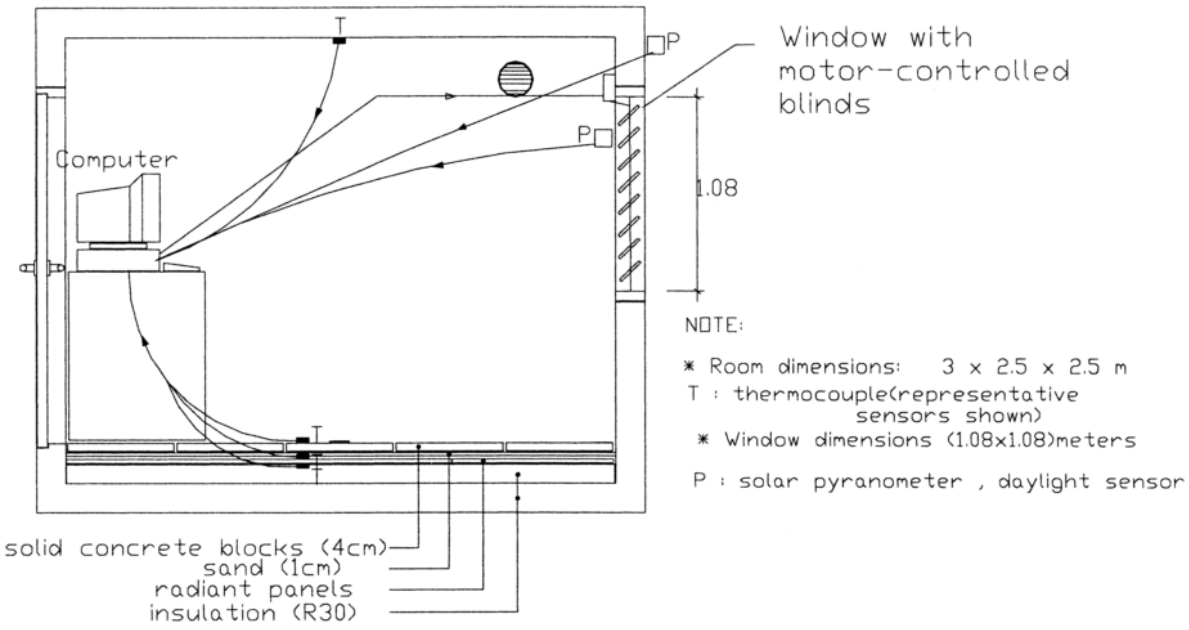

Figure 2-7. Schematic of the test room (Athienitis and Tzempelikos 2002)

2.3.3 Occupant behavior

Office occupants interact with many building components, including windows, window blinds, and lighting, and this introduces a great uncertainty over the performance of the building (Gunay and O'Brien 2016). They also introduce extra plug loads from small appliances that are not included in the design stage (Athienitis and O'Brien 2015). If the occupant comfort is not achieved in a building, occupants may react in unexpected ways and adapt themselves to the environment, by adjusting thermostats or opening windows and shades. This may increase the energy consumption of the building (Athienitis and O'Brien 2015). The occupant behavior can affect the energy performance of offices by a factor of two or more (Haldi and Robinson 2011; Reinhart 2004).

Villafana and Federspiel (2003) studied a user interface for energy and maintenance systems in commercial buildings. They suggested that building occupants should also be considered users of energy and maintenance systems. They state that they need more data to define the effect of the user interface on the frequency of service request. However, they conclude that this interface could reduce the labor regarding phone calls service requests, improve the quality of data in a maintenance database and enhance thermal comfort.

Lehrer and Vasudev (2010) studied methods of visualizing information to improve building performance. Their survey showed an agreement for better methods of communicating with building occupants. They mention that many users prefer data exported from Building Management Systems (BMSs), and use spreadsheet programs for monitoring and analysis. However, they state that the level of detail of information depends on the type of user (occupants, engineers, building operators).

2.4 Model-based predictive control (MPC)

MPC uses weather forecast and occupancy patterns in a mathematical model of the system, which is then used to choose the best action for the near future (Athienitis and O'Brien 2015). The basic structure of MPC is presented in Figure 2-8:

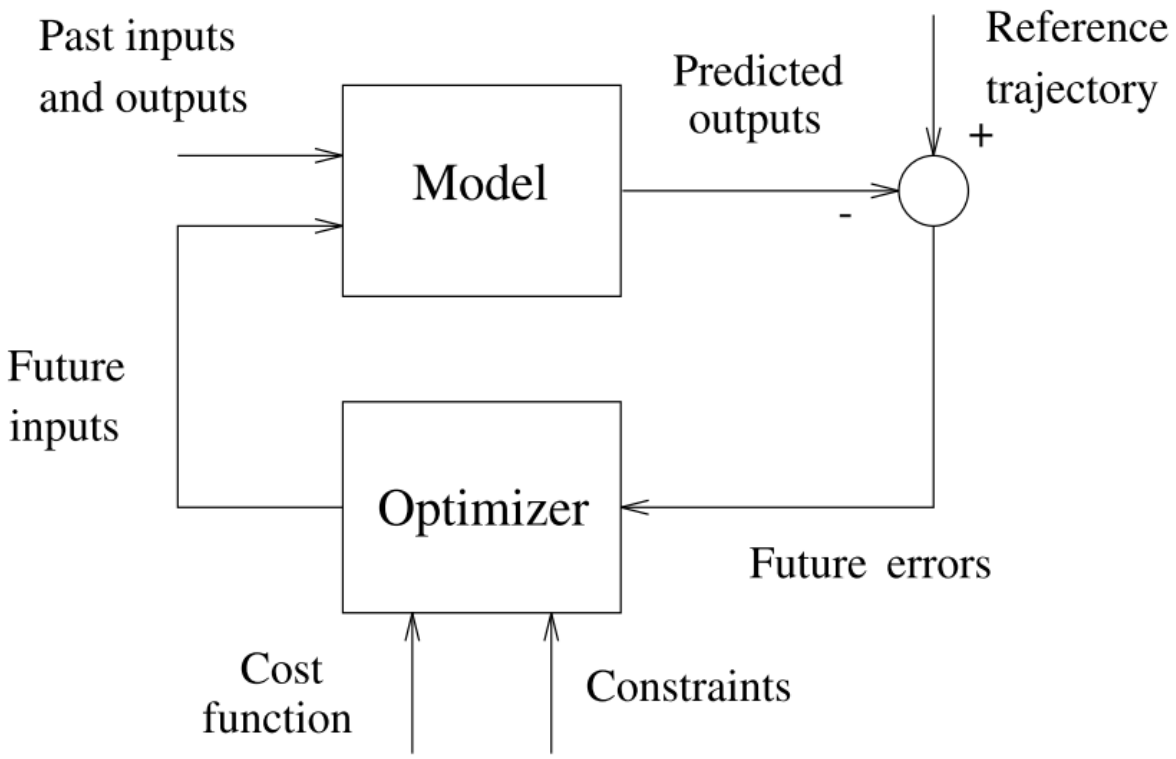

Figure 2-8: Basic structure of MPC (Camacho and Bordons 2003)

Camacho and Bordons (2003) give a description of the above figure in their book: "*A model is used to predict the future plant outputs, based on past and current values and on the proposed optimal future control actions. These actions are calculated by the optimizer taking into account the cost function (where the future tracking error is considered) as well as the constraints*." They state that three types of model that are used in MPC: the Truncated Impulse Response Model, the State Space Model and the Transfer Function Model. The first one measures of the output when the process is excited with an impulse input and is very common in the industry. In the State Space Model the development of the controller is simple even for a case with many variables. This model is more popular in the academic research community. The Transfer Function, also used in

academia, requires less parameters. However, the derivation of the controller is more difficult in this case.

The difference of MPC and a conventional control in a building can be seen in the following figure:

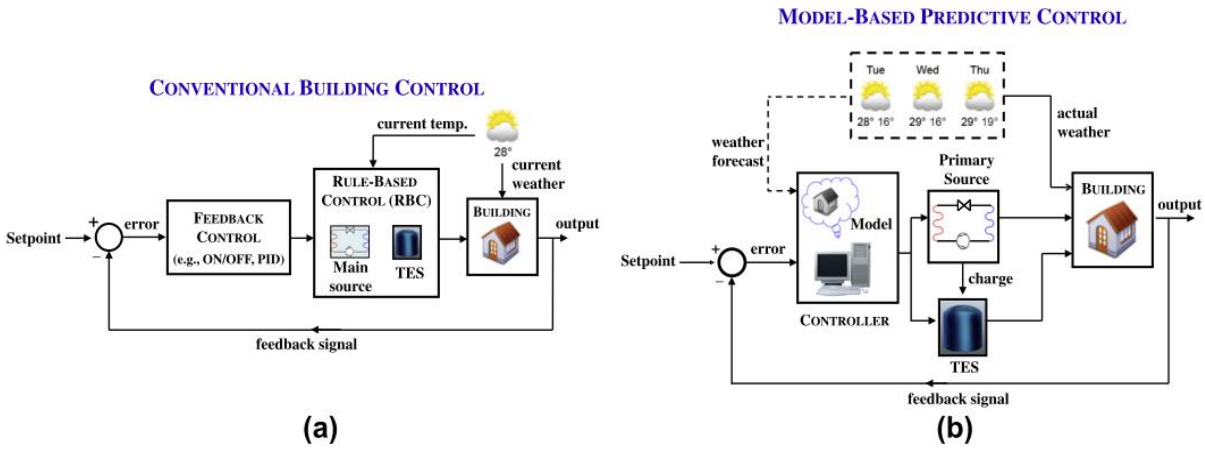

Figure 2-9: Conventional control compared to MPC (J.A. Candanedo, Dehkordi, and Stylianou 2013)

The main difference is that MPC takes into account the future disturbances. In MPC decisions are taken with anticipation considering the inertia of the system (Candanedo et al. 2011). Candanedo gives an example about that comparing the controlling of the temperature of a house with a larger thermal mass to steering an ocean liner. In both cases, actions need to be taken in advance considering the inertia of the system.

Camacho and Bordons (2003) give another example drawing a parallel between the MPC strategy and driving a car. The driver knows the preferred route (reference trajectory) for a finite time in the future (control horizon). He decides which control action to take (accelerate, brake, steer) to follow the desired trajectory, considering the characteristics of the car. He applies part of the control actions he chooses and reevaluates the situation. The procedure moves forward to the next moment when a control decision is taken for the following receding horizon. Driving a car with a

PID control strategy would be equivalent to driving the car just using the mirror, as the control actions are taken based on past errors (Figure 2-10).

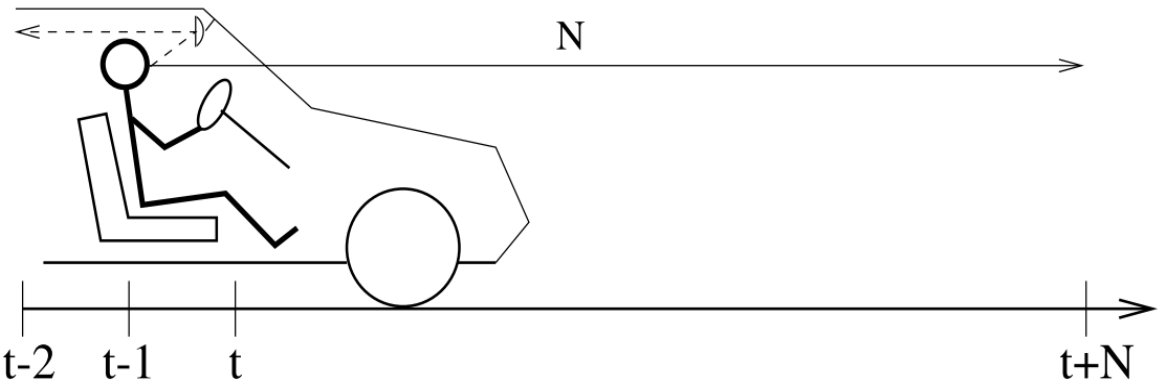

Figure 2-10: MPC analogy (Camacho and Bordons 2003)

Some preliminary steps may detect the opportunities in which knowledge of future weather and occupancy inputs may be helpful (Athienitis and O'Brien 2015). Typical information that can be gathered includes the characteristics of the energy carriers that are used, the energy storage capabilities of the building, the control variables and weather and occupancy profiles.

2.4.1 MPC and thermal mass

The most common control methods in building applications now are on/off and proportional-integral-derivative (PID) controls, which are unable to use appropriately the building dynamics and often leading to wrong performance (Ascione et al. 2016). Ideally, in order to program a thermostat for example, the expected thermal response of the building (which depends on factors such as temperature, occupancy, etc.) should be calculated with some anticipation. In this context, model-based predictive control (MPC) is a promising approach that provides an alternative to feedback-only control strategies.

MPC is suitable for slow-responding systems (e.g. thermally massive buildings) (Hu and Karava 2014; Sakellariou 2011). Energy storage capacity −such as that provided by a thermal energy storage (TES) device or a significant thermal mass−, enhances the potential of MPC, since it allows planning the capture and release of energy as a function of the expected power load and energy cost profiles (J.A. Candanedo et al. 2013). MPC creates opportunities of taking advantage of thermal storage capacities (Prívara et al. 2013). Characterizing the system's dynamic response can optimize its performance (Sakellariou 2011). An MPC algorithm can determine the optimal setpoint trajectory for the room temperature that can be close to the charging and discharging rate of the thermal mass in order to reduce and shift the power peak.

2.4.2 Model development

The model used in MPC may be developed in simulation programs such as TRNSYS and EnergyPlus, or derived from simpler physics-based or data driven models that produce sufficiently accurate and faster results (Afram and Janabi-Sharifi 2014). Many studies have investigated the implementation of MPC using building performance simulation software (Corbin, Henze, and May-Ostendorp 2012; Kummert, Leduc, and Moreau 2011; May-Ostendorp et al. 2011; Michailidis et al. 2015; Sakellariou 2011; Sturzenegger et al. 2016) and others using simplified models (Moroşan et al. 2010; Oldewurtel et al. 2012; Široky et al. 2011). However, simpler models present advantages for model based control applications, since the reduced number of parameters to calibrate makes them more robust (J. A. Candanedo, Dehkordi, and Lopez 2013; Dermardiros 2015).

Prívara et al. (2013) state that the dynamic models are of crucial importance in predictive control. They mention that the modeling is the most costly part of the automation process and consumes the most time. They describe some types of building modeling techniques that can be used in

predictive control and these are: Sub space methods (4SID), Prediction error methods (PEM), MPC relevant identification (MRI), Deterministic semi – physical modeling (DSPM) and Probabilistic semi – physical modeling (PSPM).

The sub space methods belong to the black-box identification algorithms and use a state space form for the model. Their main advantage is their ability to handle large volume of data. The most commonly used statistical identification techniques are the prediction error methods (PEM). They optimize the parameters of a pre-defined model structure to minimize one-step ahead prediction error. Autoregressive moving average with external input (ARMAX) model structures are usually preferred. MPC relevant identification (MRI) methods minimize multi-step ahead prediction errors. The horizon for error minimization is proportionate to the prediction horizon of the predictive controller. Deterministic semi – physical modeling (DSPM) is a gray-box modeling approach, using resistance capacitance (RC) network to describe the dynamics of the system. Finally, probabilistic semi – physical modeling (PSPM) describe the model using stochastic differential equations.

2.4.3 MPC applications in buildings

There are different teams studying MPC. Two of the leading projects of predictive control in buildings include the work of OptiControl team in Zurich and the University of California, Merced.

Gyalistras and OptiControl team (Oldewurtel et al. 2010, 2012) has investigated the effect of MPC and weather predictions on the energy efficiency in Integrated Room Automation (IRA) while maintaining comfort conditions for the occupants (Figure 2-11). They control the HVAC system, the position of the blinds and the electric lighting. These are control variables for typical office

buildings. The control setup is shown in figure x. They used a bilinear building model with a sampling time of one hour:

$$x_{k+1} = Ax_k + Bu_k + B_\upsilon \upsilon_k + \sum_{i=1}^{m}\left[\left(B_{\upsilon u,i}\upsilon_k + B_{xu,i}x_k\right)u_i\right] \tag{2.1}$$

where

x_k: state representing the temperatures in the room, wall, floor, and ceiling

u_k: control inputs (HVAC, blind positioning and lighting)

υ_k: disturbance (weather and occupancy input) at time step k

m: number of different control inputs available

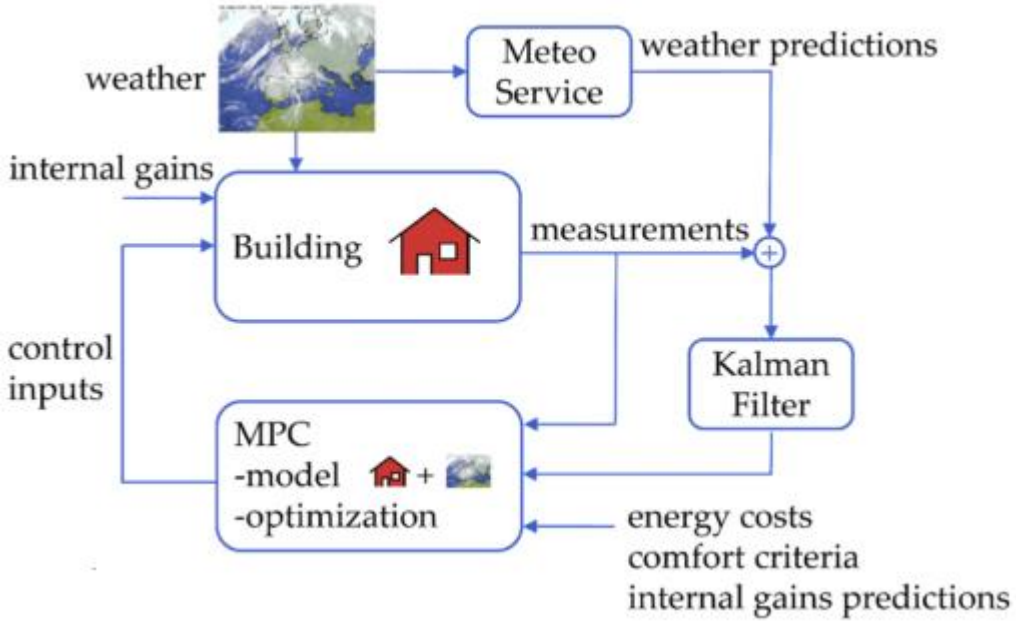

Figure 2-11: Overview of control setup (Oldewurtel et al. 2010)

The model validation was made comparing its dynamic response of the building model to simulations with TRNSYS. The numerical weather prediction model COSMO-7 operated by MeteoSwiss was used for weather predictions. COSMO-7 provides hourly predictions for a horizon of three days with an update cycle of 12 hours. The standard linear Kalman filter was used to correct the weather predictions for location-specific effects at the building site and also to consider the newest on-site weather measurements in between the 12-hourly updates.

Their results show that MPC along with real weather predictions outperforms non-predictive Rule-based Control (RBC). Also, MPC improves the thermal comfort, because it decreases the diurnal temperature fluctuations in the room. A sensitivity analysis showed that the controller is robust to model parameter mismatch. They mention that MPC is promising approach to building climate control and they state the high importance of good quality weather predictions.

A more recent study of OptiControl team (Sturzenegger et al. 2016) present measured data of a fully occupied, well instrumented typical Swiss office building, where MPC was applied. The MPC algorithm was implemented in Matlab and the communication between control levels was accomplished through a BACnet. During the experiments the switching back to the initial control strategy was possible all the times since the building was occupied. The MPC algorithm included the following steps:

1. Reading of new measurements
2. Kalman filtering
3. Preparation of predictions
4. Preprocessing of costs and constraints
5. Computing of new control inputs
6. Postprocessing of results & writing of setpoints and operating modes

The experimental results showed that MPC respected the thermal comfort constraints in the demonstrator building. Also, they used co-simulation of EnergyPlus and Matlab through Building

Controls Virtual Test Bed (BCVTB) middleware, for whole-year simulations to compare the MPC performance against the originally implemented standard rule-based controller. The simulation results indicate significant energy savings potential compared to industry standard control when MPC was applied. They state the need for model effort to be negligible in order for MPC as a product to be successful on the market.

Ma et al. (2012) study the main ingredients of a predictive control framework necessary for an actual implementation. They describe the role of active thermal storage in a predictive control scheme, showing a fundamental tradeoff between savings, losses, and uncertainty through a thermal mass model. At this study they also demonstrate that MPC may include and reproduce strategies of well-known commercial solutions for energy savings, such as demand response, economizer-mode, and precooling/preheating. They use resistance capacitance networks for the model of the systems and they separate the control to high (energy conversion system) and low (energy distribution system) level. The MPC architecture they developed is presented in Figure 2-12:

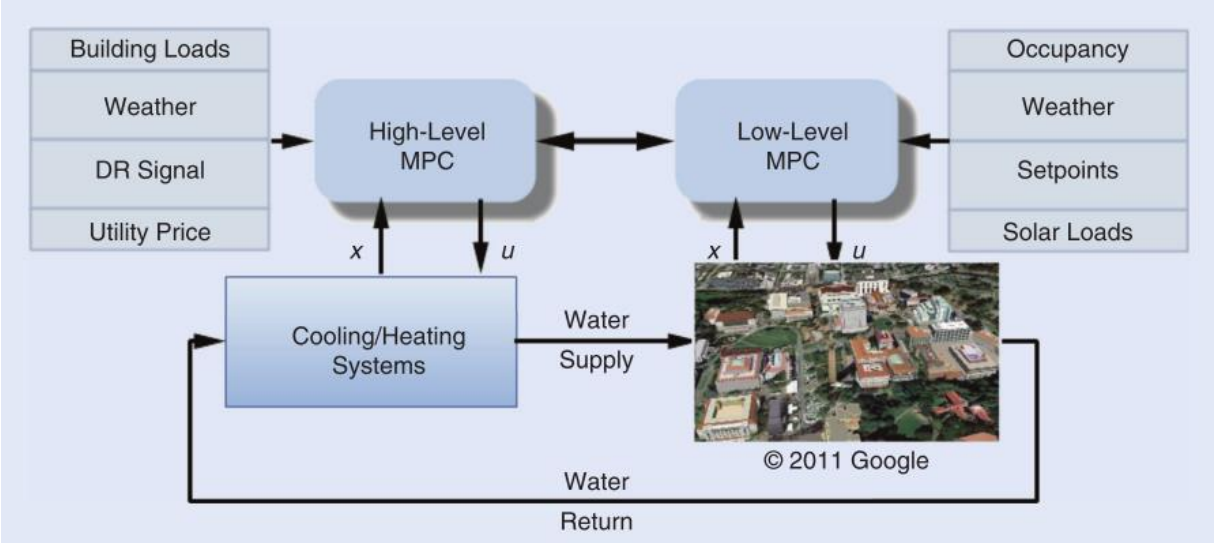

Figure 2-12: Hierarchical model predictive control (MPC) structure for a building control system. A high-level MPC (HMPC) is deployed to optimize the operation and schedule the cooling and heating systems with active thermal storage. A low-level MPC (LMPC) controls the variable air volume boxes and the air handling units by considering thermal comfort constraints of the occupants. At both levels a variety of predictions can be included in the models and in the cost function to control the system in an efficient and effective way. These predictions include building loads, load shedding signals from the power grid, utility prices, weather, occupancy, and solar loads. (Ma et al. 2012)

They conclude that an MPC scheme solved the energy conversion and distribution problems. The control scheme is effective according to simulations and experimental results. Finally, they mention some considerations regarding the design (stability and feasibility, prediction uncertainty) and the implementation (convergence to suboptimal solutions, computational complexity, and cost of additional digital sensors). The results show that the MPC does not perform well when the probability of the correct prediction decreases. Actually, MPC is unable to keep the zone

temperature within the comfort constraints due to prediction error. Another issue is the computational complexity which increases, in case of centralized MPC, when the building model becomes more complex. The solutions they suggest for that are distributed MPC (local MPC on subsystems) and offline MPC using lookup tables and pre-calculated control actions for a set of states and disturbances.

2.5 Conclusion and research needs

Thermal mass is an essential element of buildings. If it is used properly as dispatchable thermal energy storage it may significantly reduce the peak load and the temperature fluctuations in the room. The controls that are currently used in buildings are feedback controllers and are unable to efficiently control slow responding dynamic processes. A promising approach is model-based predictive control (MPC), which takes into account the thermal inertia of the space. MPC combines two mechanisms: the active storage and the optimization. However, for MPC to be integrated in commercial Building Automation and Control systems the effort to develop a model and the prediction error should be minimized.

A first step may include offline MPC, with lookup tables. Pre- calculated actions can be derived from the study of different system, starting from room level to a whole building level. The varying time constant of these systems, or in other words the different thermal inertia, shows the potentials of thermal energy storage in each case. Also, the prediction uncertainty may be decreased, using local weather forecasts from weather stations installed in the buildings or combining data from many weather stations and compare their accuracy. Based on the literature review there is a need to develop models of low resolution that can be readily calibrated for predictive control.

The following two chapters present predictive control strategies for 2 case studies with different thermal mass configurations. Chapter 3 describes the first case study of a perimeter office zone with radiant floor heating and a chiller beam. It investigates the effect on thermal mass in peak load and temperature fluctuations in the room, through predictive control strategies. The thermal mass in this case is concrete. Chapter 4 describes a test room with phase change materials integrated into a wall. It includes numerical and experimental analysis of a predictive control algorithm which calculates the best setpoint profile out of 10 predefined scenarios that minimizes a cost function.

3 The importance of thermal mass in predictive control

3.1 Case study: a perimeter zone with radiant floor heating and a chilled beam

This chapter presents a simulation study of predictive control strategies to reduce and shift peak load in a zone of a perimeter office with floor heating, convective cooling and various floor configurations, particularly carpet cover, while maintaining acceptable comfort conditions. A representative case study is considered where a building automation system controls the floor heating, convective cooling and shades. For the specific case study, the window-to-wall ratio is 75%, resulting in high solar gains. These solar gains are useful in winter but in summer they need to be reduced by controlling the shades to reduce total cooling load. The simulations results show that an exposed concrete floor (no carpet) can lead to significantly lower peak (about 40% in cooling and 45% in heating) in the auxiliary cooling/ heating as compared to a carpeted floor. A detailed model investigates the impact of model resolution in peak load reduction calculation. The comparison between the simplified and the detailed models show that the separation of the heat transfer coefficients into convective and radiative part, has a significant effect on the peak (16% in cooling and 5% in heating) and total load (12% in cooling and 16% in heating). On the other hand, increasing the number of control volumes in the floor has a low impact on the results (less than 3%). Finally, a parametric analysis on different window-to-wall ratio (WWR) and various materials commonly used on the floor surface in buildings showed that higher WWR results in higher loads and as the thermal conductivity decreases the peak and total load increase.

3.2 Methodology and model for use in predictive control

The method used to simulate the room is the explicit Finite Difference Method (FDM) (Athienitis A.K. and Santamouris M. 2002) with a thermal network of the zone. The floor is initially

discretized into two control volumes and the wall and ceiling room-side layer (gypsum board) is represented by one control volume. Initially, combined convective and radiative heat transfer coefficients, constant with temperature are used. A detailed model follows that calculates the heat transfer coefficients separately to show the difference between the accuracy of the two models and also studies the effect of more control volumes for the thermal mass.

The auxiliary heating is applied, with proportional control, at the air node when convective heating/cooling is simulated and at the floor lower control volume of concrete layer in case of radiant floor heating. The side walls of the office are considered to connect to similar offices and thus to be adiabatic.

The building is located in Laval, Quebec, Canada (Latitude 45 N) and the considered office is located on the front façade that is oriented 50 degrees west of south. Its floor area is 15.25 m^2 and its height 2.51 m. The window-to-wall ratio (WWR) is 75%, which results in high solar gains.

The internal wall layers are gypsum board and insulation and have a total thermal resistance of 5 $^oC*m^2/W$. The floor is comprised of a 2 cm layer of carpet, a layer of concrete and a layer of insulation. Its total thermal resistance varies from 1.75 °C $*m^2/W$ to 1.3 °C $*m^2/W$, depending on the thickness of the concrete and the presence of the carpet. Material properties are presented in Table 3-1.

The uncarpeted concrete floor can store 1.136 kWh per ^oC. When the floor is covered with a carpet, an extra resistance (0.333 °C $*m^2/W$) is added in series, reducing the charging of the floor thermal mass by solar gains and also reducing the heat transfer from the concrete to the room.

Equations 3.1 – 3.4 present the explicit FDM equations that were used to solve the thermal network model. Figure 3-1 shows the thermal network of the room in radiant floor heating mode, with a

carpeted floor. The auxiliary heat is applied at node 4 (lower control volume of the concrete). When convective heating/cooling is simulated, the auxiliary heat is applied at node 1. 70% of the transmitted solar radiation is assumed to be absorbed on the floor and 30% on the other interior surfaces. Later in this paper, the resolution of the model is increased, discretizing the floor into more control volumes and separating convective and radiative heat transfer coefficients.

Table 3-1. Material properties

	ρ (kg/m^3)	c_p (J/kg^{o}C)	k (W/m^{o}C)
Gypsum board	800	750	0.16
Concrete floor	2200	800	1.7
Tiles	2000	630	1.5
Parquet	800	2000	0.2
Carpet	800	750	0.06

Explicit FDM equations for zone. Energy balance equations (1) for auxiliary heat (proportional control), (2) nodes with thermal capacitance, (3) nodes without thermal capacitance and (4) time step condition for numerical stability in explicit finite difference form; p indicates the present time point and p+1 the next time point

$$q_{aux}^{p+1} = k_p (T_{sp}^p - T_1^p) \tag{3.1}$$

$$T_i^{p+1} = \frac{\Delta t}{C_i}[q_i^p + \sum_j U_{ij}(T_j^p - T_i^p)] + T_i^p \tag{3.2}$$

$$T_i^{p+1} = \frac{q_i^p + \sum_{j \neq i} U_{ij} T_j^p}{\sum_{j \neq i} U_{ij}} \tag{3.3}$$

$$\Delta t \leq \left\lfloor \frac{C_i}{\sum_j U_{ij}} \right\rfloor \tag{3.4}$$

where

q_i: heat source at node i

k_p: proportional gain

T_{sp}: Room air temperature setpoint

T_i: Temperature at node i

U_{ij}: Thermal conductance between nodes i and j

C_i: Thermal capacitance of node i

Δt: Simulation time step

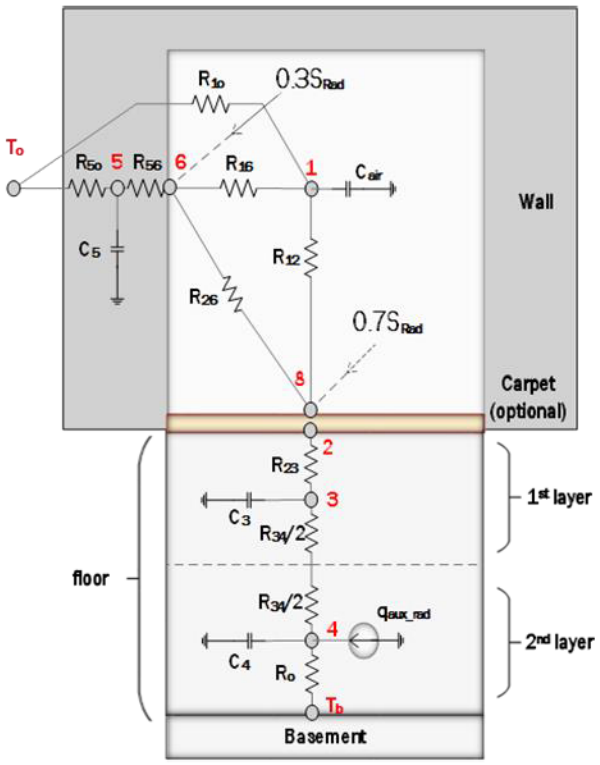

Figure 3-1: Room thermal network

3.3 Simulations

Simulations were performed for an exposed concrete and a carpeted concrete floor in cooling (convective) and heating (convective and radiant floor) mode. For both cases, clear sunny day profiles are used: a hot sunny day in the summer and a cold sunny day in the winter.

Initially, the motorized shades are assumed to be fully open, in order to study the potential effect of the carpet on peak and total load and also on temperature swings in the room. The response of the zone is tested for different setpoint profiles (constant, night setback, ramp function) of room air temperature. The setpoint profiles are presented in Figure 3-4 for cooling mode. In heating mode instead of a night setup, there is a night setback, reducing the setpoint from 22 °C during the day to 20 °C during the night.

Different floor configurations are studied to present the potential of thermal energy storage in the room. Simulation studies include carpeted and uncarpeted floor and a comparison of two concrete thicknesses, 10 cm and 15.24 cm. which represents the existing case. Finally, a control strategy is recommended for the existing configuration (carpeted floor, 15.24 cm concrete) of the office. This strategy combines the previous results of the setpoint profile with a more optimal control of the motorized shades for cooling mode, when high solar gains need to be blocked.

Before applying any shading control, the light sensor on the ceiling is correlated with manual measurements of daylight taken at various points on the work plane and the inner side of the window. The current control strategy for the shades in the room has the ceiling sensor setpoint set to 600lx. This results in almost 1800lx on the work plane. The recommended light level for an office is 400lx (ANSI/ASHRAE 2007). The proposed control action uses a three hour ramp for the room temperature setpoint and lowers the motorized shades when the daylight level is more than 500lx on the work plane to satisfy daylight needs while limiting excessive solar gains. All of these parameters (carpet, floor thickness, Tsp profile, and shades) affect the peak load and the total load, as well as the thermal comfort of the occupants. Table 3-2 summarizes the different simulations parameters and the key design and control variables.

Table 3-2: Main design and control variables

Qaux	convective cooling, convective and radiant floor heating
Tsp profile	fixed, night setback, 1h ramp, 2h ramp, 3h ramp
Control Variables	Tsp profile, motorized blinds position
Floor Surface	carpeted, exposed
Floor Thickness	10 cm, 15.24 cm

A parametric analysis was performed showing the effect of different WWR values and other materials commonly used as floor covering on peak and total load. Also, simulations include a more detailed model of the room with increasing number of control volumes of the floor and separating the film heat transfer coefficients into convective and radiative part.

3.4 Model Validation

Simulated and experimental data of room air temperature were compared to validate the model. The setup used for this comparison was: room setpoint at 22 °C constant and shades fully open. The outdoor temperature fluctuates form 22 to 32 °C. The outdoor temperature and the solar radiation as measured on the south-west façade for this day are presented in Figure 3-2. The model is the simplified one, with combined heat transfer coefficients and two control volumes in the floor. The results presented in Figure 3-3 show that there is good agreement between the model and the measurements. The maximum difference between the measured and the simulated data is 1.18 °C. The temperature in the test room was measured with a digital temperature sensor with ±0.2 °C accuracy.

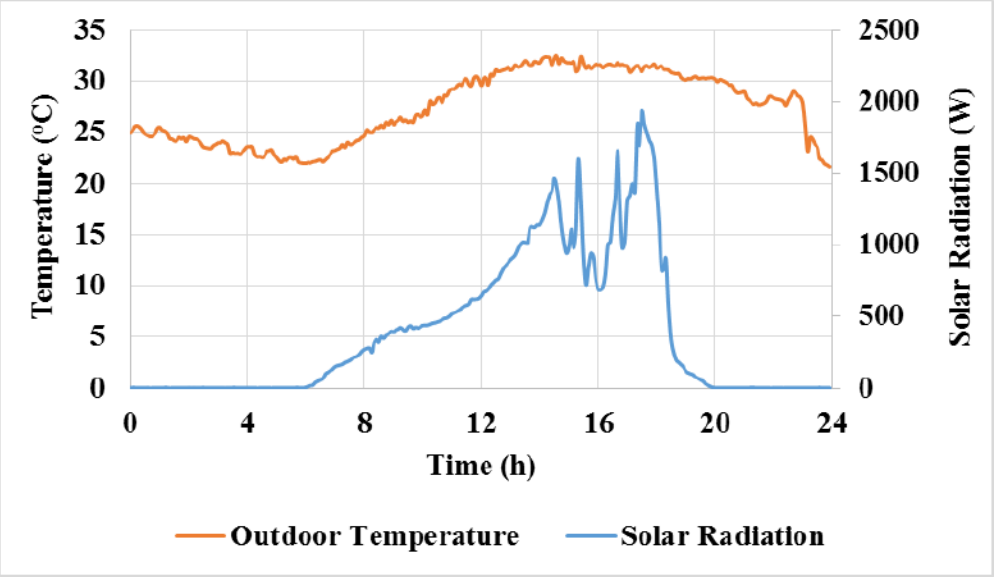

Figure 3-2: Measured outdoor temperature and solar radiation

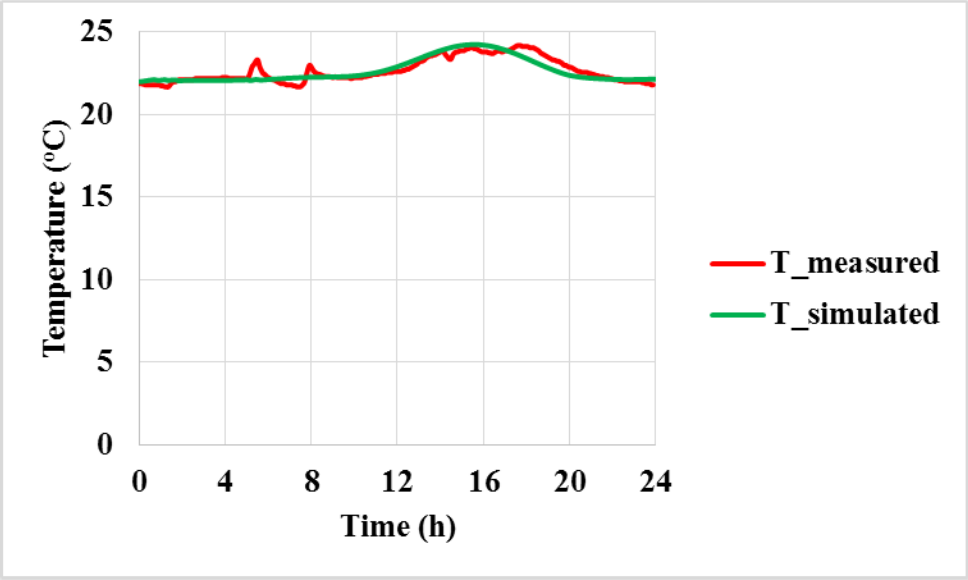

Figure 3-3: Room air temperature, Tsp=22 °C (constant), shades fully open

3.5 Results and discussion

Results below present the carpet effect on peak load and temperature swings in the office, shifting of peak load, the thermal mass thickness effect and a shading control for the cooling mode.

Furthermore, a comparative analysis shows the effect of different floor coverings and WWR on peak load. These materials are commonly used in office buildings.

3.5.1 Carpet effect on peak load

Various setpoint profiles of room air temperature are studied for a carpeted and uncarpeted floor. The results of carpeting in the zone during cooling mode are shown in Table 3-3 and Table 3-4. An exposed concrete floor enables the charging and discharging of the thermal mass and therefore less cooling is required. In this case, a three hour ramp in the room temperature profile leads to 35% reduction in peak load and 16% reduction in total load, compared to a carpeted floor.

When convective heating is used, attention is required for calculation of convective heat transfer coefficients, because the heat flow is downwards. In case of a cold floor and warm air the convective heat transfer coefficient may be of the order of 1 W/ °C *m^2 , while for a heated floor and cold air it is around 3 W/ °C *m^2 (Athienitis and O'Brien 2015; Date 2015). Results, presented in Table 3-5 and Table 3-6, show a 17% reduction in power peak and 30% in energy between the exposed and the carpeted floor, for 1 hour ramp.

The carpet has a very significant effect on the radiant floor heating. After heating the concrete, the heating system has to overcome the carpet resistance before the room air node begins to absorb heat. Comparing the different setpoint profiles, the three hour ramp leads to 41% reduction in peak heating load (Table 3-7) and 56% in total heating load (Table 3-8).The maximum heating and cooling capacity of the system is 2kW. The carpeted floor requires the maximum capacity of the system to reach the temperature setpoint while for the case with the exposed floor we need only 59% of the maximum capacity. Note that for Tables 3-8 the percent change is calculated by the following formula:

*Percent change = (Value_Carpet – Value_No_Carpet) / Value_Carpet * 100%* (3.5)

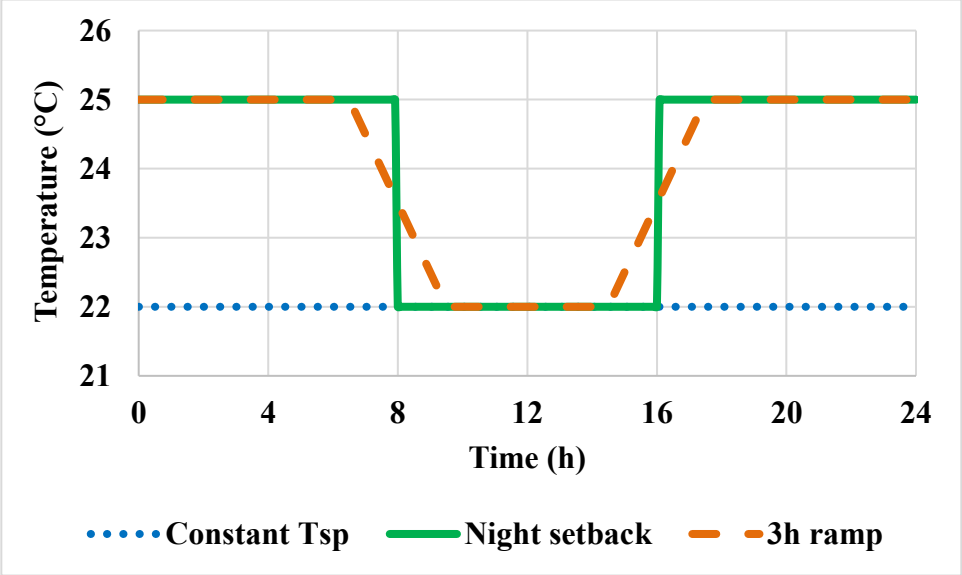

Figure 3-4: Room setpoint profiles – Cooling mode

Table 3-3: Peak load with different setpoint profiles for convective cooling with and without carpet (shades open)

	Floor cover	Temperature setpoint profiles				
		"Constant"	"Night setback"	"1h ramp"	"2h ramp"	"3h ramp"
Peak load (W)	No Carpet	1629	1693	1594	1591	1482
Peak load (W)	Carpet	2270	2277	2224	2225	2278
Percent change		28%	26%	28%	28%	35%

Table 3-4: Total cooling load with different setpoint profiles for convective cooling with and without carpet (shades open)

	Floor cover	Temperature setpoint profiles				
		"Constant"	"Night setback"	"1h ramp"	"2h ramp"	"3h ramp"
Total Cooling load (Wh)	No Carpet	15235	10209	9907	10086	11313
Total Cooling load (Wh)	Carpet	16637	13782	12945	12981	13456
Percent change		8%	26%	23%	22%	16%

Table 3-5: Peak load with different setpoint profiles for convective heating with and without carpet (shades open)

	Floor cover	Temperature setpoint profiles				
		"Constant"	"Night setback"	"1h ramp"	"2h ramp"	"3h ramp"
Peak load (W)	No Carpet	488	941	780	700	630
Peak load (W)	Carpet	588	1100	937	820	738
Percent change		17%	14%	17%	15%	15%

Table 3-6: Total heating load with different setpoint profiles for convective heating with and without carpet (shades open)

	Floor cover	Temperature setpoint profiles				
		"Constant"	"Night setback"	"1h ramp"	"2h ramp"	"3h ramp"
Total Heating load (Wh)	No Carpet	4065	3089	2974	3076	3070
Total Heating load (Wh)	Carpet	4801	4178	4222	4163	4152
Percent change		15%	26%	30%	26%	26%

Table 3-7: Peak load with different setpoint profiles for radiant floor heating with and without carpet (shades open)

	Floor cover	Temperature setpoint profiles				
		"Constant"	"Night setback"	"1h ramp"	"2h ramp"	"3h ramp"
Peak load (W)	No Carpet	885	1231	1229	1222	1177
Peak load (W)	Carpet	2000	2000	2000	2000	2000
Percent change		56%	38%	39%	39%	41%

Table 3-8: Total heating load with different setpoint profiles for radiant floor heating with and without carpet (shades open)

	Floor cover	Temperature setpoint profiles				
		"Constant"	"Night setback"	"1h ramp"	"2h ramp"	"3h ramp"
Total Heating load (Wh)	No Carpet	7153	5524	5292	5494	5480
Total Heating load (Wh)	Carpet	15357	12241	12492	12309	12361
Percent change		53%	55%	58%	55%	56%

3.5.2 Carpet effect on room air temperature swings

The carpet also affects the temperature swings in the room, because it delays the charging and discharging of the thermal mass. Table 3-9 presents the temperature swings of the room air and the concrete surface and also the time lag. The results are for a hot summer day with constant setpoint at 22 °C in the office and shades fully open. Temperature swing is the difference between the maximum and minimum temperature and the time lag is the difference in time between the concrete and the air room temperature peaks.

Table 3-9: Carpet effect on temperature swings with shades open

	ΔT_room (°C)	*ΔT_concr. (°C)*	*Time lag (h)*
No Carpet	1.5	4.2	0.8
Carpet	2.2	1.4	2.8

Figure 3-5 shows simulation results for this day. Temperature profiles are shown for: a) the uncarpeted floor and b) carpeted case. The temperature at the carpeted floor surface reaches 31.1ºC, while the maximum for an uncarpeted floor surface is around 27.8 °C. The temperature

swing between the maximum and the minimum room air temperature for the uncarpeted floor is 1.5 °C while for the carpeted floor is 2.2 °C.

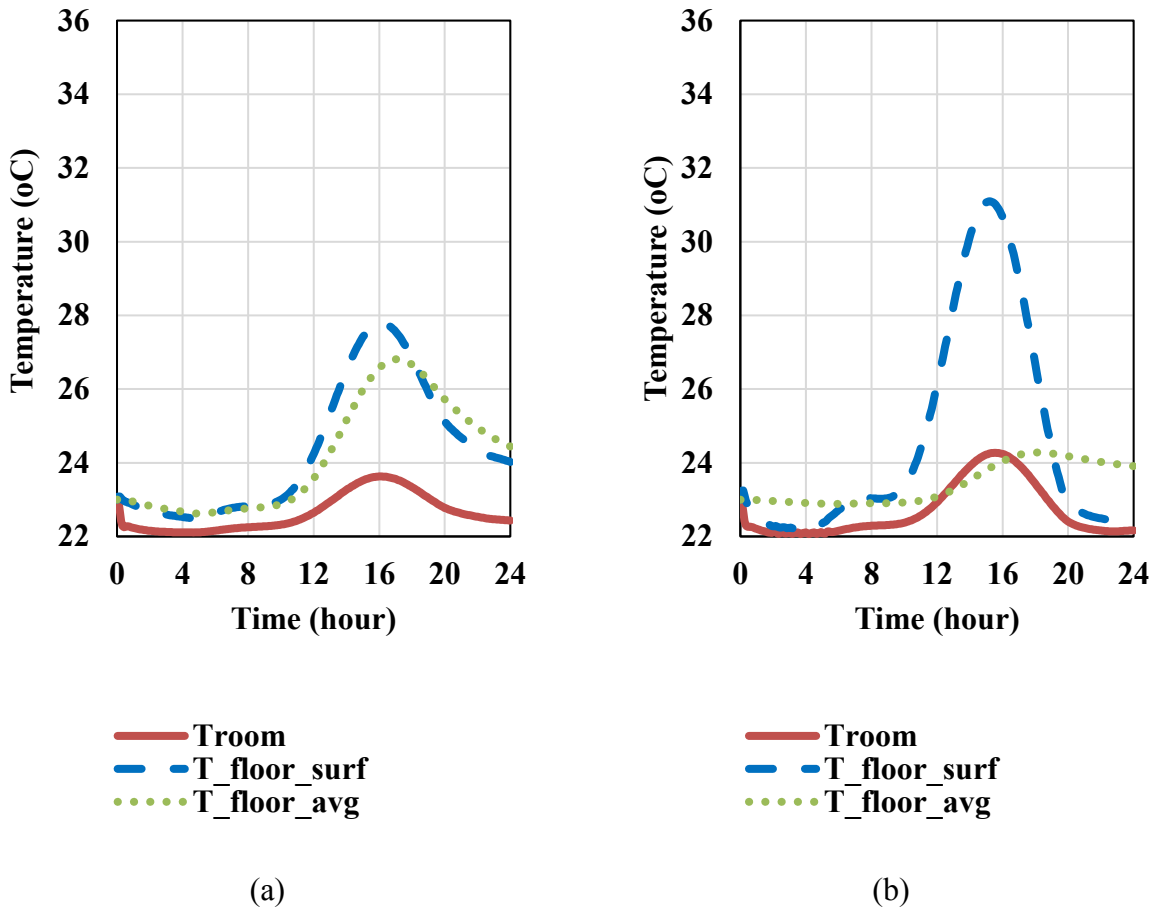

Figure 3-5: Carpet effect on temperature swings with shades open and Tsp constant at 22 °C on a hot summer day: a) exposed floor b) carpeted floor

Carpet introduces a weak thermal coupling that produces larger temperature difference in the room air and smaller temperature difference of the thermal mass (Chen 2013). Also, a weaker thermal coupling leads to a larger time lag between the room and concrete temperatures.

3.5.3 Shifting of peak load

Thermal mass is important for predictive control strategies – both heuristic and fully implemented real time MPC with online use of weather forecasts. Knowing its properties and the amount of energy that can be stored and released later, the peak of load can be shifted by modifying setpoint profile. Figure 3-6 shows this peak shifting in cooling mode, for an uncarpeted floor. The three hour ramp (green dotted line) brings the peak of cooling load closer to the peak of solar radiation, compared to a constant setpoint (red continuous line). The blue (dashed) line represents the solar radiation. The results for all the setpoint profiles are presented in Table 3-10.

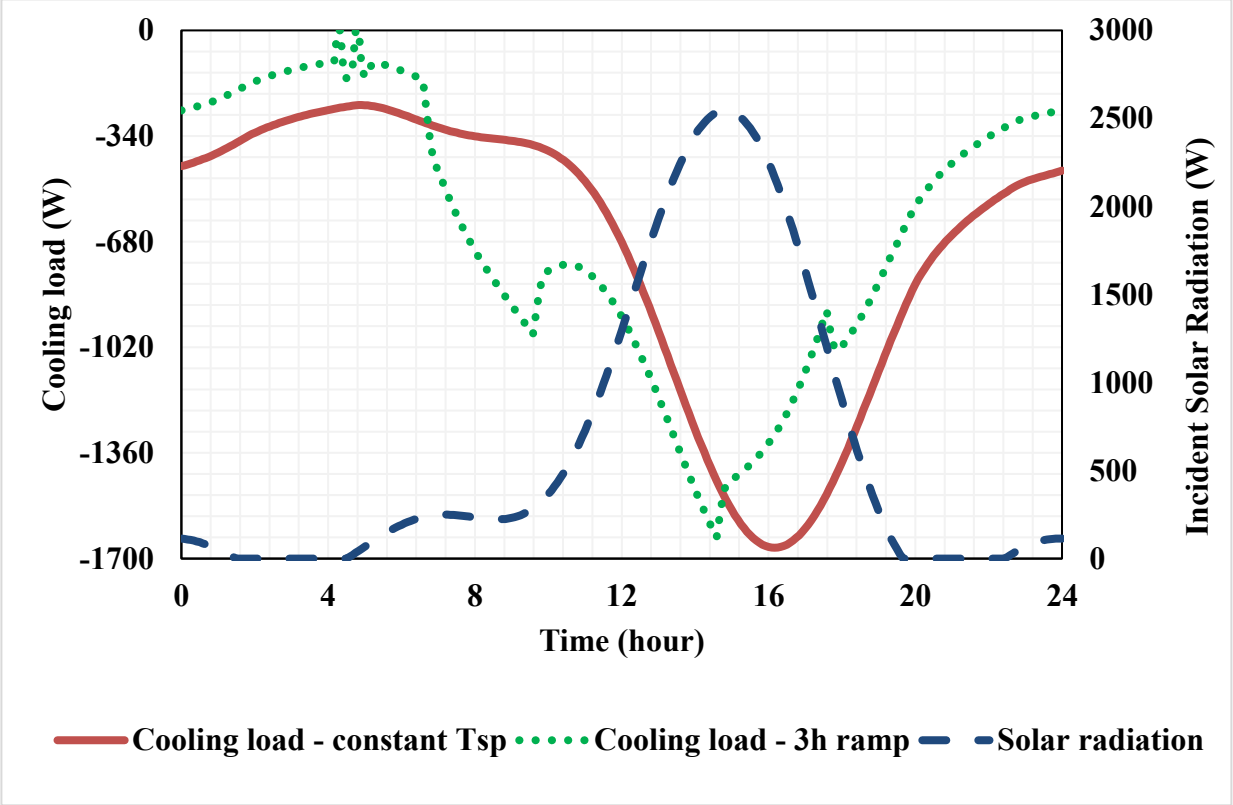

Figure 3-6: Cooling load shifting for an exposed floor with shades open

Table 3-10: Peak shifting for different setpoint profiles during cooling (Delay is the time difference in minutes between the minimum of auxiliary cooling and the maximum solar radiation)

	Floor Cover	Temperature setpoint profile				
		"Constant"	"Night Set-up"	"1h ramp"	"2h ramp"	"3h ramp"
Delay (min)	No Carpet	80	75	15	15	-15
Delay (min)	Carpet	50	50	15	15	50
Difference (min)		30	25	0	0	-65

The delay is defined as the difference between the time of the maximum/minimum auxiliary heat (heating/cooling) and the time of the maximum solar radiation. A negative delay corresponds to the load peak leading the solar radiation peak. The optimal algorithm matches the two peaks.

The optimal solution for this case study is between a 2 and a 3 hour ramp function for an uncarpeted floor and between 1 and 2 hour ramp for a carpeted floor. The last row of Table 3-10 shows the difference in time lag between the two simulations for every setpoint profile. This illustrates the possibilities of optimal use of the system if proper characterization of the thermal mass properties is performed.

Figure 3-7 shows the shifting of peak load in radiant floor heating mode with an uncarpeted floor. The effect of a three hour ramp (green dotted line) compared to a constant setpoint (red continuous line) is shown. Table 3-11 presents the results for a carpeted and uncarpeted floor in heating mode, with all the simulated setpoint profiles. In this case the peak occurs during the night or early in

the morning when the setpoint changes. At this time the ambient temperature is low. The peak in load will always lead the peak of solar radiation, corresponding to the negative delay value.

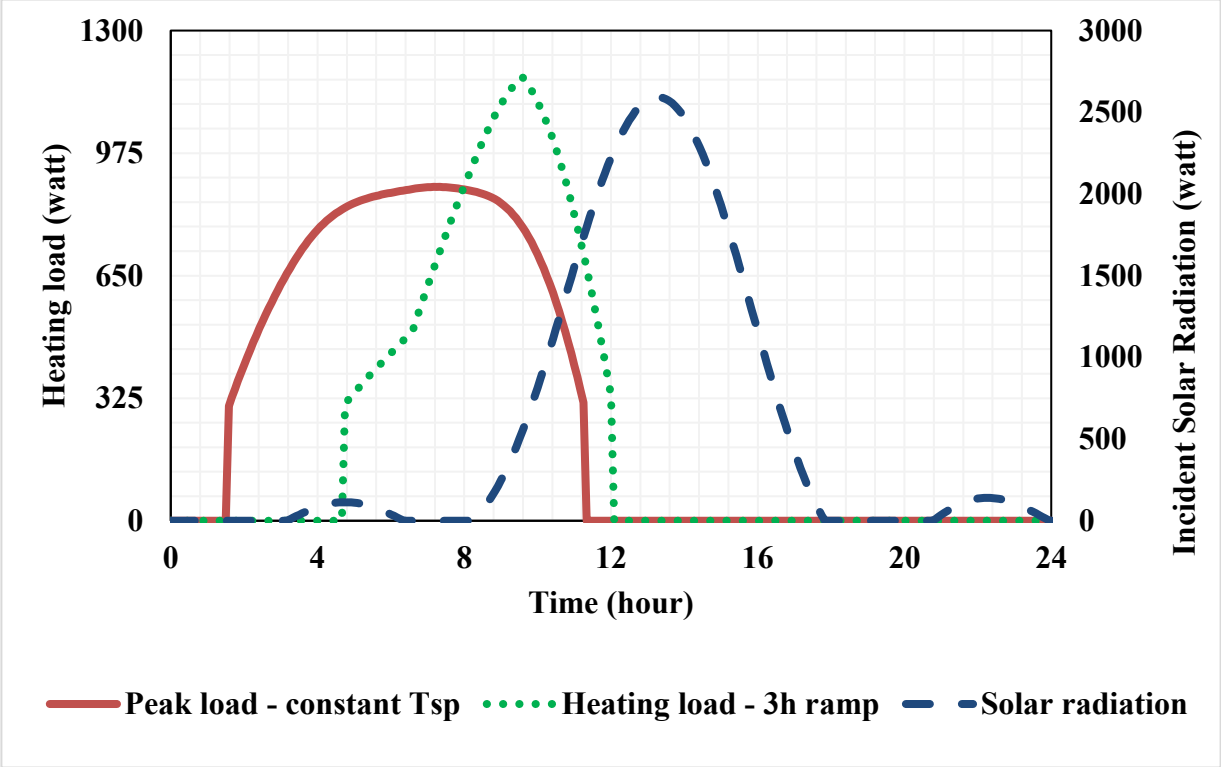

Figure 3-7: Heating load shifting for an exposed floor with shades open.

Although a carpeted floor has less delay between the two peaks, an uncarpeted one offers more flexibility in control. Also, it should be noted that, even without shades, an uncarpeted floor may maintain the room temperature between comfortable levels during summer and winter for all room temperature setpoint profiles. Transferring the peak of the auxiliary heating/cooling system closer to the peak of solar radiation allows the power demand to be offset by solar electricity generated by photovoltaics. On-site electricity generation can partly offset daily electricity consumption,

eliminate grid transmission losses and potentially result in reduced need for peak- capacity power plants (Gaiddon, B., Kaan, H., & Munro n.d.).

Table 3-11: Peak shifting for different setpoint profiles during heating (Delay is the time difference in minutes between the maximum of auxiliary heating and the maximum solar radiation)

	Floor Cover	**Temperature setpoint profile**				
		"Constant"	**"Night Set-up"**	**"1h ramp"**	**"2h ramp"**	**"3h ramp"**
Delay (min)	**No Carpet**	-360	-265	-250	-250	-220
Delay (min)	**Carpet**	-240	-185	-185	-185	-185
Difference (min)		-120	-80	-65	-65	-35

Depending on the control strategy used and optimality criteria, a predictive control algorithm will prescribe the action that minimizes the cost of an appropriate control function. This could mean changing the setpoint profile duration or the setpoint value according to the present state of the thermal mass and the expected disturbance (weather, occupancy profile).

For example, during a weekend in the summer, when the office is not occupied, a predictive controller may fully discharge the thermal mass by lowering the setpoint value and closing the motorized blinds so it can store more energy at the beginning of next week, if Monday is expected to be a hot sunny day. The optimal use of all the control variables should maintain the thermal comfort in the space when occupied. The predictive control strategy should reduce peak demand and energy consumption according to criteria that take into account flexibility in comfort constraints and energy pricing schemes by optimizing charging and discharging of thermal storage.

3.5.4 Thermal mass thickness effect

Two thermal mass thicknesses, 10 cm and 15.24 cm, are simulated in convective cooling and radiant floor heating mode for an exposed floor. The results are presented in the Figure 3-8 and Figure 3-9 for cooling and heating respectively. There is no significant change in peak power demand (less than 5% for all simulated cases) and energy consumption reduction (less than 10% for all tested profiles). For this 24-hour cycle with modest temperature swings in room surface and air temperatures, a concrete thickness of 10 cm is satisfactory, with no significant benefit in a higher thickness. Beyond that, very little is added to the effective diurnal storage capacity of the mass for the properties and configuration considered.

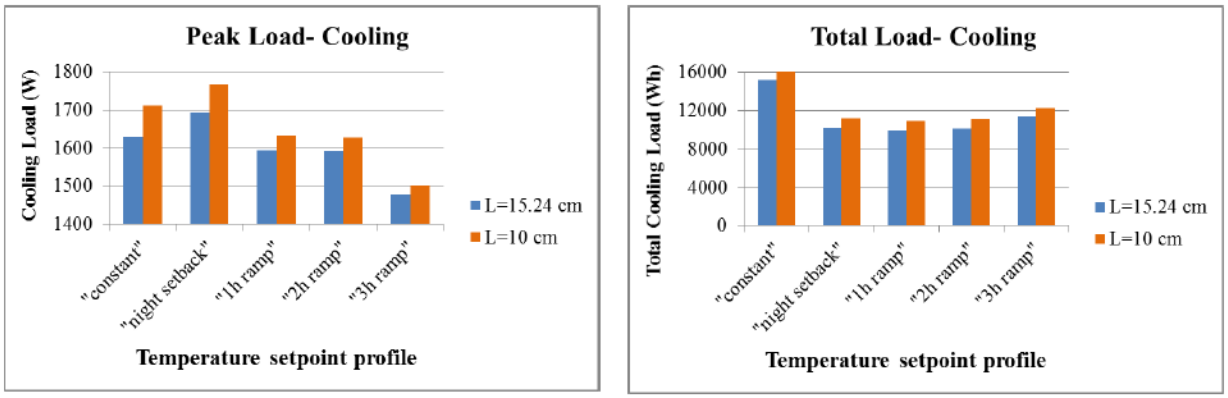

Figure 3-8: Floor mass thickness effect – Cooling – No carpet

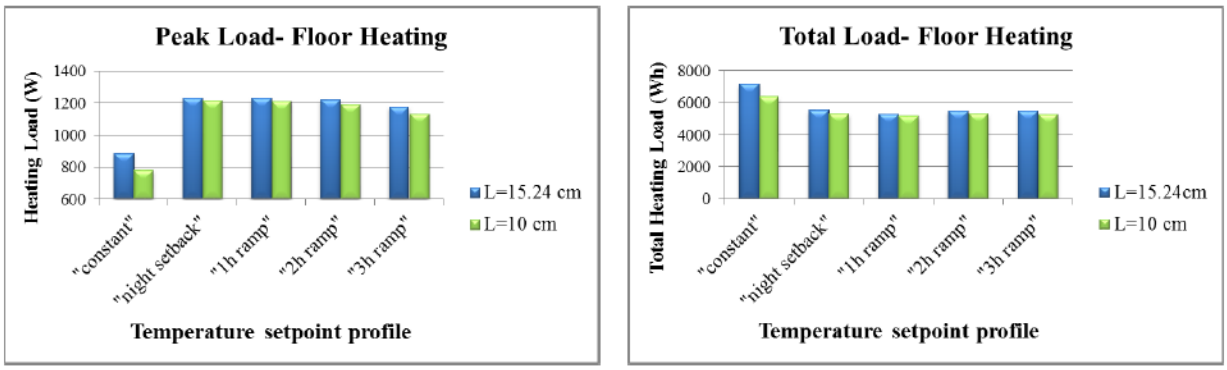

Figure 3-9: Floor mass thickness effect – Heating – No carpet

3.5.5 Shading control – cooling mode

The room receives high solar gains because the WWR is 75%. In the case of carpeted floor the temperature of the room and also the temperature on the carpet surface are above the comfort levels, unless shades are controlled optimally or closed. Results are improved when a simple control is applied for the motorized blinds. The maximum temperature of the carpeted floor reaches more comfortable levels, down from 30.9 °C with shades open to 26.8 °C with shades closed. Moreover, the shading control keeps the maximum room air temperature below 24 °C when the office is occupied. According to international standards, the recommended floor temperature range in occupied zones, is 19 °C to 29 °C (Olesen 2002).

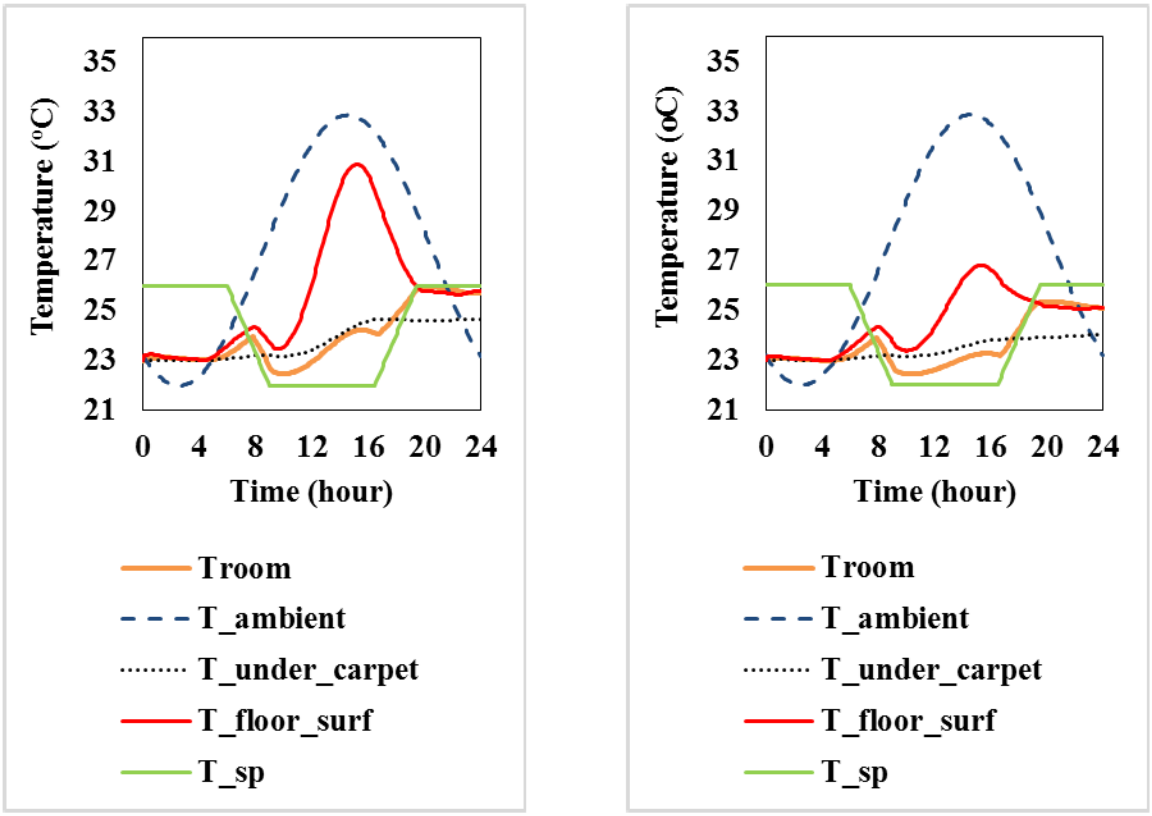

(a) (b)

Figure 3-10: Shading control for a room with carpeted floor in cooling mode with a 3 hour ramp setpoint profile (a) simulation with shades fully open (b) simulation with control of motorized shades

In the case of fully open shades the cooling system reaches its maximum capacity and is inadequate to maintain the temperature setpoint in the room. When the motorized shades are controlled the peak load is reduced by 43% and total cooling load is reduced by 40%.

Figure 3-10 shows the simulation results for (a) the case with shades fully open and (b) shades operating with controls. This control strategy blocks the solar radiation when the light level on the

work plane is above 500 lx. This equals almost to 150 W/m^2 on the window. As can be seen from the figure, room temperature follows closely the setpoint profile in case of shading control.

3.5.6 Comparison of different interior layers of thermal mass

There are other common materials that are used on the floor surface in buildings. Such materials are tiles or parquet. The following figures present a comparison of the peak and total load of the perimeter zone using these materials.

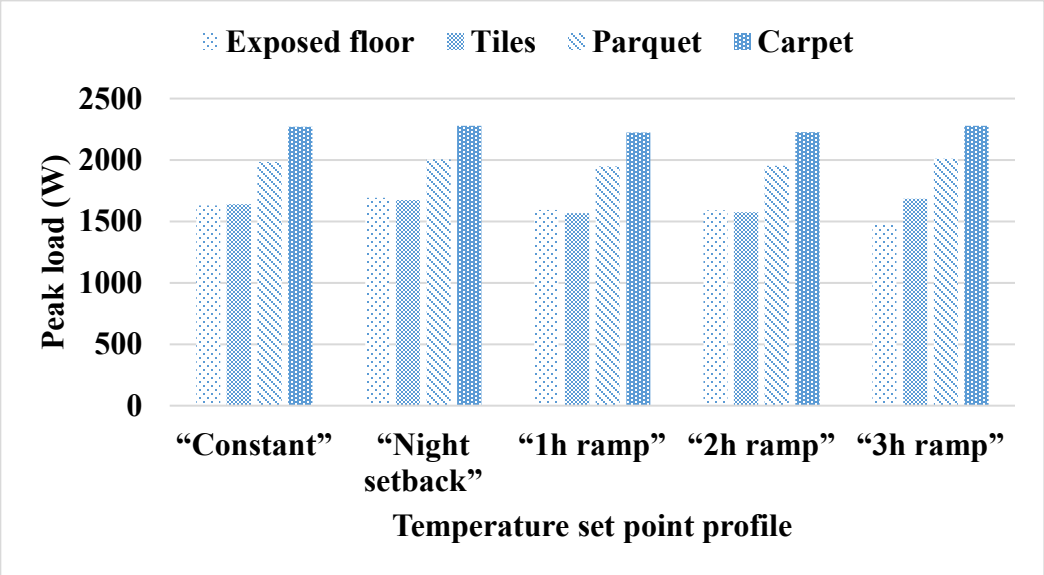

Figure 3-11: Peak load for different interior layers for convective cooling at different setpoint profiles (shades open)

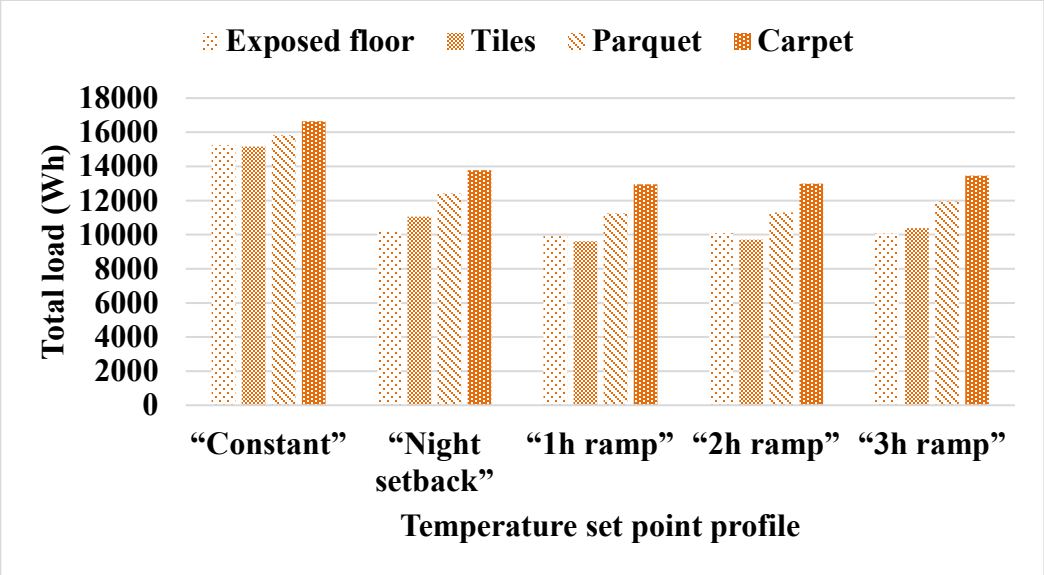

Figure 3-12: Total cooling load for different interior layers for convective cooling at different setpoint profiles (shades open)

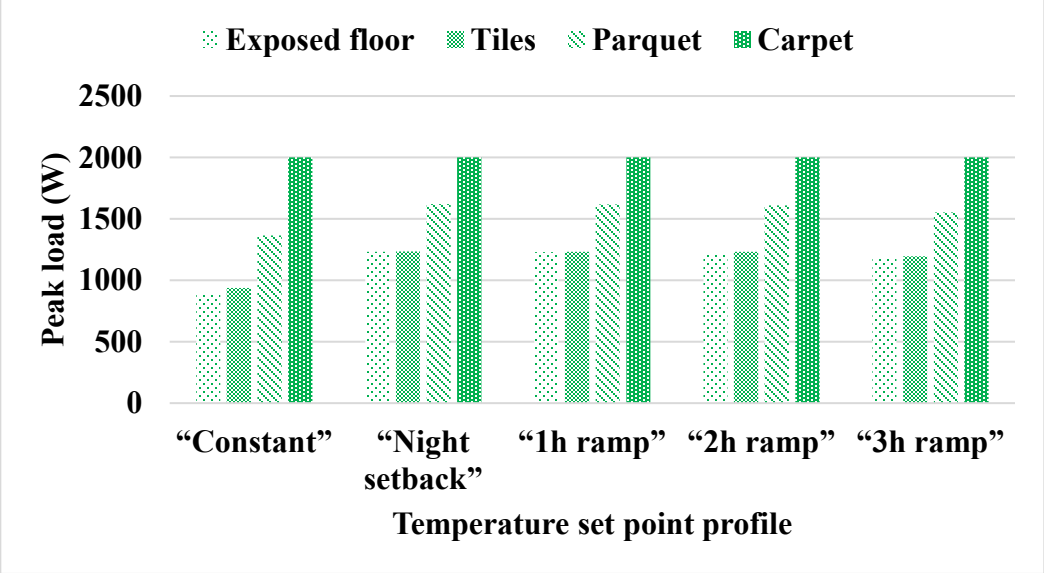

Figure 3-13: Peak load for different interior layers for radiant floor heating at different setpoint profiles (shades open)

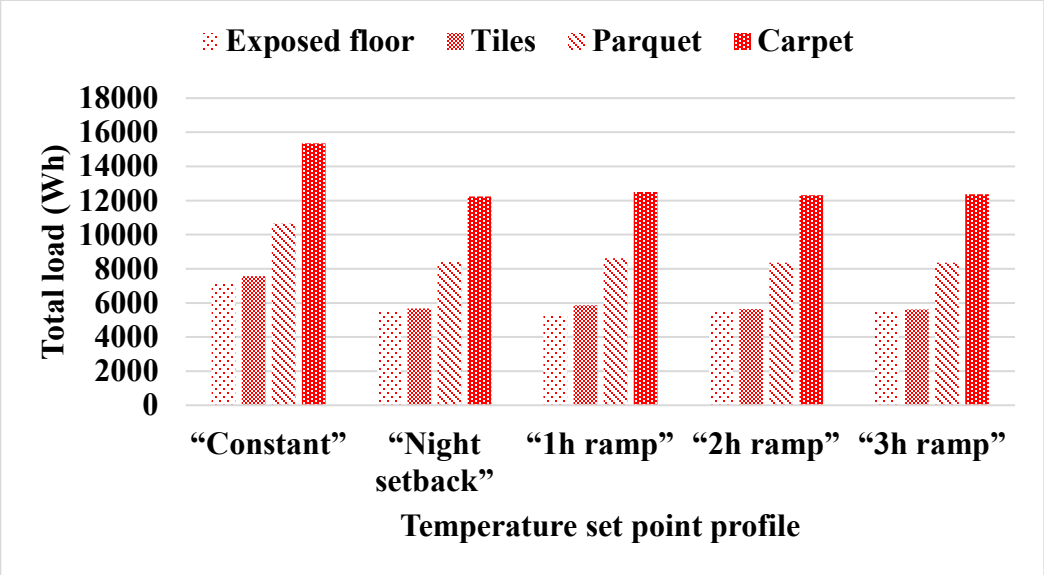

Figure 3-14: Total heating load for different interior layers for radiant floor heating at different setpoint profiles (shades open)

As the thermal conductivity decreases (see Table 3-1), the peak and total load increase. Also, a floor cover with tiles and an exposed one have similar behavior in cooling and heating mode.

3.5.7 The effect of WWR

This specific case study, has 75% WWR, which results in high solar gains and cooling load. The WWR is varied, to illustrate its effect on peak load, at similar offices. The shades remain open and the floor is covered with carpet. Figure 3-15 and Figure 3-16 show the results of the parametric analysis for cooling and Figure 3-17 and Figure 3-18 for heating mode.

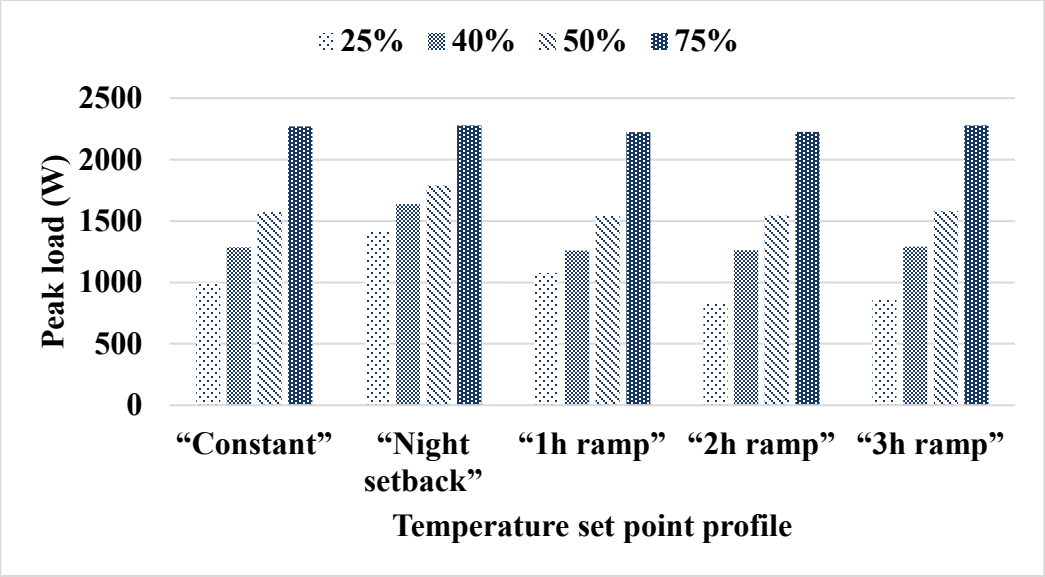

Figure 3-15: Peak load for different WWR for convective cooling at different setpoint profiles (shades open)

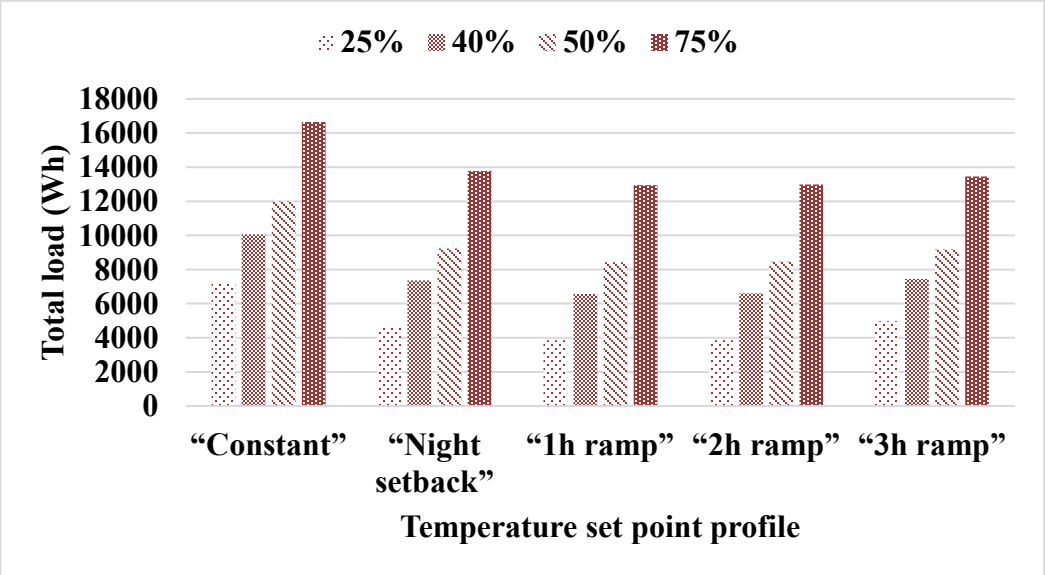

Figure 3-16: Total cooling load for different WWR for convective cooling at different setpoint profiles (shades open)

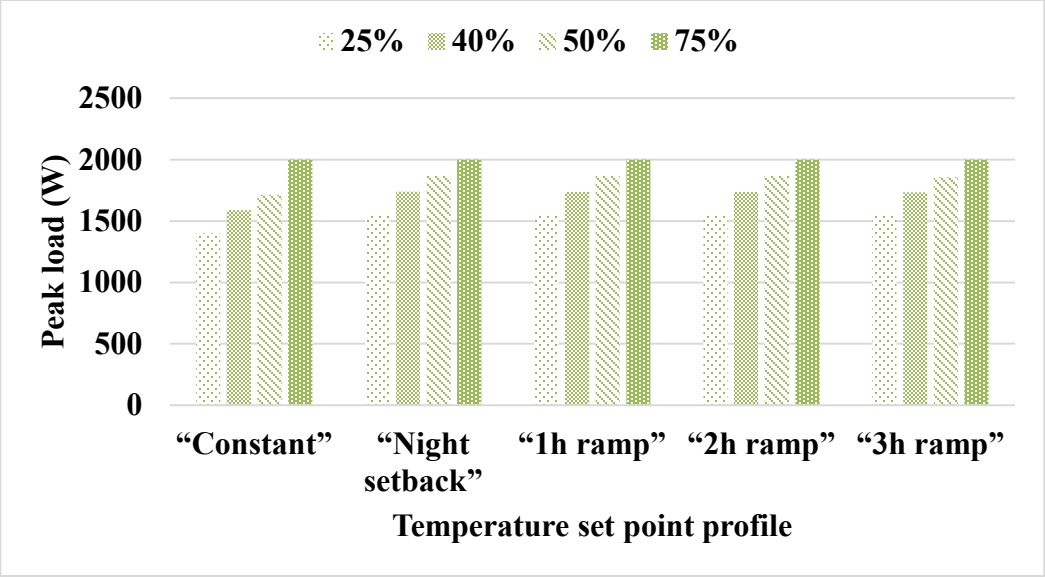

Figure 3-17: Peak load for different WWR for radiant floor heating at different setpoint profiles (shades open)

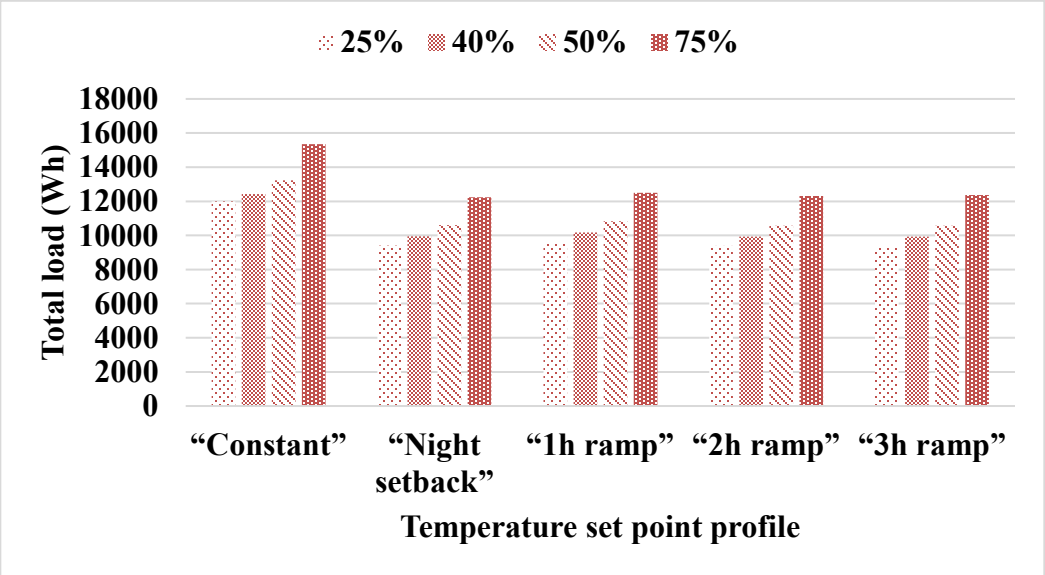

Figure 3-18: Total cooling load for different WWR for radiant floor heating at different setpoint profiles (shades open)

Higher window-to-wall ratio results in higher loads, because windows have smaller thermal resistance than walls.

3.6 Detailed model

A more detailed model is used to investigate the impact of model resolution in peak load reduction. The detailed model uses separated convective and radiative heat transfer coefficients and discretizes the floor into more control volumes.

3.6.1 Separate convective and radiative heat transfer coefficients

The detailed model separates the combined heat transfer coefficients that were used before, in the radiative and convective part. These coefficients change every time step, depending on the temperature of the relative surfaces, while at the simplified model they were considered constant. The radiative heat transfer coefficient is calculated from the following equation (Athienitis and O'Brien 2015; McAdams 1959):

$$h_r = 4 * \sigma * T_m^3 * F_{ij}^* \tag{3.6}$$

$$\mathrm{T}_m = \frac{T_1 + 273 + T_2 + 273}{2} \tag{3.7}$$

$$F_{ij}^* = m_{ij} * \varepsilon_1 * \varepsilon_2 / \rho_i \tag{3.8}$$

where $4\mathrm{Tm}^3$ is a linearization factor for radiation heat transfer. $\mathrm{F_{ij}}^*$ is the radiation exchange factor between surfaces i and j (Athienitis and O'Brien 2015). The convective heat transfer coefficients are calculated as follows (McAdams 1959):

$$h_{conv} = 1.52 * (T_{floor} - T_{air})^{1/3} ... heat\_flow\_upward \tag{3.9}$$

$$h_{conv} = 0.59 * (\frac{T_{air} - T_{floor}}{x})^{0.25} ... heat\_flow\_downward \quad (3.10)$$

$$x : characteristic\_dimension$$

$$h_{conv} = 1.31 * (T_{wall} - T_{air})^{1/3} ... for\_vertical\_surfaces \quad (3.11)$$

Figure 3-19 presents the convective heat transfer coefficient between the wall and the room air node. Figure 3-20 shows the combined heat transfer coefficient (convective between floor and room air node and radiative between floor and wall) of the floor surface. The results are for 5 days. The values of these coefficients vary significantly compared to the previous analysis, where they were considered constant.

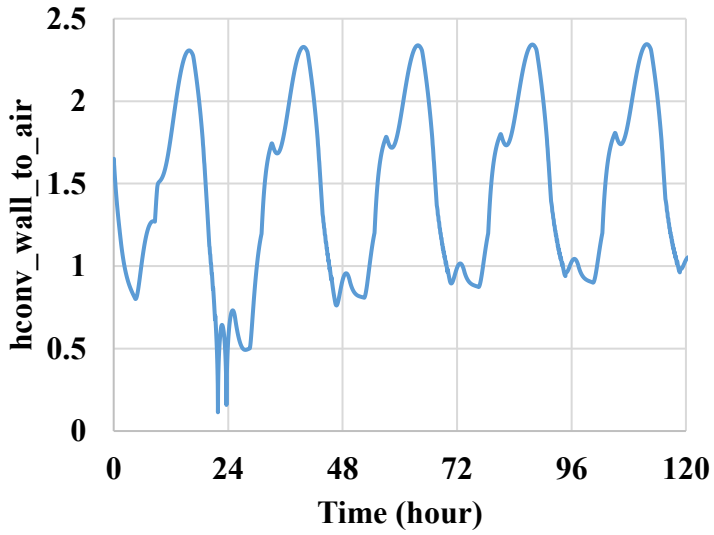

Figure 3-19: Convective heat transfer coefficient for vertical surfaces

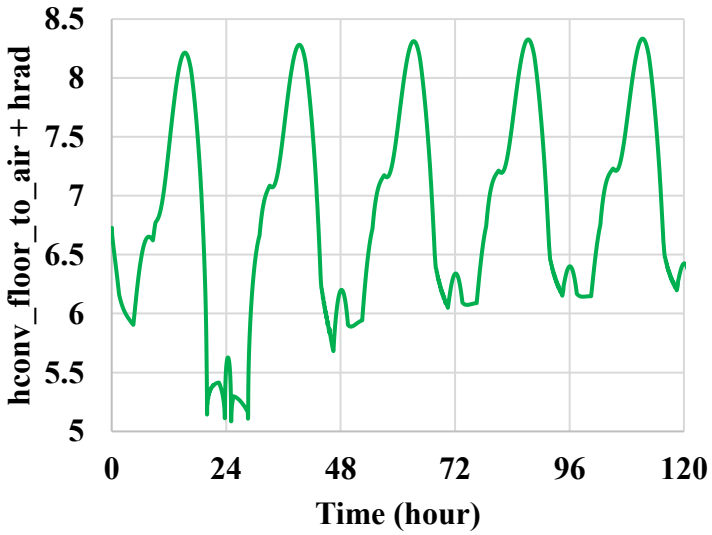

Figure 3-20: Convective and radiative heat transfer coefficients of the floor surface

3.6.2 Discretization of thermal mass in the floor

In the previous analysis, the floor was discretized into 2 control volumes. The analysis was repeated with the floor discretized into 4, 6, 8 and 10 control volumes, to increase the level of detail and test the accuracy of the results.

3.6.3 Compared results between the simplified and the detailed model

The detailed model was used, to simulate the case with a three hour ramp change for the temperature setpoint profile and the shades controlled by the proposed algorithm. The following tables include comparative results between the simple model and the detailed one. The reference point is the value of the simplified model. This is compared with the detailed model showing the effect of the heat transfer coefficients separation and the different number of control volumes. Table 3-12 and Table 3-13 show the results of peak and total load in cooling mode and compare them with the same setup of the simplified model. The results of heating mode are presented in

Table 3-14 and Table 3-15. Note that for Tables 12-15 the percent change is calculated by the following formula:

$$Percent\ change = (Value\_separated - Value\_combined) / Value\_separated * 100\% \quad (3.12)$$

Table 3-12: Peak load comparison between simplified and detailed model – cooling mode

	Heat transfer coefficient	Number of control volumes in the floor				
		"2CV"	"4CV"	"6CV"	"8CV"	"10CV"
Peak load (W)	h_combined	1287	1287	1297	1306	1308
Peak load (W)	h_separated	1106	1122	1139	1156	1160
Percent change		-16%	-15%	-14%	-13%	-13%

Table 3-13: Total load comparison between simplified and detailed model – cooling mode

	Heat transfer coefficient	Number of control volumes in the floor				
		"2CV"	"4CV"	"6CV"	"8CV"	"10CV"
Total Cooling load (Wh)	h_combined	6974	6867	6989	7135	7166
Total Cooling load (Wh)	h_separated	6217	6196	6319	6470	6508
Percent change		-12%	-11%	-11%	-10%	-10%

Table 3-14: Peak load comparison between simplified and detailed model – heating mode

	Heat transfer coefficient	Number of control volumes in the floor				
		"2CV"	"4CV"	"6CV"	"8CV"	"10CV"
Peak load (W)	h_combined	1736	1738	1779	1818	1827
Peak load (W)	h_separated	1821	1825	1858	1890	1897
Percent change		5%	5%	4%	4%	4%

Table 3-15: Total load comparison between simplified and detailed model – heating mode

	Heat transfer coefficient	Number of control volumes in the floor				
		"2CV"	"4CV"	"6CV"	"8CV"	"10CV"
Total Heating load (Wh)	h_combined	17673	18073	18460	18707	18792
Total Heating load (Wh)	h_separated	20827	21261	21868	21738	21734
Percent change		15%	15%	16%	14%	14%

The comparison of the simulated results between the simplified and the detailed model, indicates that the major difference comes from the separation of the heat transfer coefficients in convective and radiative part, while the discretization of the floor into more control volumes has a small effect. Analytically, in cooling mode, the separation of the heat transfer coefficients and its variation at every time step, leads to 16% decrease in peak load and 12% in total load, compared to the case of combined h, constant in time.

In heating mode, the separation of the heat transfer coefficients results in 5% increase in peak load and 16% in total load, compared to the case of combined h, constant in time. The discretization of floor into more control volumes has a small impact on the results (3% maximum difference in all cases).

3.7 Conclusion

This chapter presents a simulation study of predictive control strategies to reduce and shift peak load in a zone of a perimeter office with floor heating, convective cooling and various floor thermal storage configurations. The floor is covered by a carpet and the WWR is 75%. A case without carpet is considered and the simulated results show the potential of energy savings and occupancy comfort through some predictive control strategies. A predictive control algorithm will find the optimal action for the control variables of the room (Tsp profile and motorized blinds position) in

order to reduce peak load while maintaining comfortable temperature and daylight levels. Therefore, it will control the charging and discharging rate of the thermal mass according to its present state and the expected disturbances (weather and occupancy profiles).

Thermal mass and its coupling with the occupied space is very important for MPC. The results show the effect of the carpet in power reduction and comfort conditions in the office. The importance of the thermal mass and its thermal coupling are illustrated through different setpoint profiles that are possible actions of an MPC controller.

Simulations compare the case of an exposed concrete floor to a carpeted one. The carpet adds an extra resistance in series with the floor and delays the charging and discharging of the thermal mass. In cooling mode the reduction in peak load of an uncarpeted floor compared to a carpeted one is 35% with a 16% reduction in total load. In radiant floor heating mode simulations show 41% reduction of peak load and 56% in total load. An exposed floor requires less maximum capacity for the heating/cooling system compared to the carpeted one. Simulations show that there is no significant difference in peak power demand and energy consumption, between the case with 10cm and 15.24cm floor concrete mass thickness. A practical thickness of a concrete storage layer is about 10 cm for diurnal energy storage.

Besides the temperature set point profile, another variable that can be controlled to improve the energy consumption and the occupancy comfort in the room is the position of motorized roller shades. A simple control strategy of the motorized shades for the cooling mode, may lead to proper illuminance and thermal comfort levels in the room. At the same time, excessive direct solar gains are blocked, reducing the peak cooling load in the zone.

A detailed model for the perimeter zone calculates separately the convective and radiative heat transfer coefficients, varying them at every time step and discretizes the floor into 10 control volumes. The comparison between the simplified and the detailed model showed that the separation of the heat transfer coefficients has a significant effect on the peak and total load. On the other hand, increasing the number of control volumes in the floor has a small impact on the results. The level of accuracy depends on the application. However, the simplified model provides enough information about the dynamic response of the system and can be used in predictive control algorithms that can be robust providing quick and accurate results.

Finally, a parametric analysis illustrated the important effect of WWR on peak and total heating/cooling loads. Also, alternative floor covers, such as tiles or parquet may offer more energy efficient solutions, while satisfying the aesthetics of the space.

4 MPC for PCM: a numerical and experimental study of simple predictive control in a perimeter zone with phase change materials

4.1 Introduction

This chapter presents a simulation and experimental study of simple predictive control strategies in a perimeter test cell using a phase change material (PCM) as a means of thermal storage. The PCM, embedded in a wall of the test cell, is actively charged through forced air circulation. The objective of the study is to investigate how MPC can be used to leverage the performance of a PCM wall. This study also shows how a low-order thermal network model can be used as an effective tool in the design of the MPC strategy. The proposed model predictive control (MPC) algorithm uses a set of linear ramp functions to change the room temperature setpoint to reduce and shift peak power demand. These ramp setpoint profiles allow the effective charging and discharging of the wall-integrated PCM. The algorithm applied in the experimental facility uses the outdoor temperature as input to select the best charging and discharging rate over a prediction horizon. A low-order model of the room and the PCM wall is used in the predictive control algorithm. It was found that this model can predict accurately the peak power demand (CV-RSME 28.2% and NMBE 3.4%) and the temperature profile in the room. As the process moves forward in time, the weather profile is updated periodically and the algorithm calculates the new outputs over the new control horizon. The whole procedure is automated and the outputs of the algorithm are transferred to the local variables of physical the controller of the test room through BACnet. The results of the predictive control algorithm are presented and discussed.

4.2 The test room

Experiments were conducted at Concordia University Paul Fazio Solar Simulator Environmental Chamber (SSEC) Research Laboratory (Concordia University 2011, 2014). The Environmental Chamber allows accurate and repeatable testing of advanced building enclosures under standard conditions with fully programmable temperature, humidity and pressurization profiles and temperature ranges from -40 °C to +50 °C. The test room is located inside the Environmental Chamber (Figure 4-1).

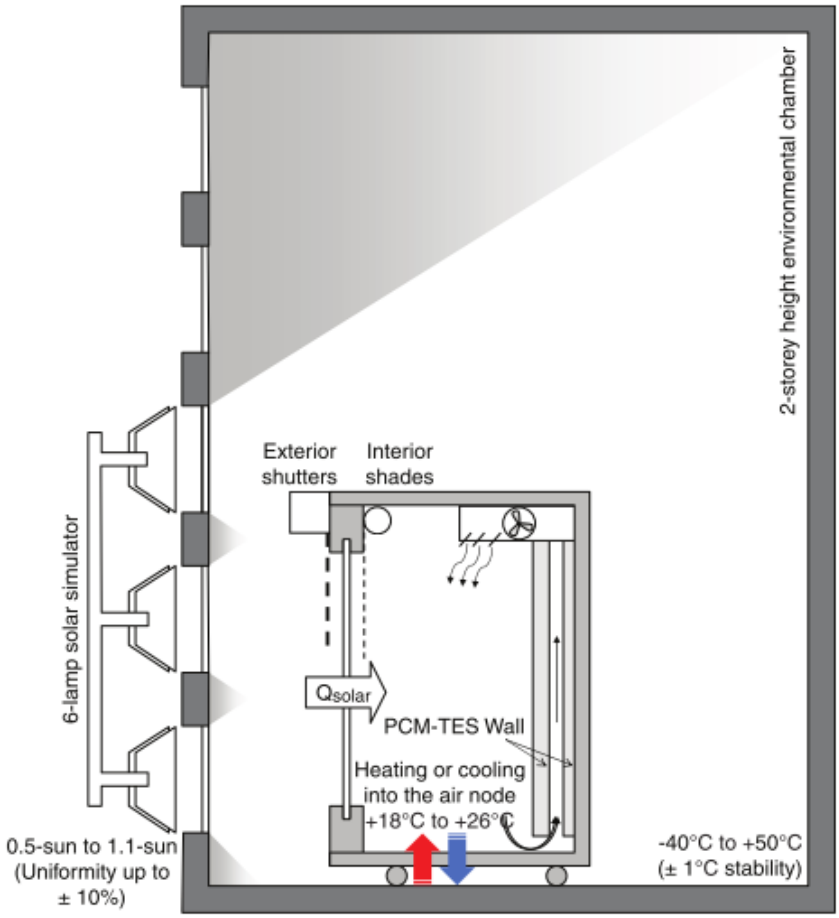

Figure 4-1: Schematic of the environmental chamber with the PCM test room inside showing the controllable parameters (Dermardiros 2015)

The test room has interior dimensions 3 x 1.5 x 2.7 m with PCM panels integrated into its back wall. An air channel between the PCM panels and a plenum fan on the ceiling allow the active charge and discharge of the material. A 984-W electric heater provides heat to the room. Double-pane windows in the front of the room allow emulated daylight from the mobile solar simulator to enter and heat the space; part of the energy is stored in the PCM. This energy will be released into the room at night when room temperature will decrease, reducing the energy consumption of the heater.

Outdoor temperature conditions were simulated in the Environmental Chamber. Sinusoidal profiles with a 24-h period and varying amplitude were applied. The experimental results were used in the model to tune its parameters. The heater in the model is controlled with a PI controller that has the same parameters of the actual controller in the experiment. Initially the goal of the experiments was to determine the dynamic response of the system, the charge and discharge rate of the PCM under a temperature range of 16.5 °C to 25 °C in the test room. The linear ramp durations were tested under a heuristic control process to investigate the effect of their use on reduction and shifting of peak power demand.

After the simple predictive control model was developed in MATLAB (Mathworks 2016), it was then implemented in the test room for model validation. The model can predict with sufficient accuracy the peak power demand.

4.3 Methodology

The study consists of two parts: (a) the creation of a model of the PCM test room; (b) the development and experimental implementation of the predictive control algorithm.

4.3.1 Model of room with PCM wall

The model of the test room was created in MATLAB and it is based on the results of a previous study (Dermardiros 2015). Dermardiros (2015) studied the performance of the same type of phase change material used in this study, and created models of varying levels of complexity for the PCM wall. In the present study, Dermardiros' second order model is chosen for the wall (Figure 4-2b); this model predicts the energy stored by the PCM and the temperature at the outlet of the channel accurately (1.7% error in the energy balance during charging and 4.1% during discharging after 6 hours). The test room itself (Figure 4-2a) was modeled with one effective thermal capacitance and one effective thermal resistance (see Appendix A.4 Test room thermal model). The models were implemented in MATLAB. The equations 4.1-4.4 (Dermardiros and Athienitis 2015) were solved with the implicit finite difference method to calculate the total heat provided at the room air node.

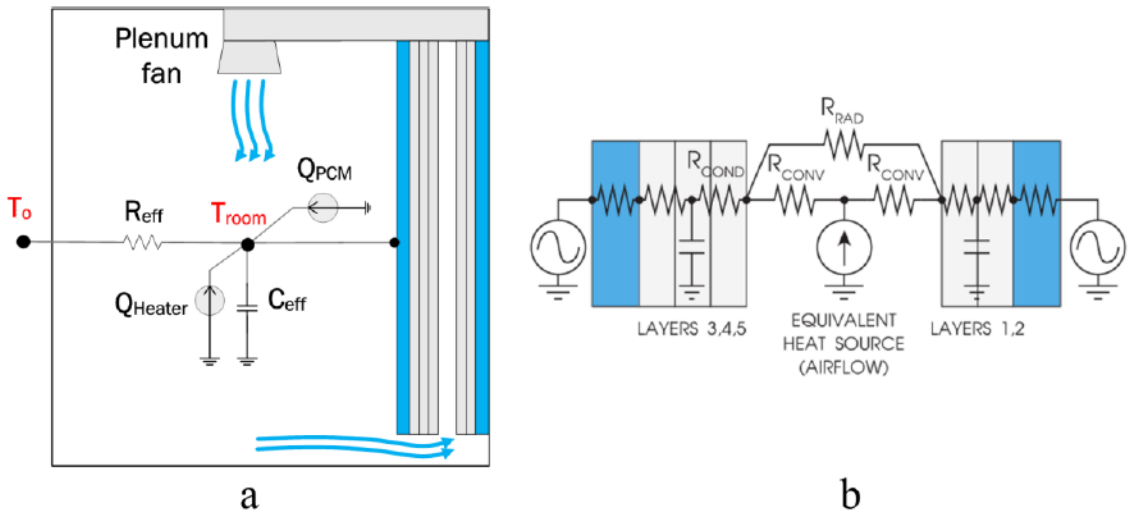

Figure 4-2: (a) Thermal model of the test room (b) 2nd order model for the PCM wall (Dermardiros 2015)

Equation 4.1 is the heat balance equation. Equation 4.2 is the effective heat capacity of the PCM as a function of its temperature. Equation 4.3a is the air control volume differential equation which is solved for the outlet air temperature (Equation 4.3b) to calculate the equivalent heat source at the air channel control volume (Equation 4.4). Equation 4.5 calculates the heat provided by the electric heater with proportional integral control (PI control).

$$\sum_j [U_{ij}^{t+1}(T_j^{t+1} - T_i^{t+1})] - \frac{C(T)_i^t}{\Delta t} T_i^{t+1} + \dot{Q}_i^{t+1} = -\frac{C(T)_i^t}{\Delta t} T_i^t \tag{4.1}$$

$$C_p(T) = \Delta h \cdot \frac{1}{\sqrt{2\pi}} \cdot \exp\left(\frac{-(T - T_c)^2}{2 \cdot \omega^2} \right) \cdot \left[1 + erf\left(\frac{skew \cdot (T - T_c)}{\sqrt{2} \cdot \omega} \right) \right] + c_{p,average} \tag{4.2}$$

$$(\dot{m} \cdot C_p \cdot dT)_{air} = depth \cdot dy \cdot (h_{conv,front} \cdot (T_{front} - T_{air}) + h_{conv,back} \cdot (T_{back} - T_{air})) \tag{4.3a}$$

$$T_{air,outlet} = T_{air,inlet} \cdot \exp\left(\frac{-h_{conv} \cdot A_{PCM}}{\dot{m}_{air} \cdot C_{p,air}} \right) + T_{surface} \left[1 - \exp\left(\frac{-h_{conv} \cdot A_{PCM}}{\dot{m}_{air} \cdot C_{p,air}} \right) \right] \tag{4.3b}$$

$$\dot{Q}_{PCM}^t = \dot{m}_{air} \cdot C_{p,air} \cdot (T_{air,outlet}^t - T_{air,inlet}^t) \tag{4.4}$$

$$Q_{Heater}^t = k_p \cdot (T_{setpoint}^t - T_{room,air}^t) + k_i \cdot \int (T_{setpoint}^t - T_{room,air}^t) dt \tag{4.5}$$

where

- Δh, enthalpy of fusion, $J \cdot kg^{-1}$;

- T_c, approximate temperature of peak phase change, °C;
- ω, temperature range of phase change;
- skew, skewness factor; and,
- $C_{p,\,average}$, average specific heat of PCM in the sensible range, $J \cdot kg^{-1} \cdot K^{-1}$;
- k_p, proportional gain of the controller, W/ °C
- k_i, integral gain of the controller, W/°C ·s
- $\dot{Q}i$, heat flux into the node, W

At the air node two heat sources are applied, one from an electric 960W heater and the other from the energy released from the Phase-change material based thermal energy storage (PCM-TES). The PCM melts above 21 °C and solidifies when its temperature drops below 19 °C. After a full charge and discharge cycle the PCM-TES releases 2.66kWh. The material was charged by supplying air at 28 °C, and discharged with 13 °C air. In the present study temperatures in the range of 16.5 to 25 °C, were simulated and implemented in the experiment to come close to full charge/discharge of the PCM. The goal is to test the behavior of the material in realistic conditions used in buildings. Therefore, the daytime setpoint is set to 25 °C and the nighttime setpoint to 16.5 °C. The daytime setpoint is higher than the ones normally used in buildings, in order to allow the PCM-TES to charge during the day. However, it enables validation of the model and control algorithm so that it can be applied to other buildings with actively charged building-integrated thermal storage.

Different setpoint profiles, with diverse periods of "charging" and "discharging" are tested. The charging/discharging ramps refer to the transition periods between nighttime and daytime setpoints (16.5 and 25 °C). Figure 4-3 shows the setpoint profile. The length of the charging and the discharging ramps allow the material to absorb heat and release it before the day time period, when

the setpoint is increased, to reduce the amount of heat provided by the electric heater. Although electric heat is used for ease of control, the strategies can be applied to other forms of heating like floor heating with hydronic pipes connected to a heat pump or solar heating. The experimental facility at the SSEC laboratory has a mobile solar simulator that can be used to heat up the test room through emulated sunlight and charge the PCM. In this case, the position of the motorized roller shades can be added as control variable to the algorithm and control the solar gains entering the zone.

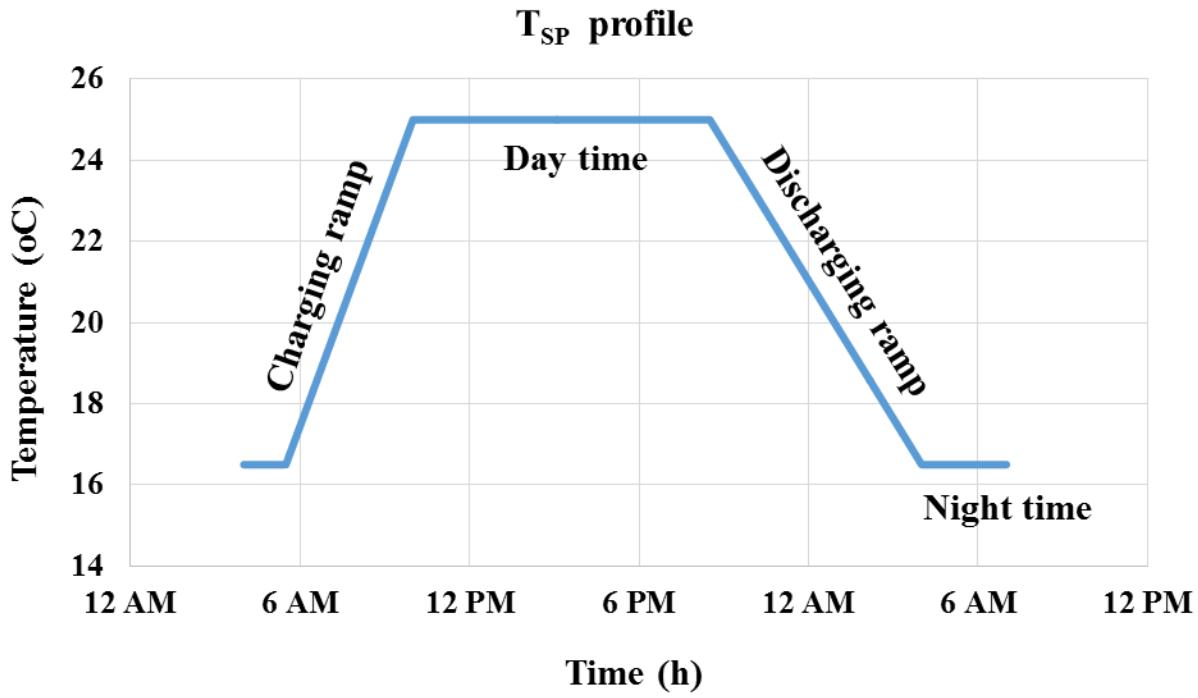

Figure 4-3: Tsp profile example with 4.5h charging and 7.5h discharging period

It should be noted that the specific profile was chosen to illustrate the potential in energy and peak power reduction through the utilization of PCM. It is worth pointing out that there is no mechanical system or any dampers that can isolate the PCM wall. Therefore, the room temperature setpoint profile and the air circulation through the wall allow charging the PCM during daytime and

discharging it before the transition between night-time and daytime. This transition is the moment when the morning electric peaks are observed and by fully discharging the PCM at that time the peak power is reduced by releasing energy that was stored in the PCM during the charging period.

Dermardiros studied variations of this system, where the PCM can be integrated into the HVAC system or zone-coupled. He studied the impact of PCM-TES on heating peak during the morning start-up for varying amounts of PCM and for different HVAC activation times (Dermardiros and Athienitis 2016). However, in the present study the main way to control the behavior of the PCM is the temperature profile. Dermardiros also showed that increasing the number of air channels between the PCM panels, the charging and discharging durations decrease and lead to faster and more easily controllable thermal energy storage (Dermardiros and Athienitis 2015).

4.3.2 Simple MPC algorithm

An algorithm for simple predictive control was implemented based on the previous model of the test room. The algorithm (see Appendix A.5 Simple MPC Algorithm) solves the energy balance equations of the room and calculates the best setpoint profile of the ten available in order to minimize a cost function (Equation 4.6). The cost function consists of the energy consumption and the discomfort and takes values from 0 to 100. Energy and discomfort are normalized (see Appendix A.3 Energy consumption and Discomfort normalization) with similar process described by Sakellariou (2011).

$$CF = a \times Energy(normalized) + (1-a) \times Discomfort(normalized) \tag{4.6}$$

where α and 1-α are the energy and the discomfort weighting factors respectively. The simple MPC algorithm chooses one of the available scenarios (Table 4-1), which are combinations of different charging and discharging times that minimize the cost function. Five scenarios use linear ramps of

the same duration for charging and discharging. Some of these ramps were also used by Date (Date et al. 2015). However, during the experiments a heuristic control process (see Appendix A.1 Heuristic control experimental results) lead to the result that the linear ramp durations from daytime to nighttime setpoint and vice versa should not always be equal. Initially the goal was to reduce the peak power demand. Controlling the ramp durations was the only way to control the charging and discharging rate of the PCM and release the stored energy at the proper time.

Table 4-1: Available scenarios – Tsp profiles

Tsp profiles		
# Scenario	**Charging ramp duration (h)**	**Discharging ramp duration (h)**
1	**1**	**1**
2	**2**	**2**
3	**3**	**3**
4	**3.5**	**3.5**
5	**3**	**6**
6	**4.5**	**4.5**
7	**4**	**6**
8	**4.5**	**7**
9	**4**	**7.5**
10	**4.5**	**7.5**

A batch file that is executed every 12h runs the model "looking ahead" at a prediction horizon of 3 days (72h); the results are then applied to a control horizon of 12h. The reason for choosing a control horizon of 12h is to allow a full charge and discharge of the PCM. Sakellariou (Sakellariou 2011) showed that the performance of MPC is not affected substantially by the control horizon; it is improved though by increased forecasting accuracy.

The charging and discharging durations that minimize the cost function are then written in an Excel file. Then, the external temperature is updated and the model is executed again. The process is repeated, moving forward in time by a period equal to the control horizon (12h). Every time a scenario is chosen, the values of the charging and discharging ramps are transferred to the variables of the actual controller through BACnet. A second batch file is used to write the outcome of the simple MPC algorithm to the controller 30 min after the execution of the first batch file to avoid any discard time in the whole process. The procedure is summarized in the following flow chart:

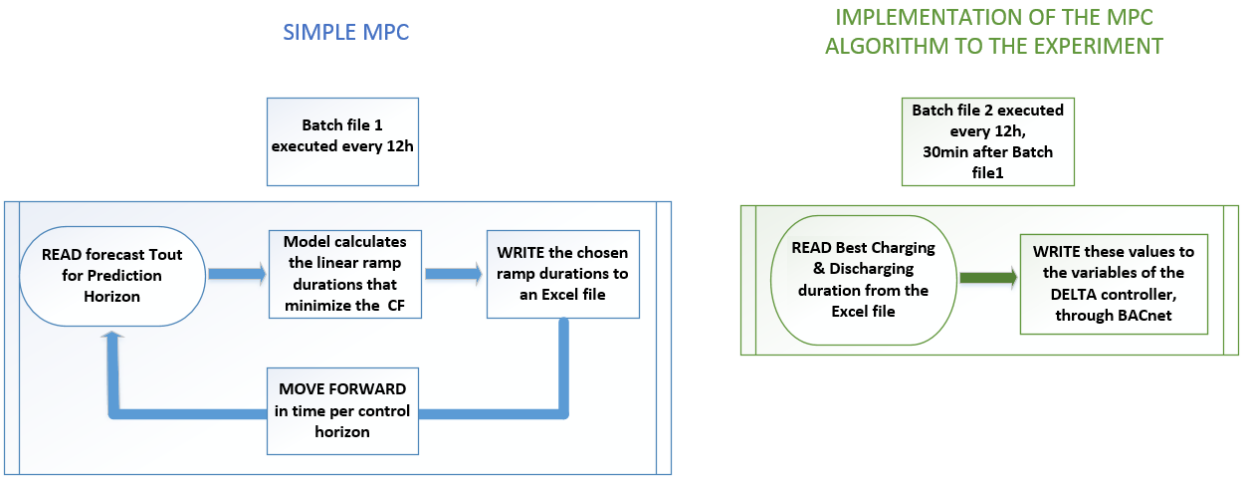

Figure 4-4: Flow chart of simple predictive control and experimental application

Discomfort is calculated (see Appendix A.2 Discomfort Calculation) according to ISO 7730 based on Fanger model and PPD index (ISO7730 2005). The analysis is for the winter months and people's clothing is 1clo. A space of thermal Category C is considered, with activity 70W/m^2, the acceptable operative temperature range is 19-25 °C for the heating season. The cost function is

$$CF = 0.1 \times Energy_{norm} + 0.9 \times Discomfort_{norm} \quad (4.7)$$

where $Energy_{norm}$ and $Discomfort_{norm}$ are the normalized energy and discomfort as described earlier. A similar CF is used by Sakellariou (Sakellariou 2011). Usually a cost function aims to reduce the peak demand, energy consumption and discomfort, or in other words enhance the thermal comfort. Depending on the objective of each case, terms can be added and also their weighting factors may be varied to highlight the importance of every term. In this case, a larger weighting factor is set for discomfort, as it is considered the most important objective. Thermal comfort affects the performance and enables better work productivity (Appleby et al. 2008; Frontczak and Wargocki 2011; Kosonen and Tan 2004a, 2004b; Roelofsen 2015; Simmonds 1993; Yang et al. 2014). The cost of productivity translated in employee's salaries in office buildings may be 10 to 100 times greater than the costs of operation and maintenance of the building (J.E. Skåret 1992; Woods 1989).

The cost function and the external temperature profile were intentionally chosen to illustrate the operation of the algorithm, while respecting the limitations of the experiment. Smoother transitions in the weather or a different CF would cause smaller changes to the room setpoint profile, which corresponds better to realistic conditions. A sensitivity analysis on the weighting factor α is performed (see Appendix A.7 Sensitivity Analysis on Cost Function Weighting Factors) and it

showed that as α increases, the weighting factor of energy increases and the algorithm chooses the profile that minimizes more the energy and less the discomfort term.

The weighting factors of the terms of the cost function depend on the objective of the algorithm. For example, if the space was a solarium, the discomfort would not be so important parameter and higher priority would be given to minimize the energy from the electric heater, combined with the optimal use of the solar gains.

4.3.3 Rationale for a simple heuristic approach

The algorithm presented above is called "simple" since the decision-making process focuses on a small number of available scenarios. All these scenarios share similar profiles with constant values for the daytime and nighttime setpoints and linear ramps for the transitions. A formal MPC algorithm based on mathematical optimization would search for the optimal setpoint profile minimizing the cost function without restricting the number of possible solutions nor the shape of the setpoint profile.

This simple approach, however, is practical and is based on an understanding of the physics of the problem. The PCM-TES used in this experiment cannot be turned "on" or "off". The proposed setpoint scenarios take into account the time and the amount of energy that can be stored in the system and later released gradually. Finally, the proposed algorithm could easily be implemented in a programmable thermostat, without requiring too much processor speed and memory capacity.

4.4 Control implementation and BACnet communication

The test room uses a DELTA controller box (Delta Controls 2016) that controls the electric heater and the plenum fan in the room. The controller was installed from Regulvar Inc. (Regulvar Inc. 2016) and was programmed in GCL+. A batch file is executed every 12h (corresponding to the

control horizon); this file executes the model in MATLAB to calculate and compare the performance of the different charging and discharging ramp durations.

A second batch file is executed half an hour after the first one. The purpose of this file is to write the chosen charging and discharging ramps in the analog variables of the controller through BACnet Stack (ASHRAE 2016a, 2016b). The MATLAB code (see Appendix A.6 BACnet Stack Demo Tools) that enables this communication uses BACnet Stack Demo Tools, specifically the read and write objects properties with the **bacrp** and **bacwp** tools. Some object properties need to be entered in the command. These properties include the device instance (i.e. which device on the network), object type (analog input, binary input, analog variable etc.), object instance (i.e. which analog input) and the property (present value, object name, status flags etc.).

4.5 Results and discussion

This section includes:

- An initial assessment of experimental results comparing the peak power obtained with the use of linear ramps versus step changes for the room air temperature setpoint.
- Simulation results of the heuristic predictive control under varying outdoor temperature profiles.
- Comparison of numerical and experimental results of the predictive control algorithm showing also the validation of the room model.

4.5.1 Use of linear ramps

The purpose of using linear ramps for the transition between night time and day time setpoints is to reduce and shift the peak power demand. The following figures present the effect of a linear ramp on peak power as compared to a step change, which is the case that is most commonly used

in buildings. Figure 4-5 shows the results for the power of the electric heater (green solid line) and the temperature in the room with the PCM wall (red dashed line) when the temperature setpoint increases from 16.5 °C to 25 °C with a step change. Figure 4-6 shows the results with linear ramps; it is clear that the use of linear ramps (4.5h charging and 7h discharging in this case) lead to a significant reduction in peak power demand (19.5%) and shifting of about 35min. In both cases, the imposed "outdoor" temperature (blue dotted line) follows a sinusoidal profile fluctuating between -10 °C to 0 °C, with a 24 h period, peaking at 3pm.

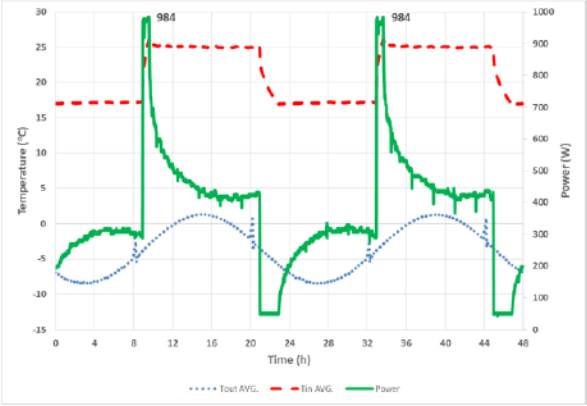

Figure 4-5: Experimental results of step change for Tsp

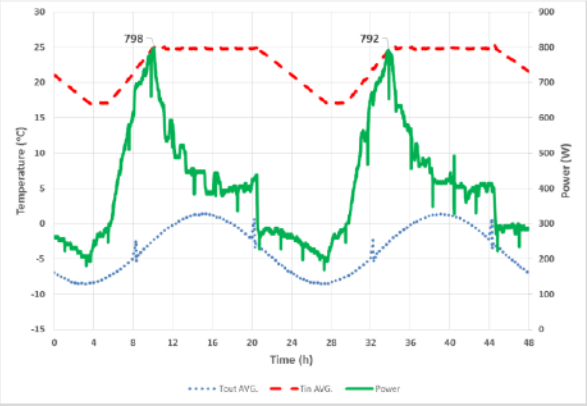

Figure 4-6: Experimental results of Linear ramps: 4.5h charging and 7h discharging

4.5.2 Simple MPC

Three different external temperature profiles were simulated and tested in the lab to demonstrate the operation of the algorithm. The environmental chamber is used to impose sinusoidal "outdoor" temperature profiles, described by three parameters: (a) mean temperature; (b) peak-to-peak wave amplitude (i.e., difference between maximum and its minimum temperatures); (c) the time of the maximum temperature.

The algorithm finds the minimum cost function among 10 different scenarios of charging and discharging time. These scenarios use linear ramps for the transition between daytime and nighttime setpoint. The available profiles, that the algorithm solves, are profiles that can be used in a programmable thermostat, without significant memory and processor capacity. They are profiles that correspond to reality and can be applied in buildings to reduce peak power demand and energy consumption while maintaining occupancy comfort. For the specific case study, though, some profiles were tested with longer charging and discharging periods (e.g. 4.5h charging and 7.5h discharging), in order to take advantage of the PCM and the energy that can be stored and released at specific time and with a specific rate depending also on the external temperature conditions. The simulated results for 3 days are presented in Table 4-2. Figure 4-7 and Figure 4-8 show the temperature profiles and the power of the heater.

Table 4-2: Simulation parameters and results for 3 days

Experiment Progress		**External T Profile**		**Best Scenario Chosen**	
Control horizon (12 h step)	**Time (h)**	**Tout mean (°C)**	**Tout p-p amplitude (°C)**	**Charging ramp dur. (h)**	**Discharging ramp dur. (h)**
1st	**1-12**	**-5**	**10**	**4.5**	**7.5**
2nd	**13-24**	**-5**	**10**	**4.5**	**7.5**
3rd	**25-36**	**0**	**5**	**3**	**6**
4th	**37-48**	**0**	**5**	**3**	**6**
5th	**49-60**	**2.5**	**5**	**1**	**1**
6th	**61-72**	**2.5**	**5**	**1**	**1**

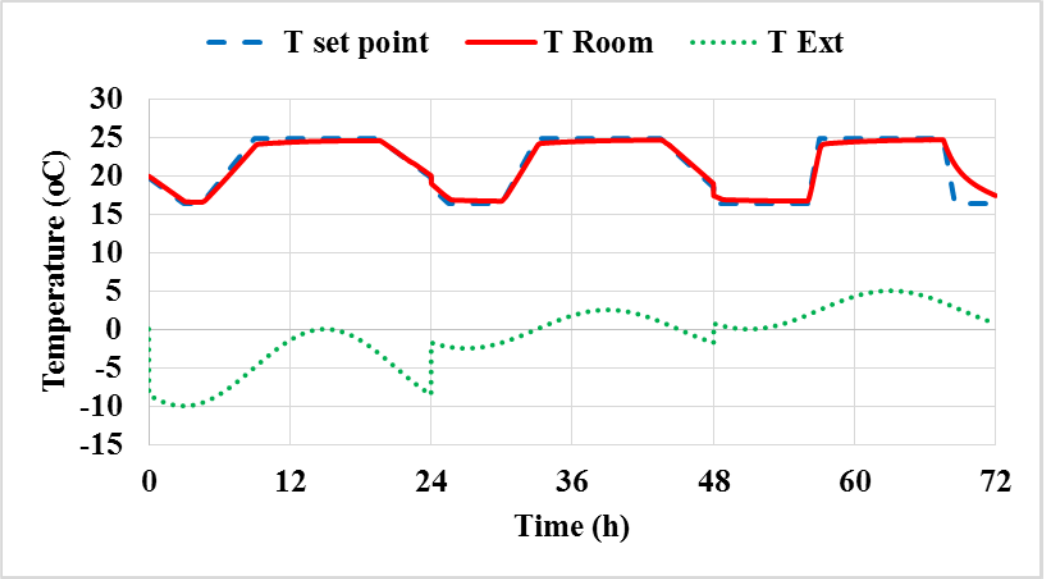

Figure 4-7: Simulation results of setpoint, room and ambient temperature profiles for 3 days

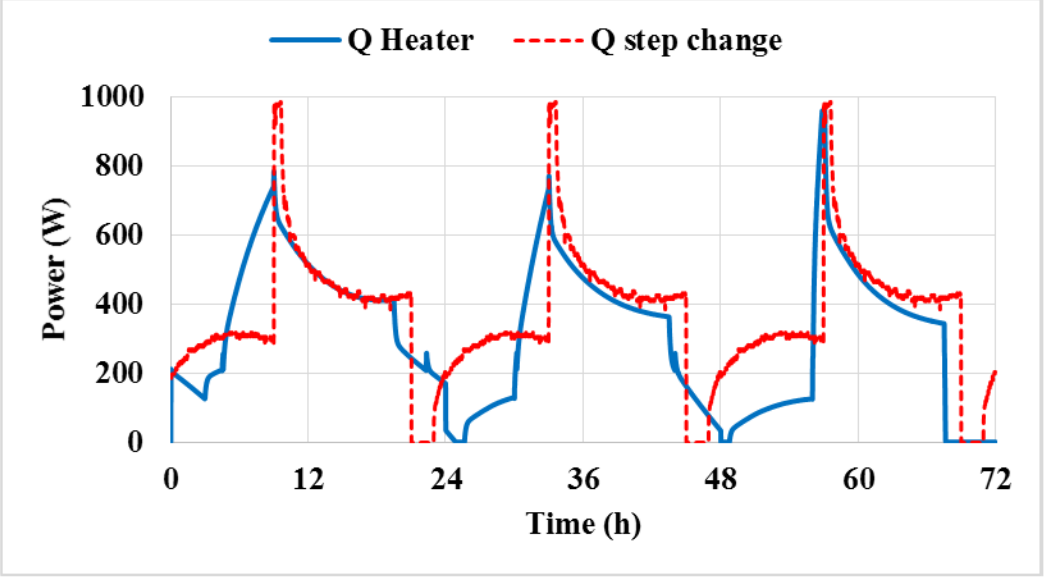

Figure 4-8: Simulation results for power of the electrical heater for 3 days

When the ambient temperature changes, the algorithm adjusts the setpoint profile to minimize the cost function. Figure 4-9 shows the performance of the selected cost function. The cost function that was used here, leads also to reduction of peak power demand compared with the case of step change, when the peak power demand is 984W. The results show 20.4% reduction the first day and 21.6% the second day. There is no peak power demand reduction the last day, as the algorithm uses 1h linear ramps to minimize the cost function. Moreover, the room air temperature follows the different set point profiles that the algorithm chooses every day according to the specific cost function.

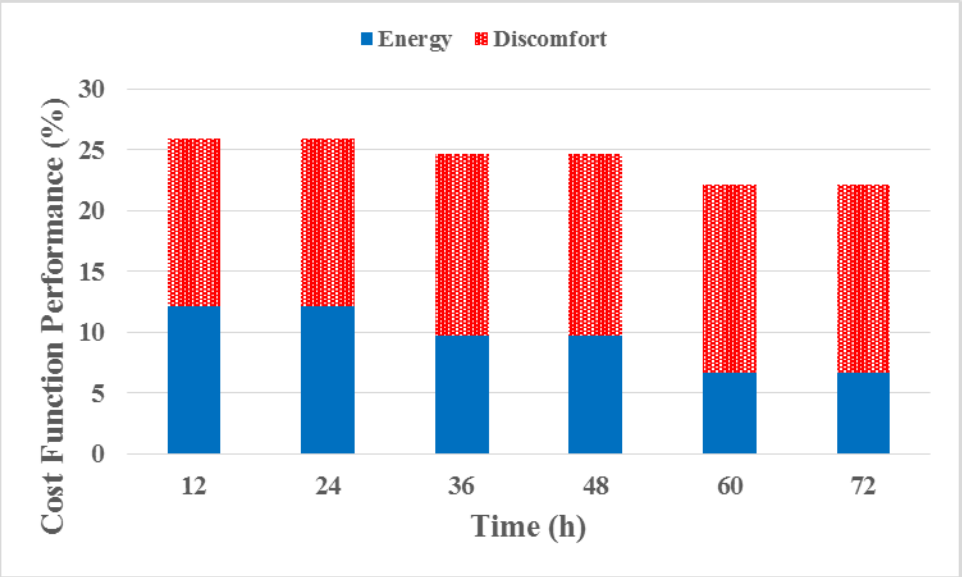

Figure 4-9: Simulation results of the cost function for 3 days

4.5.3 Model Validation

The simulated T_{out} profile was applied in the SSEC laboratory and the results of the power of the heater for the model and the experiment are presented in the following Figure 4-10. As can be seen the modelled and the experimental are in good agreement.

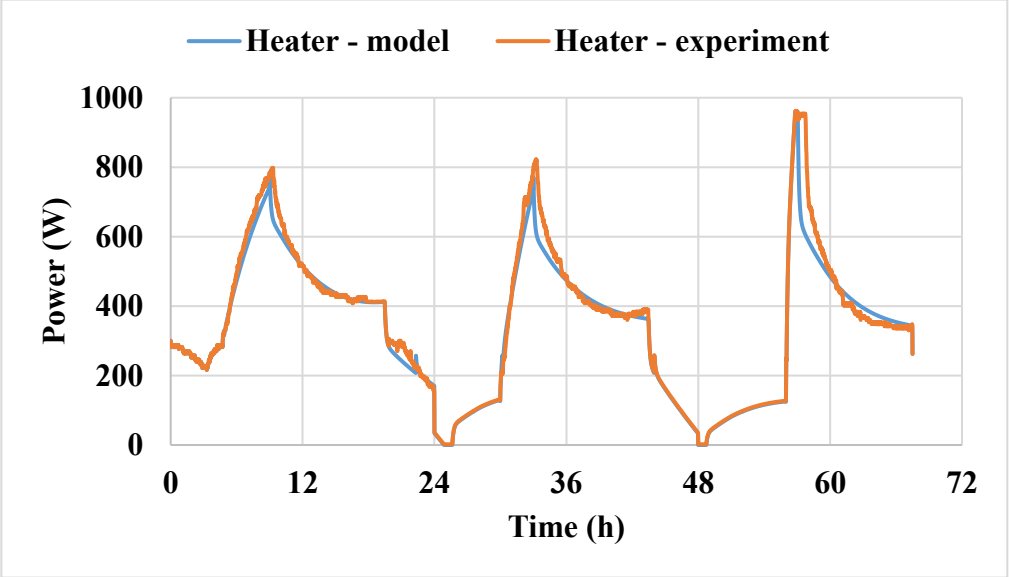

Figure 4-10: Modeled and experimental results of simple MPC for the power of the heater

Figure 4-11 shows the modeled and experimental data of the room air temperature. The maximum difference between the experimental and the simulated values is 1.6 °C.

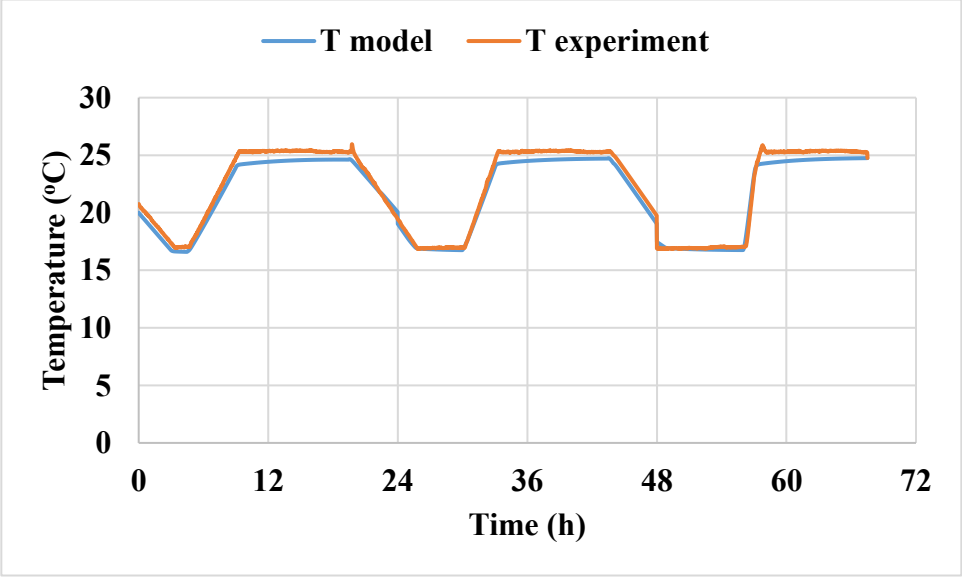

Figure 4-11: Modeled and experimental results of simple MPC for the power of the heater

Statistical indices of the coefficient of variation of the root-mean-square error (CV-RSME) and normalized mean bias error (NMBE) provide additional information about the performance of the model. According to ASHRAE Guideline 14, a maximum CV-RMSE of 30% and NMBE of 10% on an hourly basis ensures a calibrated model when the whole-building energy use is compared (ANSI/ASHRAE 2002). Table 3 shows that the model is calibrated.

Table 4-3: Model calibration according to ASHRAE Guideline 14

Calibrated parameter	CV-RSME (%)	NMBE (%)
Power of the Heater	28.2%	3.4%
Guideline 14 (ASHRAE 2002)	30%	10%

The maximum difference between the simulated and the measured temperature in the test room is 1.6 °C. The temperature in the test room was measured with thermocouples type T, with ±0.5 °C (Dermardiros 2015).

4.6 Summary

This chapter documents simulation studies and data from experiments with simple predictive control strategies intended to reduce and shift peak load in a perimeter zone which uses phase change materials for thermal storage. It also shows how a low-order thermal network can be used as an effective tool in the design of the MPC strategy. The process can be easily implemented in a programmable thermostat, providing the final user a more comfortable and less energy expensive environment. The thermostat, instead of trying to reach the desired value, through a classic control process, will take into account the building thermal mass and the expected weather conditions and choose the best one of some anticipatory actions.

5 Conclusion

In this thesis predictive control strategies were investigated with different thermal mass configurations. Thermal mass can store thermal energy and release it later, reducing the peak power demand and the energy consumption of the building. It can also minimize the temperature fluctuations in a space by absorbing excessive heat and it that way enhancing thermal comfort. The type and amount of thermal mass as well as its thermal coupling with the space are important parameters defining the rate of heat exchange. The controls that are commonly used in buildings are feedback controllers (e.g. PI controllers) and are unable to control slow responding systems. Model-based predictive control (MPC) is a promising approach that takes into account the thermal inertia of the space. The present study investigated two approaches and case studies with different type of thermal mass (concrete versus phase change materials).

The first case study describes a perimeter office zone with radiant floor heating system and a chilled beam. The thermal mass is concrete and it is covered with a carpet. The effect of the carpet on peak and total load is investigated through predictive control strategies with use linear ramps for the setpoint change by comparing the response of the zone with and without carpet covering the concrete. The carpet also affects the temperature fluctuations in the room. Two models are tested; a simplified one with 2 control volumes in the floor and combined heat transfer coefficients, constant with time and a more detailed model which separates the heat transfer coefficients in convective and radiative part and calculates them every time step depending on the temperature of the surfaces in the zone. Finally a sensitivity analysis is performed, varying the window-to-wall (WWR) ratio and type of floor covering. The results for peak and total heating/cooling load are presented.

The second case study considered a test room with phase change materials (PCMs) integrated into its back wall. An air channel between the PCM panels and a plenum fan on the ceiling allow the active charge and discharge of the material. Experiments have been conducted in a large scale environmental chamber to help us develop a calibrated simple model of the system and establish the charging and discharging rate under different outdoor temperature profiles. A numerical model is created for the test cell simulating a predictive control algorithm. Then this algorithm is implemented in the environmental chamber using BACnet Stack Demo Tools. The numerical and experimental data are in good agreement.

5.1 Main contributions

Simulation results have shown that an exposed floor leads to significant lower peak (35% in cooling and 41% in heating mode) and total (16% in cooling and 56% in heating mode) load compared to a carpeted floor. An exposed floor may also reduce the temperature fluctuations in the room significantly. Carpet can be replaced by tiles which have similar effect on peak and total load with the exposed concrete. Other materials may offer alternative solutions, depending on their thermal properties.

Increasing the model resolution, it was shown that calculating separately the convective and radiative heat transfer coefficients has a significant effect on peak heating/cooling (16% reduction in cooling and 5% increase in heating mode) and total heating/cooling load (12% decrease in cooling and 16% increase in heating mode) compared to the simplified model. The simplified model uses combined heat transfer coefficients constant with temperature. The detailed model varies them every time step depending on the temperature of each surface.

A low order model of a test room which uses PCM was developed in MATLAB. This model was used in predictive control which was applied in the experimental facility showing that it can predict accurately the peak power demand (CV-RSME 28.2% and NMBE 3.4%) and the room air temperature.

5.2 Future Work

The model of the PCM test room, which was presented in chapter 4, can be extended to consider external conditions. Spaces like the one in this paper, may be used as solariums. The PCM can be charged using solar energy and release the stored energy to a neighboring space at a later time to reduce the peak load of a heating system.

Moreover, the simple MPC algorithm can be tested to spaces with different thermal mass configurations (exposed concrete floor, carpeted floor, radiant floor hating system, carpeted floor with furniture on top of it etc.). The thermal mass would be the add-on to the same algorithm, creating templates for the same type of rooms. These templates can be easily implemented in Simulink for better representation. Finally, having similar spaces in terms of thermal inertia, it would be easier to have some pre-loaded scenarios, like the ones presented in this study, in a programmable thermostat to save energy and improve occupants comfort.

The pre-calculated actions may form lookup tables that are derived from offline MPC. This will show the potential of energy storage of its system and may improve the current control strategies. Then optimization of this results combined with accurate forecast weather data and occupancy profiles will lead to full MPC implementation in building automation systems.

References

Afram, Abdul and Farrokh Janabi-Sharifi. 2014. “Theory and Applications of HVAC Control Systems - A Review of Model Predictive Control (MPC).” *Building and Environment* 72:343–55.

ANSI/ASHRAE. 2002. “ASHRAE Guideline 14-2002 Measurement of Energy and Demand Savings.” *Ashrae* 8400:170.

ANSI/ASHRAE. 2007. *ANSI/ASHRAE/IESNA Standard 90.1*.

Appleby, Paul, Guy Newsham, Derek Clements-croome, and Ashak Nathwani. 2008. “Research Note - Thermal Comfort.”

Ascione, Fabrizio, Nicola Bianco, Claudio De Stasio, Gerardo Maria Mauro, and Giuseppe Peter Vanoli. 2016. “Simulation-Based Model Predictive Control by the Multi-Objective Optimization of Building Energy Performance and Thermal Comfort.” *Energy and Buildings* 111:131–44.

ASHRAE. 2007. *Thermal Storage. ASHRAE Handbook - HVAC Applications. SI Ed. Atlanta, GA, US: American Society of Heating Refrigerating and Air-Conditioning Engineers (ASHRAE)*.

ASHRAE. 2009. *ASHRAE Handbook - Fundamentals. SI Ed. Atlanta, GA, US: American Society of Heating Refrigerating and Air-Conditioning Engineers (ASHRAE)*.

ASHRAE. 2010. “Standard 55-2010. Thermal Environmental Conditions for Human Occupancy.Atlanta: American Society of Heating Refrigerating and Air Conditioning Engineers.”

ASHRAE. 2016a. “BACnet.” Retrieved June 15, 2016 (http://www.bacnet.org/).

ASHRAE. 2016b. “BACnet Stack.” Retrieved June 15, 2016 (http://bacnet.sourceforge.net/).

Athienitis, A. K., C. Liu, D. Hawes, D. Banu, and D. Feldman. 1997. “Investigation of the Thermal Performance of a Passive Solar Test-Room with Wall Latent Heat Storage.” *Building and Environment* 32(5):405–10.

Athienitis, A. K. and W. O’Brien. 2015. *Modeling, Design, and Optimization of Net-Zero Energy Buildings*. Ernst & Sohn.

Athienitis, A. K. and A. Tzempelikos. 2002. “A Methodology for Simulation of Daylight Room Illuminance Distribution and Light Dimming for a Room with a Controlled Shading Device.” *Solar Energy* 72(4):271–81.

Athienitis A.K. and Santamouris M. 2002. *Thermal Analysis and Design of Passive Solar Buildings*. London UK.: James and James.

AUTODESK. 2016. “SUSTAINABILITY WORKSHOP-Human Thermal Comfort.” Retrieved September 10, 2016 (http://sustainabilityworkshop.autodesk.com/buildings/human-thermal-comfort).

Balaras, C. A. 1996. “The Role of Thermal Mass on the Cooling Load of Buildings. An Overview of Computational Methods.” *Energy and Buildings* 24:1–10.

Braun, James. 2003. “Load Control Using Building Thermal Mass.” *Solar Energy Engineering* 125(August):292–301.

Buonomano, Annamaria, Umberto Montanaro, Adolfo Palombo, and Stefania Santini. 2014. “Indoor Air Temperature Control in Buildings via an Optimal Tuned PI Strategy.” *International Journal of Engineering and Innovative Technology (IJEIT)* 4(4).

Caliskan, Hakan, Ibrahim Dincer, and Arif Hepbasli. 2012. "Thermodynamic Analyses and Assessments of Various Thermal Energy Storage Systems for Buildings." *Energy Conversion and Management* 62:109–22.

Camacho, E. F. and C. Bordons. 2003. *Model Predictive Control*. 2nd ed. edited by E. F. Camacho and C. Bordons. Springer.

Candanedo, J. A., S. Bucking, A. Allard, and A. K. Athienitis. 2011. "Model-Based Predictive Control Applications for Solar Homes and Communities." 1–31.

Candanedo, J. A., V. R. Dehkordi, and P. Lopez. 2013. "A Control-Oriented Simplified Building Modelling Strategy." *Proceedings of BS2013: 13th Conference of International Building Performance Simulation Association, Chambery, France, Aug. 26-28* 3682–89.

Candanedo, J. A., V. R. Dehkordi, A. Saberi-Derakhtenjani, and A. K. Athienitis. 2015. "Near-Optimal Transition between Temperature Setpoints for Peak Load Reduction in Small Buildings." *Energy and Buildings* 87:123–33.

Candanedo, J. A., V. R. Dehkordi, and M. Stylianou. 2013. "Model-Based Predictive Control of an Ice Storage Device in a Building Cooling System." *Applied Energy* 111:1032–45.

Chen, Yuxiang. 2013. "Methodology for Design and Operation of Active Building- Integrated Thermal Energy Storage Systems." Ph.D. Thesis, Concordia University, Montreal, Canada.

Concordia University. 2011. "Concordia University Launches the Solar Simulator-Environmental Chamber and NSERC Smart Net-Zero Energy Buildings Strategic Network." Retrieved June 21, 2016 (http://www.concordia.ca/content/shared/en/news/main/releases/2011/12/15/concordia-

university-launches-the-solar-simulator-environmental-chamber-and-nserc-smart-net-zero-ene.html).

Concordia University. 2014. “Solar Buildings Research Network.” Retrieved June 21, 2016 (http://www.solarbuildings.ca/index.php/en/).

Corbin, Charles D., Gregor P. Henze, and Peter May-Ostendorp. 2012. “A Model Predictive Control Optimization Environment for Real-Time Commercial Building Application.” *Journal of Building Performance Simulation* 1493(March 2014):1–16.

Date, J. A. 2015. “A Study of Impact of Thermal Model Resolution and Zone Set Point Profiles on Peak Heating Load and Its Calculation.” Master’s Thesis, Concordia University, Montreal, Canada.

Date, J. A., A. K. Athienitis, and M. Fournier. 2015. “A Study of Temperature Set Point Strategies for Peak Power Reduction in Residential Buildings.” *ScienceDirect* 0:6–11.

Delta Controls. 2016. “Delta Controls.” Retrieved June 15, 2016 (https://www.deltacontrols.com/).

Dermardiros, V. 2015. “Modelling and Experimental Evaluation of an Active Thermal Energy Storage System with Phase-Change Materials for Model-Based Control.” Master’s Thesis, Concordia University.

Dermardiros, V. and A. K. Athienitis. 2015. “Comparison of PCM-Active Thermal Storage Systems Integrated in Building Enclosures.” in *10th Conference on Advanced Building Skins*. Bern, Switzerland.

Dermardiros, V. and A. K. Athienitis. 2016. “BUILDING-INTEGRATED PCM-TES FOR PEAK

LOAD REDUCTION." Pp. 380–86 in *eSim 2016 - Conference Proceedings*. Hamilton, ON.

Dermardiros, V., A. Daoud, Y. Chen, and A. K. Athienitis. 2016. "Development of Reduced-Order Thermal Models of Building-Integrated Active PCM-TES." *ASHRAE Transactions* 122:267–77.

Dincer, I. 2002. "On Thermal Energy Storage Systems and Applications in Buildings." *Energy and Buildings* 34(4):377–88.

Dincer, I., S. Dost, and X. Li. 1997. "Performance Analysis of Sensible Heat Storage Systems for Thermal Applications." *International Journal of Energy Research* 21:1150–71.

Dincer, I. and M. A. Rosen. 2001a. "Energetic, Environmental and Economic Aspects of Thermal Energy Storage Systems for Cooling Capacity." *Applied Thermal Engineering* 21(11):1105–17.

Dincer, I. and M. A. Rosen. 2001b. *Thermal Energy Storage Systems and Applications*. London: Wiley.

DOE US. 2016. "Buildings Energy Data Book." Retrieved September 10, 2016 (http://buildingsdatabook.eren.doe.gov).

Eurostat. 2016. "Russia-EU – Basic Statistical Indicators." Retrieved September 10, 2016 (http://ec.europa.eu/eurostat/statistics-explained).

Fernandes, D., F. Pitié, G. Cáceres, and J. Baeyens. 2012. "Thermal Energy storage: 'How Previous Findings Determine Current Research Priorities.'" *Energy* 39(1):246–57.

Frontczak, Monika and Pawel Wargocki. 2011. "Literature Survey on How Different Factors Influence Human Comfort in Indoor Environments." *Building and Environment* 46(4):922–

37.

Fukai, Jun, Makoto Kanou, Yoshikazu Kodama, and Osamu Miyatake. 2000. “Thermal Conductivity Enhancement of Energy Storage Media Using Carbon Fibers.” *Energy Conversion and Management* 41(14):1543–56.

Gaiddon, B., Kaan, H., & Munro, D. n.d. *Photovoltaics in the Urban Environment: Lessons Learnt from Large-Scale Projects*. (1st ed.). London, UK: Earthscan.

La Gennusa, M. et al. 2010. “Multi-Agent Systems as Effective Tools for the User-Based Thermal Comfort: An Introduction.” *World Applied Science Journal* 10(2):179–95.

Gunay, B. and W. O’Brien. 2016. “Implementation and Comparison of Existing Occupant Behaviour Models in EnergyPlus.” *Journal of Building Performance Simulation* 1493(January).

Haldi, F. and D. Robinson. 2011. “The Impact of Occupants’ Behaviour on Building Energy Demand.” *Journal of Building Performance Simulation* 4(4):323–38.

Hu, Jianjun and Panagiota Karava. 2014. “Model Predictive Control Strategies for Buildings with Mixed-Mode Cooling.” *Building and Environment* 71:233–44.

I, Gail S.Brager and Richard J. De Dear. 1998. “Thermal Adaptation in the Built Environment : A Literature Review.” *Energy and Buildings* 27:83–96.

Ismail, K. A. R. and J. Henriquez. 2001. “Thermally Effective Windows with Moving Phase Change Material Curtains.” *Applied Thermal Engineering* 21(18):1909–23.

ISO7730. 2005. “ISO 7730:2005 Ergonomics of the Thermal Environment -- Analytical Determination and Interpretation of Thermal Comfort Using Calculation of the PMV and

PPD Indices and Local Thermal Comfort Criteria."

J.E. Skåret. 1992. *"Indoor Environment and Economics", Project No. N 6405*. Oslo.

Kosonen, R. and F. Tan. 2004a. "Assessment of Productivity Loss in Air-Conditioned Buildings Using PMV Index." *Energy and Buildings* 36(10 SPEC. ISS.):987–93.

Kosonen, R. and F. Tan. 2004b. "The Effect of Perceived Indoor Air Quality on Productivity Loss." *Energy and Buildings* 36(10 SPEC. ISS.):981–86.

Kummert, Michaël, Marie-andrée Leduc, and Alain Moreau. 2011. "Using MPC to Reduce the Peak Demand Associated with Electric Heating." *Context*.

Kuznik, F. and J. Virgone. 2009. "Experimental Assessment of a Phase Change Material for Wall Building Use." *Applied Energy* 86(10):2038–46.

Lee, Kyoung ho and James E. Braun. 2008. "Development of Methods for Determining Demand-Limiting Setpoint Trajectories in Buildings Using Short-Term Measurements." *Building and Environment* 43(10):1755–68.

Leea, Kyoung-Ho and James E. Braun. 2008. "Evaluation of Methods for Determining Demand-Limiting Setpoint Trajectories in Buildings Using Short-Term Measurements." *Building and Environment* 43:1769–1783.

Lehrer, D. and J. Vasudev. 2010. "Visualizing Information to Improve Building Performance: A Study of Expert Users." in *ACEEE Summer Study on Energy Efficiency in Buildings*.

Li, Xiwang and Ali Malkawi. 2016. "Multi-Objective Optimization for Thermal Mass Model Predictive Control in Small and Medium Size Commercial Buildings under Summer Weather Conditions." *Energy* 112:1194–1206.

Li, Xiwang and Jin Wen. 2014. “Review of Building Energy Modeling for Control and Operation.” *Renewable and Sustainable Energy Reviews* 37:517–37.

Ma, Yudong, A. Kelman, A. Daly, and F. Borrelli. 2012. “Predictive Control for Energy Efficient Buildings with Thermal Storage: Modeling, Simulation, and Experiments.” *IEEE Control Systems* 32(1):44–64.

Manning, M. M., M. C. Swinton, F. Szadkowski, and K. Gusdorf, J.; Ruest. 2007. “The Effects of Thermostat Setting on Seasonal Energy Consumption at the CCHT Twin House Facility.” *ASHRAE Transactions* 113(1):1–12.

Mathworks. 2016. “MATLAB.” Retrieved (https://www.mathworks.com/).

May-Ostendorp, Peter, Gregor P. Henze, Charles D. Corbin, Balaji Rajagopalan, and Clemens Felsmann. 2011. “Model-Predictive Control of Mixed-Mode Buildings with Rule Extraction.” *Building and Environment* 46(2):428–37.

McAdams. 1959. *Heat Transmission*. 3rd ed. McGraw-Hill.

Merker, O., F. Hepp, A. Beck, and J. Fricke. 2002. “A New Solar Shading System with Phase Change Material (PCM).” in *Proceedings of the World Renewable Energy Congress WII*. Cologne (Germany).

Michailidis, Iakovos T., Simone Baldi, Martin F. Pichler, Elias B. Kosmatopoulos, and Juan R. Santiago. 2015. “Proactive Control for Solar Energy Exploitation: A German High-Inertia Building Case Study.” *Applied Energy* 155:409–20.

Moon, Jin Woo and Seung Hoon Han. 2011. “Thermostat Strategies Impact on Energy Consumption in Residential Buildings.” *Energy and Buildings* 43(2–3):338–46.

Moroşan, Petru-Daniel, Romain Bourdais, Didier Dumur, and Jean Buisson. 2010. "Building Temperature Regulation Using a Distributed Model Predictive Control." *Energy and Buildings* 42(9):1445–52.

Natural Resources Canada. 2013. *Energy Use Data Handbook: 1990 to 2010*.

Nicol, J. F. and M. A. Humphreys. 2002. "Adaptive Thermal Comfort and Sustainable Thermal Standards for Buildings." *Energy and Buildings* 34(6):563–72.

Oldewurtel, Frauke et al. 2010. "Increasing Energy Efficiency in Building Climate Control Using Weather Forecasts and Model Predictive Control." *REHVA World Congress Clima* 8pp.

Oldewurtel, Frauke et al. 2012. "Use of Model Predictive Control and Weather Forecasts for Energy Efficient Building Climate Control." *Energy and Buildings* 45:15–27.

Olesen, Bjarne W. 2002. "Radiant Floor Heating in Theory and Practice." *ASHRAE Journal* 44(July):19–26.

Parameshwaran, R., S. Kalaiselvam, S. Harikrishnan, and A. Elayaperumal. 2012. "Sustainable Thermal Energy Storage Technologies for Buildings: A Review." *Renewable and Sustainable Energy Reviews* 16(5):2394–2433.

Peffer, Therese, Marco Pritoni, Alan Meier, Cecilia Aragon, and Daniel Perry. 2011. "How People Use Thermostats in Homes: A Review." *Building and Environment* 46(12):2529–41.

Peng Xu, P. E. 2009. "Case Study of Demand Shifting with Thermal Mass in Two Large Commercial Buildings." *ASHRAE Transactions* 115 PART 2:586–98.

Prívara, Samuel et al. 2013. "Building Modeling as a Crucial Part for Building Predictive Control." *Energy and Buildings* 56:8–22.

Py, Xavier, Régis Olives, and Sylvain Mauran. 2001. "Paraffin/porous-Graphite-Matrix Composite as a High and Constant Power Thermal Storage Material." *International Journal of Heat and Mass Transfer* 44(14):2727–37.

Regulvar Inc. 2016. "Regulvar." Retrieved June 15, 2016 (http://www.regulvar.com/en).

Reinhart, Christoph F. 2004. "Lightswitch-2002: A Model for Manual and Automated Control of Electric Lighting and Blinds." *Solar Energy* 77(1):15–28.

Reinhart, Christoph F., John. Mardaljevic, and Zack. Rogers. 2013. "Dynamic Daylight Performance Metrics for Sustainable Building Design." *The journal of the illuminating Engineering Society of North America* 3(1):7–31.

Roelofsen, Paul. 2015. "A Computer Model for the Assessment of Employee Performance Loss as a Function of Thermal Discomfort or Degree of Heat Stress." *Intelligent Buildings International* 8975(June):1–20.

Sakellariou, F. 2011. "Model Predictive Control for Thermally Activated Building Systems." Master's Thesis, Technische Universiteit Eindhoven.

Sattari, S. and B. Farhanieh. 2006. "A Parametric Study on Radiant Floor Heating System Performance." *Renewable Energy* 31(10):1617–26.

Seo, Jungki, Jisoo Jeon, Jeong Hun Lee, and Sumin Kim. 2011. "Thermal Performance Analysis according to Wood Flooring Structure for Energy Conservation in Radiant Floor Heating Systems." *Energy and Buildings* 43(8):2039–42.

Sharma, Atul, V. V. Tyagi, C. R. Chen, and D. Buddhi. 2009. "Review on Thermal Energy Storage with Phase Change Materials and Applications." *Renewable and Sustainable Energy Reviews*

13(2):318–45.

Shen, Hui and Athanasios Tzempelikos. 2012. “Daylighting and Energy Analysis of Private Offices with Automated Interior Roller Shades.” *Solar Energy* 86(2):681–704.

Simmonds, P. 1993. “Thermal Comfort and Optimal Energy Use.” in *ASHRAE Transactions: Symposia*.

Široky, Jan, Frauke Oldewurtel, Jirí Cigler, and Samuel Prívara. 2011. “Experimental Analysis of Model Predictive Control for an Energy Efficient Building Heating System.” *Applied Energy* 88(9):3079–87.

Sturzenegger, David, Dimitrios Gyalistras, Manfred Morari, and Roy S. Smith. 2016. “Model Predictive Climate Control of a Swiss Office Building.” *Implementation, Results, and Cost–Benefit Analysis* 24(1):1–12.

Taleghani, Mohammad, Martin Tenpierik, Stanley Kurvers, and Andy Van Den Dobbelsteen. 2013. “A Review into Thermal Comfort in Buildings.” *Renewable and Sustainable Energy Reviews* 26:201–15.

Telkes, M. 1975. “Thermal Storage for Solar Heating and Cooling.” in *Proceedings of the Workshop on Solar Energy Storage Subsystems for the Heating and Cooling of Buildings*. Charlottesville (Virginia, USA).

Tyagi, Vineet Veer and D. Buddhi. 2007. “PCM Thermal Storage in Buildings: A State of Art.” *Renewable and Sustainable Energy Reviews* 11(6):1146–66.

Villafana, Luis and Clifford C. Federspiel. 2003. “Design of an Energy and Maintenance System User Interface for Building Occupants.” *ASHRAE Transactions* 109(2):665–76.

Wienold, Jan. 2007. “Dynamic Simulation of Blind Control Strategies for Visual Comfort and Energy Balance Analysis.” *IBPSA 2007 - International Building Performance Simulation Association 2007* 1197–1204.

WIKIPEDIA. 2016. “Flooring - WIKIPEDIA.” Retrieved June 18, 2016 (https://en.wikipedia.org/wiki/Flooring).

Wolisz, Henryk, Tuule Mall Kull, Rita Streblow, and Dirk Müller. 2015. “The Effect of Furniture and Floor Covering Upon Dynamic Thermal Building Simulations.” *Energy Procedia* 78:2154–59.

Woods, J. E. 1989. “Cost Avoidance and Productivity in Owning and Operating Buildings.” *Occup Med* 4(4):753–70.

Yang, Liu, Haiyan Yan, and Joseph C. Lam. 2014. “Thermal Comfort and Building Energy Consumption Implications - A Review.” *Applied Energy* 115:164–73.

Zalba, Belén, José Ma Marín, Luisa F. Cabeza, and Harald Mehling. 2003. *Review on Thermal Energy Storage with Phase Change: Materials, Heat Transfer Analysis and Applications*.

Zhang, Rui and Khee Poh Lam. 2011. “Comparison of Building Load Performance between First Principle Based and Implementable Shading Control Algorithms.” *Building Simulation* 4(2):135–48.

Appendices

A.1 Heuristic control experimental results

The experiments initially tested different outdoor temperature profiles and varying linear ramp durations for the room setpoint in order to get the dynamic response of the system under the desired conditions. The following figures show the average temperature of each layer of the PCM, during charging. The material was considered fully charged (melted) when the outer layer (layer A) reached temperature above 22ºC.

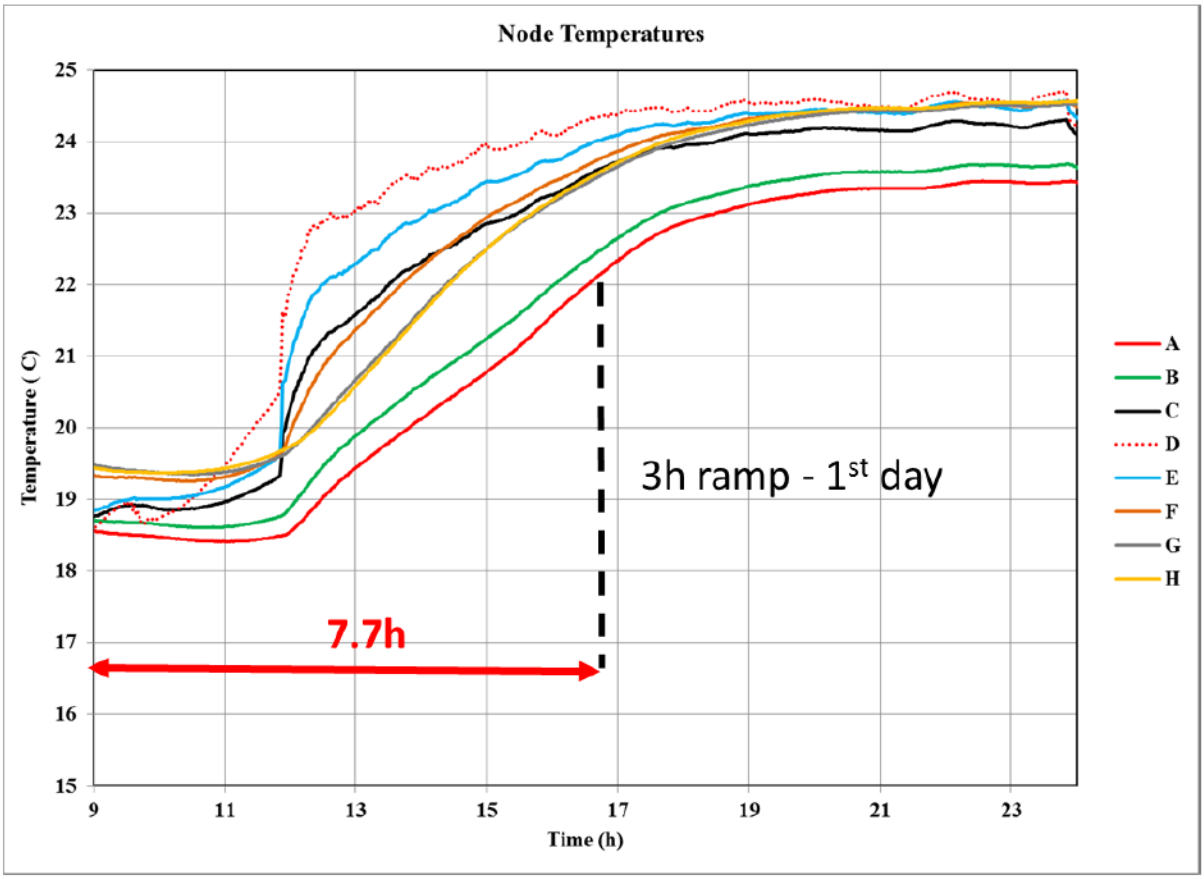

Figure A-1: Average temperature of the PCM layers - Charging with a 3h linear ramp

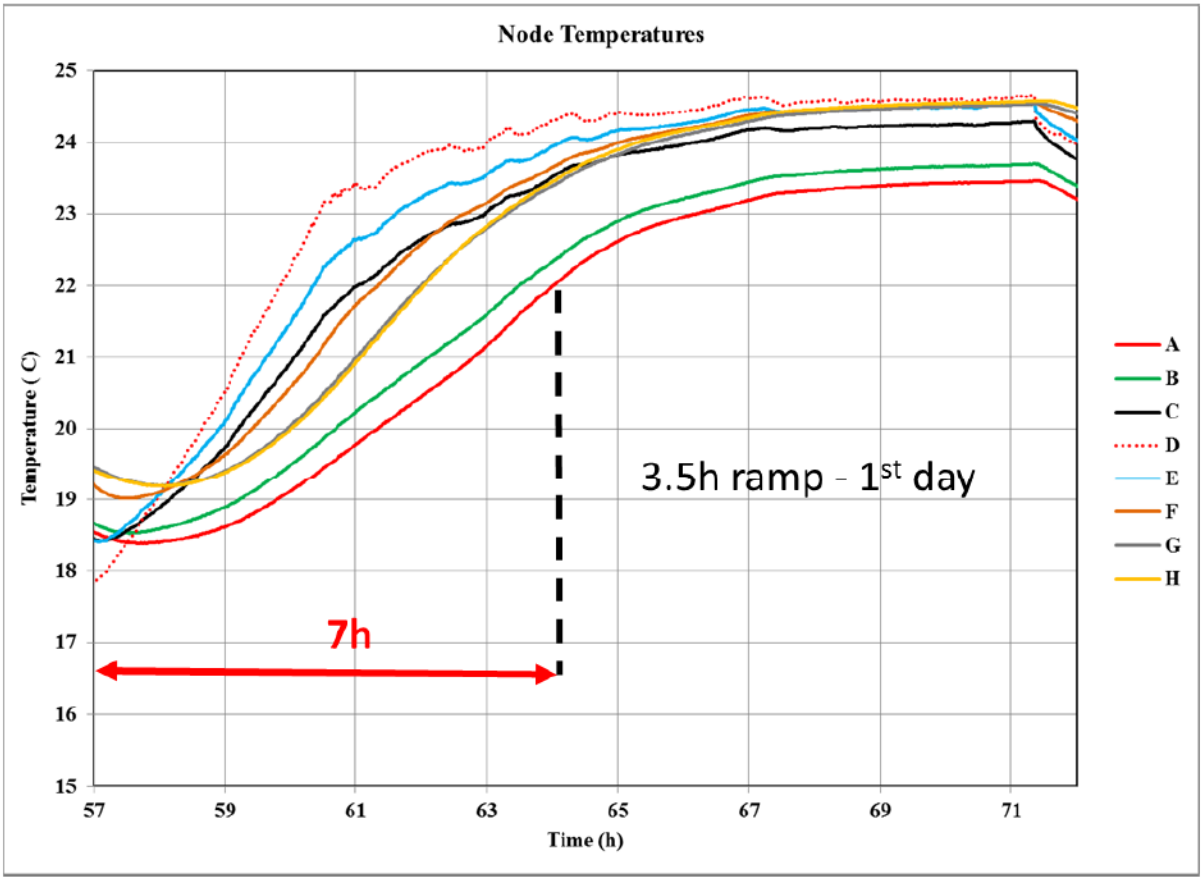

Figure A-2: Average temperature of the PCM layers - Charging with a 3.5h linear ramp

Each experiment lasted for 2 days to allow the temperatures profiles to be stabilized. The following figure shows a 4 day experiment with 3h linear ramps for charging and discharging the first 2 days and 3.5h linear ramps the last 2 days. The outdoor temperature is applied as a sinusoidal wave from 0 to -10°C. Different ramp durations were tested to investigate their effect on peak power demand.

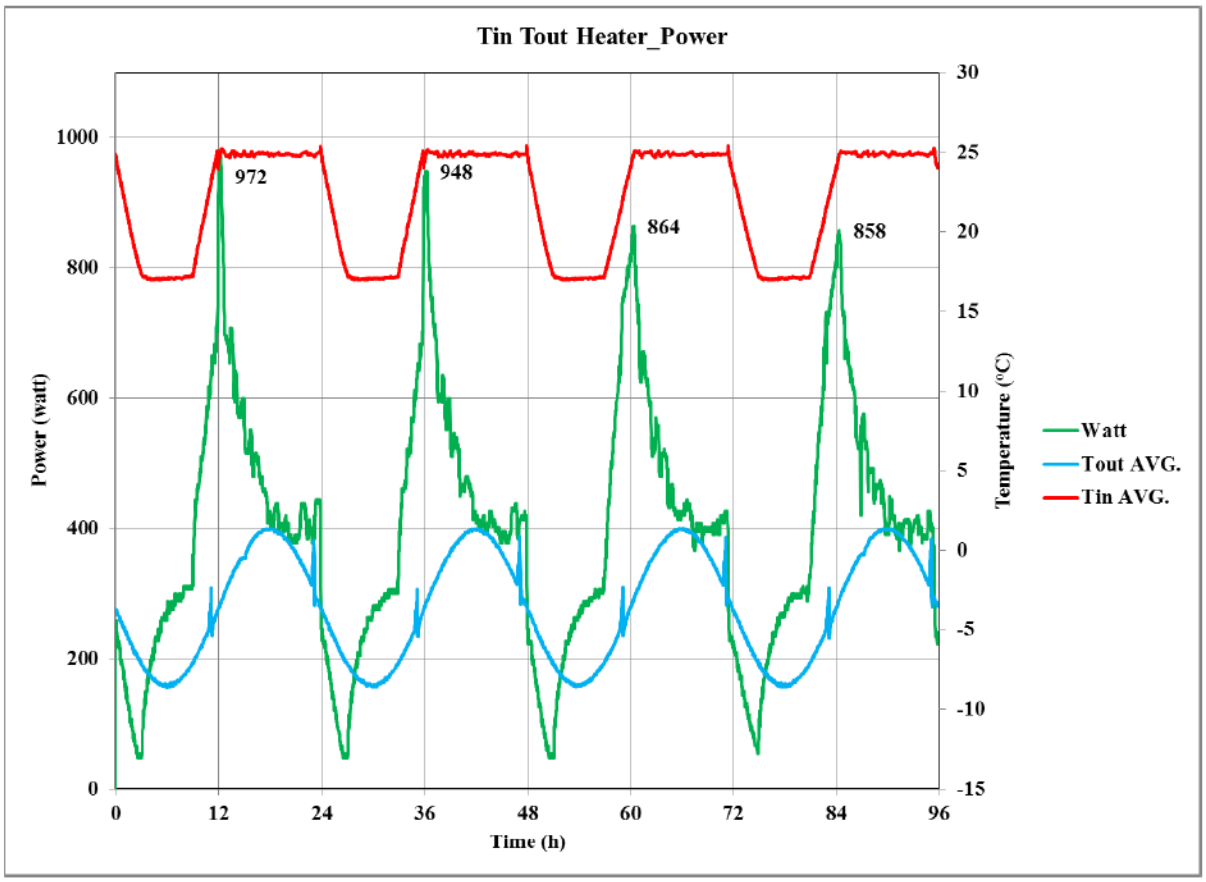

Figure A-3: 4 days experiment with 3h ramps the first 2 days and 3.5h ramps the last 2 days. Results of Tout, Tin and power of the electric heater

This experimental process helped to understand the dynamic response of the system and calibrate the parameters of the model developed in Matlab. Also, it lead to the result that the plenum fan should be turned off during the discharging period, so it will last longer. It should be noted once again here, that the only way to control the charging and discharging rate of the PCM was the room setpoint profile. There is no mechanical equipment, including grilles and dampers to isolate the PCM and release its stored energy at a desired time.

A.2 Discomfort Calculation

The Discomfort is calculated according to **ISO 7730 (2005)** based on **Fanger model** and Predicted Percentage of Dissatisfied (**PPD) index**, which predicts the percentage of people that are thermally dissatisfied. The method also calculates the Predicted Mean Vote (PMV). This is an index that predicts the mean value of the votes of a large group of persons on the following 7- point scale of thermal sensation:

- +3 hot
- +2 warm
- +1 slightly warm
- 0 neutral
- -1 slightly cool
- -2 cool
- -3 cold

The following figure presents PPD as function of PMV:

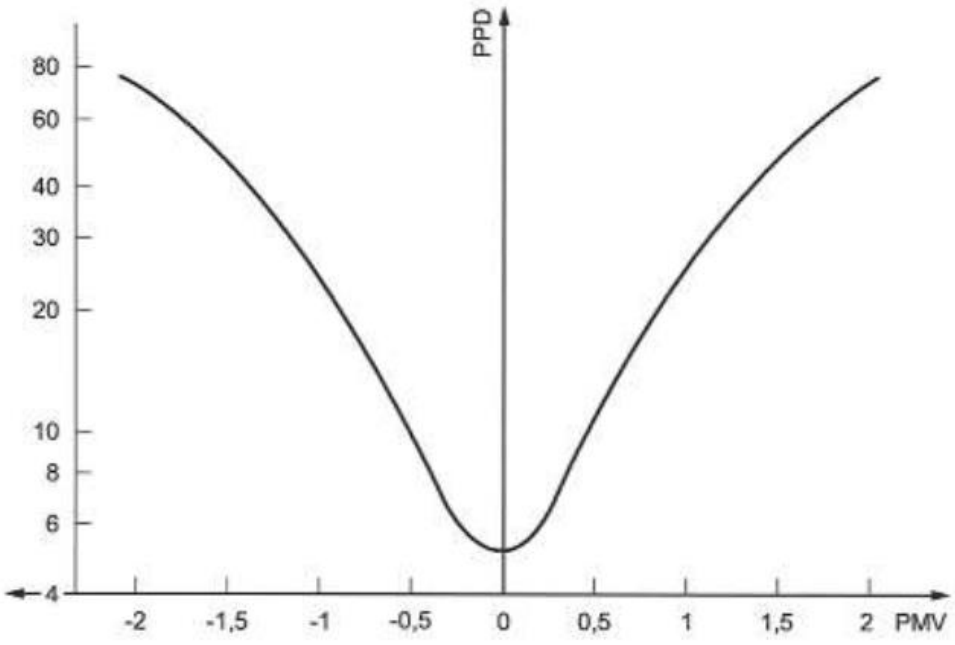

Figure A-4: PPD as function of PMV (ISO7730 2005)

PMV was calculated using this formula (Athienitis and O'Brien 2015):

$$\begin{aligned} PMV &= (0.303 * exp(-0.036 * M) + 0.028) * \\ &...((M - W) - 3.05 * 10^{(-3)} * (5733 - 6.99 * (M - W) - p_a) - 0.42 * ((M - W) - 58.15)... \\ &-1.7 * 10^{(-5)} * M * (5867 - p_a) - 0.0014 * M * (34 - t_a)... \\ &-3.96 * 10^{(-8)} * f_{clo} * ((t_{clo} + 273.15)^4 - (t_{mr} + 273.15)^4) - f_{clo} * hc * (t_{clo} - t_a)) \end{aligned} \quad \text{(A.1)}$$

PPD was calculated using this formula (Athienitis and O'Brien 2015):

$$PPD = 100 - 95 * \exp(-0.03353 * PMV^4 - 0.2179 * PMV^2) \quad \text{(A.2)}$$

The clothing surface temperature was calculated using this formula (Athienitis and O'Brien 2015):

$$\begin{aligned} t_{clo} &= 35.7 - 0.028 * (M - W) - 0.155 * I_{clo} * ((M - W) - 3.05 * \\ &...10^{(-3)} * (5733 - 6.99 * (M - W) - p_a) - 0.42 * \\ &...((M - W) - 58.15) - 1.7 * 10^{(-5)} * \\ &...M * (5867 - p_a) - 0.0014 * M * (34 - t_a)) \end{aligned} \quad \text{(A.3)}$$

where

M: Metabolic activity, M ∈ [0.8, 4] met

W: effective mechanical power in W/m^2, normally ignored for most activity (Chemical Encyclopedia)

I_{clo}: Clothing insulation, I_{cloth} ∈ [0, 2] clo

f_{clo}: Clothing surface area factor, f_{clo} ∈ [0, 2]

t_a: Ambient air temperature, Ta ∈ [10, 30] ^{o}C

t_{mr}: Mean radiant temperature, t_{mr} ∈ [10, 40] ^{o}C

υ_a: Relative air velocity, υ_a ∈ [0, 1] m/s

t_{clo}: Clothing surface temperature, t_{clo} ∈ [10, 30] ^{o}C

p_a: Partial pressure of water vapor in ambient air ∈ [0, 2700] Pa

The analysis is for the **winter months** and people's clothing is **1clo**. A space of thermal **Category C** is considered, with activity 70W/m^2, the acceptable operative temperature range is 19-25ºC for the heating season.

The Matlab code that used for the calculation of discomfort:

```
% Formulas by Athienitis & O'Brien book chapter 3 or ISO 7730:2005
M = 70;                     % metabolic activity in W/m2 for a Sedentary
                            % activity (office, school, laboratory)
                            % equals to 1.2 met
W = 5/4.5;                  % effective mechanical power in W/m2, normally
                            % ignored for most activity(Chemical Encyclopedia)
I_clo = 1;                  % clothing insulation during winter in clo
f_clo = 1.05 + 0.1 * I_clo;% clothing surface area factor since Icl>0.5 clo
ta = T(t,10);               % air temperature in degrees C
t_mr = T(t,2);              % mean radiant temperature in degC
v_air = v_air_chan;         % relative air velocity in m/s
p_a = 2310;                 % partial pressure of water vapor in ambient
                            % air, range [0,2700] Pa
hc = h_int;                 %convective heat transfer coefficient in W/m2*K

% clothing surface temperature in degC
t_clo = 35.7 - 0.028 * (M - W) - 0.155 * I_clo * ((M - W) - 3.05 *...
        10^(-3) * (5733 - 6.99 * (M - W) - p_a) - 0.42 *...
        ((M - W) - 58.15) - 1.7 * 10^(-5) *...
        M *(5867 - p_a) - 0.0014 * M * (34 - ta));

% Predicted mean vote
PMV = (0.303 * exp(-0.036 * M) + 0.028) * ...
    ((M - W) - 3.05 * 10^(-3) * (5733 - 6.99 * (M - W) - p_a) - 0.42 *...
    ((M - W) - 58.15) - 1.7 * 10^(-5) * M *(5867 - p_a) - 0.0014 * M *...
    (34 - ta) - 3.96 * 10^(-8) * f_clo *...
    ((t_clo + 273.15)^4 - (t_mr + 273.15)^4) - f_clo * hc * (t_clo - ta));

% Predicted percentage of dissatisfied
PPD= 100 - 95 * exp( - (0.03353 * PMV.^4 + 0.2179 * PMV.^2));
```

A.3 Energy consumption and Discomfort normalization

Energy consumption is normalized based on the expected minimum and maximum consumption. It takes values from 0 to 100. The energy consumption was normalized using this formula (Sakellariou 2011):

$$E_n = \frac{100*(Energy - E_{\min})}{E_{\max} - E_{\min}} \quad \text{(A.4)}$$

The maximum energy is calculated as the maximum heating power of the electric heater during the optimization horizon, for a period of 1 day. Therefore, the optimization horizon in this study is 3 days. The algorithm solves the equation for 3 days, finds the maximum power of the heater. The maximum energy equals this maximum power constant for a period of one day. The minimum energy is consider zero. Alternatively, as minimum energy it can be used the constant energy consumption of the fan of the heater in case it's constantly on.

Total Discomfort is normalized based on the expected minimum and maximum discomfort. It takes values from 0 to 100. The discomfort was normalized using this formula (Sakellariou 2011):

$$D_n = \frac{100*(D_{total} - D_{\min})}{D_{\max} - D_{\min}} \quad \text{(A.5)}$$

Discomfort is calculated according to ISO 7730 based on Fanger model and Predicted Percentage of Dissatisfied (PPD) index (ISO7730 2005). The analysis is for the winter months and people's clothing is 1clo. A space of thermal Category C is considered, with activity 70W/m^2, the acceptable operative temperature range is 19-25^{o}C for the heating season. This equals to a PPD limit of 15%. Sakellariou (Sakellariou 2011) mentions that the PPD index is obtained for steady state conditions. However, he calculated it with hourly averaged values considered (PPD hourly average). In the present study the PPD index is calculated for every time step (1 minute). This approximation is based on the observation of minor fluctuations of temperature in the room during occupied hours, 9am to 7pm. Then with a similar process with the one used by Sakellariou, the weighting factors (w.f.) of discomfort were calculated:

$$w.f. = \frac{PPD_{step}}{PPD_{limit}} \_ if \_ PPD_{step} > PPD_{limit} \quad (A.6)$$

The weighting factors are summed to give the total discomfort for the considered time:

$$D_{total} = \sum w.f. \quad (A.7)$$

For maximum discomfort, the discomfort limit constant for a period of one day was considered.

The minimum discomfort is zero.

A.4 Test room thermal model

The Matlab code for the model of the test room is:

```
function [cost,charg,discharg,heater,T_ext,Ts_p,Tr,E_n,D_n,Q_PCM] = Best_scenario_function
(charg_ramp_dur, dischar_ramp_dur, Tout_mean, dTout)

% Material Properties
rho = 850;        % kg/m^3
dx = 0.0052*[3,2]; % m
h_out = 34;
h_int = 4;
h_chn = 18;       % W/m^2K; Convection coefficient in the air channel
e_chn = 0.90;     % emissivity of painted PCM panels (0.85 to 0.95)
sig = 5.67*10^-8;  % Stefan-Boltzman constant
A = 4.8;          % m^2
m_air = 400/3600;  % kg/s; Air massflow rate - This should be a variable~fan speed
Cp_air = 1005;    % J/kgK
R_ins = 0.36;     % m^2K/W 0.6-1.0, 1.32 real; but leaks etc
R_back = 1.00;    % quite well insulated back side
k_fctr = 0.80;    % representing contact resistance applied to the conductivity of PCM
ksolid = 0.18;
kliquid = 0.14;
Tk = 22.2;

%Room properties
Reff = 0.105;     % Calculated in Mathcad and double checked from table of materials
Ceff = 2.2E5;     % Calculated in Mathcad

% Control
nN = 10;          % Number of nodes
st = 60;          % steps per hour
```

```
d = 3;            % number of days
H = d*24;         % number of hours, simulation only
nT = st*H;        % number of timesteps, simulation only
dt = 3600/st;     % s (3600s = 1 hour)
maxErr = 1e-3;    % maximum temperature difference between iterations of a given timestep


max_time = 15;
Text = zeros(nT,1);
w = 2*pi/1440;
% max_time should be given in 24hour format e.g. 3:15pm--> 15.25
theta = -2*(pi/24)*max_time;

% Running modes
mode = zeros(4,1);

% Tsp profile
Tsp = zeros(86400/dt,1);
Tsp_day = 25;
Tsp_night = 16.5;
Tsp_dT = Tsp_day - Tsp_night;
setback_beg = 19.5;
setback_end = 9;

if setback_beg + dischar_ramp_dur > 24
   temp = setback_beg + dischar_ramp_dur - 24;
else
   temp = 0;
end
for t = 1:86400/dt
   time = t*dt/3600;
   % Discharging ramp
   if (setback_beg <= time) && (time < (setback_beg + dischar_ramp_dur))
      Tsp(t) = Tsp_day - (time - setback_beg)*Tsp_dT/dischar_ramp_dur;
      mode(t)=1;
   % Night time
   elseif ((setback_beg + dischar_ramp_dur) <= time) || (time < (setback_end - charg_ramp_dur )
)
      Tsp(t) = Tsp_night;
      mode(t)=2;
   % Charging ramp
   elseif ((setback_end - charg_ramp_dur ) <= time) && ( time < setback_end)
      Tsp(t) = Tsp_day - (setback_end - time)*Tsp_dT/charg_ramp_dur;
      mode(t)=3;
   % Day time
   else
```

```
        Tsp(t) = Tsp_day;
        mode(t)=4;
    end
    if time < temp
        Tsp(t) = Tsp_day - (24 - setback_beg)*Tsp_dT/dischar_ramp_dur - time * Tsp_dT /
dischar_ramp_dur;
    end
end
Tsp = repmat(Tsp,nT/(86400/dt),1);
mode = repmat(mode,nT/(86400/dt),1);

% Heating system
SP_Err = zeros(nT,1);
max_Cap = 960;   % W, Heater size
min_Cap = 0;     % W, minimum heat
Kp = 50/100;
Ki = 0.001;
heat_output = zeros(nT,1);
bias0 = 24.4/ 100;
bias = zeros(nT,1);
Irate = 0.03;     % 3/100


% Declare variablles
C = zeros(nN);
T = zeros(nT,nN);
P0 = zeros(nT,1);
P1 = zeros(nT,1);
q_PCM = zeros(nT,1);
PCM_cap = zeros(nT,2);
PMVstep = zeros(nT,1);
PPDstep = zeros(nT,1);
Dis_total = 0;
Total_energy = 0;

% Auxiliary variables
 III = zeros(nT,1);
 I = zeros(nT,1);
 DT_channel = zeros(nT,1);
 h_channel = zeros(nT,1);
 air_flow = zeros(nT,1);
 Energy = zeros(nT,1);
 Discomf_period = zeros(nT,1);

% Nodes with capacitance
C(10) = Ceff;
```

```
% Initial condition
T(1,:) = 20;
phT = 'F';

%% Outer Loop

for t = 2:nT % 1:(nT-1)

    %% First Run?
    itt = 1;
    error = 100;
    Tp = T(t);


    %% Inner Loop
    while (error > maxErr) %&& (itt <= maxItt)

        %% Declare variables
        U = zeros(nN);    % W/K
        F = zeros(nN,1);  % W/K


        % How are nodes connected? "0"s is for when they are not (K/W)
        % Each timestep is calculated a few times until the temperatures
        % converge (in that timestep).
        % For radiantion heat exchange, h_rad is initialized using surface
        % temperatures from the previous timestep (t-1). Once this "inner
        % loop" is ran once, we use temperature values from timestep (t).
        % Then you run this a few times (max 10 times) until convergence is
        % achieved.
        if itt == 1
            ti = t-1;
        else
            ti = t;
        end

        if (mode(t)==1) || (mode(t)==2)
            h_chn = 10;
            m_air = 150/3600;
            v_air_chan = 1.02;
        elseif (mode(t)==3) || (mode(t)==4)
            h_chn = 18;
            m_air = 355/3600;
            v_air_chan = 1.9;
        end
```

```
% PCM Properties and Data Range

if phT == 'M'      % Melting range
   skew = -10;    % skew
   T_peak = 23;   % peak phase change temperature, C;
   rng = 4.5;     % range of phase change, C
   dh = 13100;    % enthalpy of phase change, J/kg
   Cp_avg = 3200; % average solid/liquid specific heat (full quality), J/kg
elseif phT == 'F'  % Freezing range
   skew = -4;
   T_peak = 20.8;
   rng = 5;
   dh = 12600;
   Cp_avg = 3200;
end

% Change of PCM state
 if T(t,3) < 19
   phT = 'F';
 elseif T(t,3) > 20
   phT = 'M';
 end


ehAmCp = exp(-h_chn*2*A/(m_air*Cp_air));

% Radiation exchange in the channel
TfK = T(ti,4) + 273.15;
TbK = T(ti,6) + 273.15;
Urad = A*sig*(TfK^2+TbK^2)*(TfK+TbK) / (1/e_chn + 1/e_chn - 1);
U(4,6) = Urad;

clear rad TfK TbK Urad

% Connected to room air node
F(10) = 1 / Reff;
F(8) = (R_back/A + 1/(h_out*A))^(-1); % Back side to outside

%PCM
% node 1: inlet of the air channel
U(2,3) = (2*A*k_fctr*fk_erfc([T(ti,2) T(ti,3)])) /dx(1) ;
U(3,4) = (2*A*k_fctr*fk_erfc([T(ti,3) T(ti,4)]))/ dx(1);
U(4,5) = (h_chn*A);
U(5,6) = (h_chn*A);
```

```
U(6,7) = (2*A*k_fctr*fk_erfc([T(ti,6) T(ti,7)])) / dx(2) ;
U(7,8) = (2*A*k_fctr*fk_erfc([T(ti,7) T(ti,8)])) / dx(2);

% node 9 : outlet of the air channnel
% Towards the room air, node 10
U(2,10) = (2 * R_ins/A + 1/(h_int*A))^(-1); % Front side to room

C(3) = rho*A*dx(1)*fCp_skewnormal(T(t-1,3), skew, T_peak, rng, dh, Cp_avg);
C(7) = rho*A*dx(2)*fCp_skewnormal(T(t-1,7), skew, T_peak, rng, dh, Cp_avg);

PCM_cap(t,1:2) = [C(3) C(7)];
P0(t) = T(ti,1);
P1(t) = P0(ti)*ehAmCp + 0.5*(T(ti, 4)+T(ti,6))*(1-ehAmCp);

q_PCM(t) = m_air*Cp_air*(P1(t) - P0(t));

DT_channel(t) =  P1(t) - P0(t);


% U matrix and its inverse
U = - U - U';
s = - sum(U,1);
for i = 1:nN
   U(i,i) = s(i) +F(i) +  C(i) / dt;
end

U(1,1) = 1;
U(9,9) = 1;

% Auxiliary heat, PI control - Regulvar setup
SP_Err(t) =  Tsp(t) - T(t,10);
III(t) = SP_Err(t)*dt;
I(t) = sum(III(t));
iTerm1 =  Ki *I(t);
% Every time the Tsp changes set iTerm = 0 (Jennifer Date 2015)
if (Tsp(t) - Tsp(t-1) > 0)
   iTerm1 = 0;
end
if SP_Err(t)>0
   bias(t) = bias0 - Irate;
elseif SP_Err(t)<0
   bias(t) = bias0 + Irate;
else
   bias(t) = bias0;
end
pterm = Kp * SP_Err(t);
```

```
CO = bias(t) + pterm + iTerm1;

if CO > 1
   output = max_Cap;
elseif  (0 < CO) && (CO <= 1)
   output = max_Cap * CO;
else
   output = min_Cap;
end
heat_output(t) = output;

Total_energy = Total_energy + heat_output(t)/st;  % to get Wh
Energy(t) = heat_output(t)/st;

% Heat flow into the node
Text(t) = Tout_mean + (dTout/2)*cos(w*t+theta);
q = zeros(nT,1);
q(5) = -m_air*Cp_air*(P1(t) - P0(t));
q(8) = F(8) * Text(t);
q(10) = F(10) * Text(t) + heat_output(t)+ q_PCM(t);


% Q vector
Q = zeros(nN,1);
for i = 1:nN
   Q(i) = q(i) + C(i) * T (t-1,i) / dt;
end
Q(1) = T(ti,1);
Q(9) = T(ti,9);

% Compute temperature

T(t,:) = U \ Q;

% Compute iteration and error
error = max(T(t,:) - Tp);


T(t,1) = T(t,10);
T(t,9) = T(t,10);

Tp = T(t,:);
% Iterate
itt = itt + 1;
```

```
        Discomfort     % call Discomfort file

        PMVstep(t)=PMV;
        PPDstep(t)=PPD;
        PPD_limit = 15; % Category C
        if PPDstep(t) > PPD_limit
            w_f = PPDstep(t)/PPD_limit;
        else
            w_f = 0;
        end
        Dis_total = Dis_total + w_f;
        Discomf_period(t) = w_f;
    end

end

% Peak load
Q_heater_max = max(heat_output(1440:end));

%Calculate the cost function every day

Dmax = (15) * 1440;
Dmin = 0;

Emax = Q_heater_max/st * 1440;
Emin = 0;

    Discom = sum(Discomf_period(1440:2880));
    Energ = sum(Energy(1440:2880));

    % Discomfort Normalization
    Dn = 100 / (Dmax - Dmin) * (Discom - Dmin);

    %Energy Normalization
    En = 100 / (Emax - Emin) * (Energ - Emin);

% Cost Function
CF = 0.9 * Dn + 0.1* En;

cost = CF;
charg = charg_ramp_dur;
discharg = dischar_ramp_dur;
heater = heat_output;
Ts_p = Tsp;
T_ext = Text;
Tr = T(:,10);
```

```
E_n = En;
D_n = Dn;
Q_PCM = q_PCM;
end
```

A.5 Simple MPC Algorithm

```
clear all
clc

st = 60;          % steps per hour
d = 3;            % number of days
H = d*24;         % number of hours, simulation only
nT = st*H;        % number of timesteps, simulation only
dt = 3600/st;     % s (3600s = 1 hour)

%-------------CHARGING + DISCHARGING COMBINATIONS (10 scenarios)-------------
index = [1   1
         2   2
         3   3
         3.5 3.5
         3   6
         4.5 4.5
         4   6
         4.5 7
         4   7.5
         4.5 7.5];

number_of_scenarios = size(index,1);
% Read Outdoor temperature
Tout = xlsread('External Temperature.xlsx');

Control_horizon = 12 * dt;
optimization_horizon = nT;

%----------------MATRICES-----------------------------------------------------
cost = zeros(number_of_scenarios,1);
charg =  zeros(number_of_scenarios,1);
discharg = zeros(number_of_scenarios,1);
heater= zeros(nT,number_of_scenarios);
T_ext = zeros(nT,number_of_scenarios);
Ts_p = zeros(nT,number_of_scenarios);
Tr = zeros(nT,number_of_scenarios);
E_n = zeros(number_of_scenarios,1);
D_n = zeros(number_of_scenarios,1);
```

```
Energy_per_opt = zeros(optimization_horizon/Control_horizon,1);
Discomf_per_opt = zeros(optimization_horizon/Control_horizon,1);
heat_Optimal = zeros(nT,1);
Tsp_opt = zeros(nT,1);
Text_opt = zeros(nT,1);
Troom_opt = zeros(nT,1);
Q_PCM_opt = zeros(nT,1);
Q_PCM = zeros(nT,number_of_scenarios);
%-------------------------------------------------------------------------

tic

for ii=1:Control_horizon:optimization_horizon

   if mod(ii-1,Control_horizon) == 0
      if ii == 1
         Tout_mean = Tout(ii,1);
         dTout = Tout(ii,2);
      else
         Tout_mean = Tout(ceil(ii-1)/Control_horizon+1,1);
         dTout = Tout(ceil(ii-1)/Control_horizon+1,2);
      end
   end

   for j = 1:number_of_scenarios
      [cost(j),charg(j),discharg(j),heater(:,j),T_ext(:,j),Ts_p(:,j),Tr(:,j),E_n(j),D_n(j),Q_PCM(:,j)]
= Best_scenario_function(index(j,1),index(j,2), Tout_mean,dTout);
   end

   %-----MINIMUM Cost Function-----------------------------------------

   Optimal = min(cost);
   optimum_position = find(Optimal == cost);

   %----------RESULTS-----------------------------------------------------
   fprintf('\n External T profile:\n')
   fprintf('Tout_mean: %.1f \n',Tout_mean);
   fprintf ('dTout: %.1f \n',dTout);
   Charg_opt = charg(optimum_position);
   Discharg_opt = discharg(optimum_position);
   fprintf('Charging period: %.1f \n',Charg_opt);
   fprintf('Discharging period: %.1f \n',Discharg_opt);
   heat_Optimal(ii:(Control_horizon+ii-1)) = heater(ii:(Control_horizon+ii-
1),optimum_position);
   Tsp_opt(ii:(Control_horizon+ii-1)) = Ts_p(ii:(Control_horizon+ii-1),optimum_position);
   Text_opt(ii:(Control_horizon+ii-1)) = T_ext(ii:(Control_horizon+ii-1),optimum_position);
```

```
   Troom_opt(ii:(Control_horizon+ii-1)) = Tr(ii:(Control_horizon+ii-1),optimum_position);
   Q_PCM_opt(ii:(Control_horizon+ii-1)) = Q_PCM(ii:(Control_horizon+ii-
1),optimum_position);

   if mod(ii-1,Control_horizon) == 0
      if ii == 1
         Energy_per_opt(ii) = E_n(optimum_position);
         Discomf_per_opt(ii) = D_n(optimum_position);
         %------------WRITE THE RESULTS TO AN EXCEL FILE----------------
         xlswrite('External Temperature.xlsx', [Charg_opt Discharg_opt],
sprintf('C%d:D%d',ii+1,ii+1))
      else
         Energy_per_opt(ceil(ii-1)/Control_horizon+1) = E_n(optimum_position);
         Discomf_per_opt(ceil(ii-1)/Control_horizon+1) = D_n(optimum_position);
         xlswrite('External Temperature.xlsx', [Charg_opt Discharg_opt],
sprintf('C%d:D%d',ceil(ii-1)/Control_horizon+2,ceil(ii-1)/Control_horizon+2))
      end
   end
end

%------------PLOTS-----------------------------------------------------
tim = linspace(1,nT,nT);

figure(1);

plot(tim/60, Tsp_opt,'--b','LineWidth',2);
% title('Temperature set point');
xlabel('Time (h)');
ylabel('Temperature (^o C)');

hold on;

plot(tim/60, Troom_opt,'r','LineWidth',2);
plot(tim/60, Text_opt,':g','LineWidth',2);
legend('T Set point','T Room','Text','Location','northoutside','Orientation','horizontal');

hold off;

figure(2);

plot(tim/60, heat_Optimal,'LineWidth',2);
title('Q_{HEATER}');
xlabel('Time (h)');
ylabel('Power (W)');

figure(3);
```

```
bar(linspace(Control_horizon/60,optimization_horizon/60,size(Energy_per_opt,1)),
Energy_per_opt);
title('Energy Performance');
xlabel('Time (h)');
ylabel('Energy Normalized (%)');

figure(4);

bar(linspace(Control_horizon/60,optimization_horizon/60,size(Energy_per_opt,1)),
Discomf_per_opt);
title('Discomfort Performance');
xlabel('Time (h)');
ylabel('Discomfort Normalized (%)');

temp_har = [0.25 * Energy_per_opt' ; 0.75 * Discomf_per_opt']';

figure(5);

b = bar(linspace(Control_horizon/60,optimization_horizon/60,size(Energy_per_opt,1)),
temp_har, 'stacked');
xlabel('Time(h)');
ylabel('Cost Function Performance (%)');
legend('Energy','Discomfort','Location','northoutside','Orientation','horizontal');
b(2).FaceColor = 'r';

figure(6);

plot(tim/60, Q_PCM_opt);
title('Q_{PCM}');
xlabel('Time (h)');
ylabel('Power (W)');

toc
```

A.6 BACnet Stack Demo Tools

BACnet stands for Building Automation and Control Network. It's a communications protocol that allows building equipment and systems manufactured by different companies to work together.

BACnet Stack is an open source BACnet protocol stack for communication with BACnet devices and their objects. It contains two parts: the API (Application Program Interface) library of programs/functions for interacting with BACnet devices and objects, and demos in form of stand-alone DOS executable programs that each completes a single functionality with BACnet devices or objects. The API is coded in C, C++ and can be combined into a customized software based in Windows and UNIX. The demos, also referred to as the tools, can be used with any Windows software or programming environment (Python, MATLAB, DOS batch, etc.) that can call DOS commands. The tools use command line interface and take information from the arguments on the command line.

Some of the BACnet Stack demo tool that are commonly used are:

- bacwi: BACnet WhoIs service to display connected devices
- bacepics: BACnet EPICS: Experimental Physics and Industrial Control System
- bacrp: Read an object property
- bacwp: Write an object property

The objects are inputs, outputs, programs, trend logs, etc. The object properties parameters include:

- device instance (i.e., which device on the network)
- object type (analog input, binary input, etc.)
- object instance (i.e., which analog input)
- property (present value, object name, status flags, etc.)

The syntax of the read property service is the following:

bacrp device-instance object-type object-instance property [index]

The syntax of the write property service is:

bacwp device-instance object-type object-instance property priority index tag value [tag value...]

The Matlab code that was used during the implementation of the predictive control in chapter 4 included the following code, which was reading the value from an Excel file and writing it to the local variable of the controller through BACnet is:

```
% -------READ PROPERTY-----------------------------------------
% bacwp i) device_instance ii) object_type iii) object_instance iv) property [index]
% -----Charging ramp duration-----------------------------------

[status CmdOut] = dos ('bacrp 100800 2 17 77');
if status == 0
   Objname = CmdOut;
else
   Objname = 'Name_Error';
end


% -------WRITE PROPERTY-----------------------------------------
% bacwp i) device_instance ii) object_type iii) object_instance iv) property v) priority vi) index
vii) tag viii) value [tag value...]

dos_command = sprintf ('bacwp 100800 2 17 85 16 -1 4 %d',Charg_opt);
[status CmdOut] = dos(dos_command);
if status == 0
  ObjValue = CmdOut;
else
   ObjValue = 'Error';
End
```

A.7 Sensitivity Analysis on Cost Function Weighting Factors

A sensitivity analysis for the value of α was performed, varying it from 0.1 to 0.9 with a step of 0.1. The predictive control algorithm chooses different scenario according to the cost function coefficients. The results are presented in the following tables:

Table A-1: Sensitivity analysis on α (1)

				a = 0.1		a = 0.2		a = 0.3	
Experiment Progress		**External T Profile**		**Best Scenario Chosen**		**Best Scenario Chosen**		**Best Scenario Chosen**	
Control horizon (12 h step)	**Time (h)**	**Tout mean (°C)**	**Tout p-p amplitude (°C)**	**Charging ramp dur. (h)**	**Discharging ramp dur. (h)**	**Charging ramp dur. (h)**	**Discharging ramp dur. (h)**	**Charging ramp dur. (h)**	**Discharging ramp dur. (h)**
1st	**1-12**	**-5**	**10**	**4.5**	**7.5**	**3**	**6**	**2**	**2**
2nd	**13-24**	**-5**	**10**	**4.5**	**7.5**	**3**	**6**	**2**	**2**
3rd	**25-36**	**0**	**5**	**3**	**6**	**1**	**1**	**1**	**1**
4th	**37-48**	**0**	**5**	**3**	**6**	**1**	**1**	**1**	**1**
5th	**49-60**	**2.5**	**5**	**1**	**1**	**1**	**1**	**1**	**1**
6th	**61-72**	**2.5**	**5**	**1**	**1**	**1**	**1**	**1**	**1**

Table A-2: Sensitivity analysis on α (2)

				a = 0.4		a = 0.5		a = 0.6	
Experiment Progress		**External T Profile**		**Best Scenario Chosen**		**Best Scenario Chosen**		**Best Scenario Chosen**	
Control horizon (12 h step)	**Time (h)**	**Tout mean (°C)**	**Tout p-p amplitude (°C)**	**Charging ramp dur. (h)**	**Discharging ramp dur. (h)**	**Charging ramp dur. (h)**	**Discharging ramp dur. (h)**	**Charging ramp dur. (h)**	**Discharging ramp dur. (h)**

1st	1-12	-5	10	2	2	2	2	2	2
2nd	13-24	-5	10	2	2	2	2	2	2
3rd	25-36	0	5	1	1	1	1	1	1
4th	37-48	0	5	1	1	1	1	1	1
5th	49-60	2.5	5	1	1	1	1	1	1
6th	61-72	2.5	5	1	1	1	1	1	1

Table A-3: Sensitivity analysis on α (3)

				a = 0.7		a = 0.8		a = 0.9	
Experiment Progress		**External T Profile**		**Best Scenario Chosen**		**Best Scenario Chosen**		**Best Scenario Chosen**	
Control horizon (12 h step)	**Time (h)**	**Tout mean (°C)**	**Tout p-p amplitude (°C)**	**Charging ramp dur. (h)**	**Discharging ramp dur. (h)**	**Charging ramp dur. (h)**	**Discharging ramp dur. (h)**	**Charging ramp dur. (h)**	**Discharging ramp dur. (h)**
1st	1-12	-5	10	1	1	1	1	1	1
2nd	13-24	-5	10	1	1	1	1	1	1
3rd	25-36	0	5	1	1	1	1	1	1
4th	37-48	0	5	1	1	1	1	1	1
5th	49-60	2.5	5	1	1	1	1	1	1
6th	61-72	2.5	5	1	1	1	1	1	1

As α increases, the weighting factor of energy increases and the algorithm chooses the profile that minimizes the more the energy and less the discomfort term.